

Diploma Thesis

Recombinant production and characterization of new bacterial heme peroxidases at the origin of the peroxidase-cyclooxygenase superfamily

Performed at the

Department of Chemistry

Division of Biochemistry, Metalloprotein Research Group

BOKU - University of Natural Resources

and Life Science, Vienna

Submitted by

Stefan Alexander TEUFER

Austria, Vienna, June 2011

Table of contents

Table of contents.....	2
Index of Figures.....	6
Index of Charts.....	7
Index of Tables.....	8
1. Introduction	9
1.1 Heme peroxidases superfamily	9
1.2 <i>Microcoleus chthonoplastes</i> (PCC 7420) and <i>Lyngbya sp.</i> (PCC 8106)	14
1.3 Human peroxidases myeloperoxidase, lactoperoxidase, and eosinophil peroxidase	18
1.4 Active site of mammalian peroxidases.....	24
1.5 Reaction pathways of peroxidases	27
1.6 Co-substrate hydrogen peroxide, H ₂ O ₂	29
2. Aim of work	31
3. Material and Methods.....	33
3.1. Sequence analysis and protein parameter prediction of <i>Microcoleus chthonoplastes</i> (PCC 7420) and <i>Lyngbya sp.</i> (PCC8106) peroxidases.....	33
3.1.1. Sequence alignment of the two peroxidockerin sequences with selected mammalian peroxidases.....	34
3.1.2 Protein parameter prediction	34
3.2 Cloning of the <i>Microcoleus chthonoplastes</i> (PCC 7420) peroxidase.....	35
3.2.1. Amplification of peroxidase gene DNA and preparation of vector DNA	36
3.2.1.1 Primer design for amplification of the cyanobacterial peroxidase gene DNA from genomic DNA	37
3.2.1.2 Amplification of the cyanobacterial peroxidase gene DNA from genomic DNA by using polymerase chain reaction (PCR).....	38
3.2.1.3. Agarose gel electrophoresis (E-Gel®, Sybr® safe)	39
3.2.1.4 GFX™ PCR DNA and gel band purification.....	40
3.2.2. Plasmid preparation.....	41
3.2.2.1 Restriction cuts of peroxidase gene DNA and pET-21a (+) vector.....	41

3.2.2.2. Removal of 5'-phosphate residues from vector pET-21a (+) with CIAP	42
3.2.2.3 Ligation	42
3.2.2.4. Electroporation	43
3.3 Screening for colonies	44
3.3.1. PCR screening	44
3.3.2 Plasmid amplification and purification	46
3.3.3 Restriction screening	47
3.3.4 Expression screening	48
3.3.5 Sodium dodecyl sulfate polyacrylamide-gel-electrophoresis (SDS-PAGE)	50
3.3.6. DNA-Sequencing	52
3.3.7 Cryoculture of sequenced clone	53
3.4 Large-scale expression and purification of the two cyanobacterial peroxidases from PCC 7420 and PCC 8106	53
3.4.1 Expression of cyanobacterial peroxidases in <i>E. coli</i> BL21 (DE3) Star	54
3.4.2 Cell lysis and metal-chelate-affinity-chromatography (MCAC)	55
3.4.2.1 Cell lysis and sample preparation	55
3.4.2.2 Metal chelate affinity chromatography (MCAC)	56
3.4.3. Ultrafiltration and desalting of the protein	60
3.4.3.1 Desalting of proteins with PD-10 columns	60
3.5 Spectroscopic characterization of cyanobacterial peroxidases.	62
3.5.1 Determination of protein concentration by UV-Vis spectroscopy	62
3.5.2 Circular dichroism (CD) spectroscopy	63
3.5.2.1 Principles of CD spectroscopy	63
3.5.2.2 Sample preparations and CD measuring settings	66
3.6. Determination of peroxidase and halogenation activities.	67
3.6.1 Iodination activity	67
3.6.2 Bromination activity	68
3.6.3 Chlorination activity	68
3.6.4 ABTS-peroxidase assay	69

3.6.5 Guaiacol peroxidase assay.....	70
3.6.6. Tyrosine peroxidase assay	71
3.7 Cyanide Binding	72
3.7.1 Determination of K_d values by using spectrophotometrical cyanide titration	73
3.7.2. Determination of K_d values by using stopped-flow spectroscopy.	74
3.7.2.1 Reaction of cyanobacterial peroxidases with cyanide.....	75
3.8 Reaction of ferric enzymes with H_2O_2	76
4.Results and Discussion	76
4.1.1 Peroxidase sequence alignment.....	76
4.1.2. Protein parameters	78
4.1.2.1 Signal peptide prediction.....	78
4.1.2.2 Secondary structure prediction.....	82
4.1.2.3 Extinction coefficient, pI , M_w , and amino acid composition and secondary structure prediction.....	86
4.2.1 Agarose gel electrophoresis of PCR product containing amplified peroxidase genes.	87
4.2.2. Restriction analysis of vector and insert.....	88
4.2.3. Analysis of LB-agar _{amp} plates.....	88
4.3.1. PCR Screening.....	89
4.3.2. Restriction screening	91
4.3.3. Expression screening	93
4.3.4 DNA Sequencing.....	94
4.4.1 Enzyme purification	94
4.5. Spectroscopic analysis of cyanobacterial peroxidases	96
4.5.1 UV-Vis spectroscopy	96
4.5.2 CD spectroscopy	96
4.6. Determination of peroxidase and halogenation activity	99
4.6.1. Iodination activity.....	100
4.6.2 Bromination activity	102
4.6.3 Chlorination activity	103

4.6.4 ABTS peroxidase activity	104
4.6.5 Guaiacol peroxidase activity	106
4.6.6. Tyrosine peroxidase activity	107
4.7. Cyanide binding	108
4.7.1. Spectrophotometrical cyanide titration	108
4.7.1.1 <i>Lyngbya sp.</i> PCC 8106 peroxidase	108
4.7.1.2 PCC 7420 peroxidase	111
4.7.2 Kinetics of cyanide binding	114
4.7.2.1 Cyanide binding of PCC 8106 peroxidase	114
4.7.2.2 Cyanide binding of PCC 7420 peroxidase	116
4.8 Kinetics of hydrogen peroxide reduction	117
4.8.1 PCC 8106 peroxidase	117
4.8.2 Results of the PCC 7420 peroxidase	119
5. Conclusions	121
References	124

Index of Figures

Figure 1. The seven subfamilies of the peroxidase-cyclooxygenase superfamily.....	11
Figure 2 Domain structures of the peroxidase-cyclooxygenase superfamily.	14
Figure 3. Phylogenetic origin of the cyclooxygenase-peroxidase superfamily	15
Figure 4. Overview of the habitat of the two cyanobacteria.....	16
Figure 5. The picture shows schematic the release of MPO into the phagosome.	18
Figure 6 Structure of mature homodimeric human MPO.....	20
Figure 7 Schematic view of bovine LPO..	22
Figure 8. Ferri-Protoporphyrin IX	24
Figure 9. Active site residues of (A) bovine LPO and (B) human MPO..	25
Figure 10 General reaction scheme of peroxidases.....	27
Figure 11 pET-21a(+) expression vector	35
Figure 12.Schematic view of the pET expression system	36
Figure 13. pET-21a-d(+) cloning/expression region.	38
Figure 14. Master plate for PCR screening containing 18 colonies	45
Figure 15 Scheme of master plate for expression screening.	49
Figure 16 Components of the Sonifier II W-250 s	55
Figure 17. Sepharose with iminodiacetic acid	56
Figure 18 Amico Centriprep.....	60
Figure 19 Transition from circular polarized light to elliptic form.....	63
Figure 20 Electron structure of a six coordinated high and low spin complex	73
Figure 21 Essentials of a stopped-flow apparatus.	74
Figure 22. Multiple sequence alignment.	77
Figure 23. Agarose gel electrophoresis genome PCR.	87
Figure 24. Agarose gel electrophoresis restriction cut.	88
Figure 25. PCR screening; Agarose gel electrophoresis 1.....	89
Figure 26 PCR screening; Agarose gel electrophoresis 2.....	90
Figure 27 Restriction screening; Agarose gel electrophoresis	91
Figure 28 Electrophoretical confirmation of clone 14.	92
Figure 29. Expression screening; SDS Page.....	93
Figure 30 SDS page after MCAC purification.	95
Figure 31 Stopped flow diode array analysis of PCC 8106 peroxidase with cyanide.	115
Figure 32 Stopped flow diode array analysis of PCC 7420 peroxidase with cyanide	116
Figure 33 Stopped flow diode array analysis of PCC 8106 peroxidase with H ₂ O ₂	118
Figure 34 Stopped flow diode array analysis of PCC 7420 peroxidase with H ₂ O ₂	119

Index of Charts

Chart 1 Characteristic CD spectra	65
Chart 2 SignalP <i>Microcoleus chthonoplastes</i> of PCC 7420 sequence	79
Chart 3 Hidden Markov of the submitted sequence of PCC 7420	80
Chart 4 SignalP <i>Lyngbya sp.</i> (PCC 8106) sequence.	81
Chart 5. Hidden Markov of the submitted sequence of <i>Lyngbya sp.</i> (PCC 8106).....	82
Chart 6 Spectral features of the peroxidases of PCC 7420 and PCC 8106.....	94
Chart 7 UV-Vis absorbance spectra of PCC 7420 and PCC 8106 peroxidase solutions	96
Chart 8 Far UV CD spectra of the cyanobacterial peroxidases.	97
Chart 9 Near UV/Vis CD spectra of the cyanobacterial peroxidases.....	98
Chart 10 Specific iodinating activities.	101
Chart 11 Specific bromination activities	102
Chart 12 Specific chlorinating activities	103
Chart 13 Specific ABTS activities.	105
Chart 14 Specific guaiacol activities.	106
Chart 15 Specific tyrosine activities	107
Chart 16 Spectral changes of PCC 8106 peroxidase upon increasing cyanide concentration .	108
Chart 17 Difference spectra of PCC 8106 peroxidase.	109
Chart 18 Plot of Δ Absorption against the cyanide concentration (PCC 8106)	110
Chart 19 Double Reciprocal Plot (PCC 8106).....	110
Chart 20 Scatchard Plot (PCC 8106).....	111
Chart 21 Spectral changes of PCC 7420 peroxidase upon increasing cyanide concentration.	111
Chart 22 Difference spectra of PCC 7420 peroxidase.	112
Chart 23 Plot of Δ Absorption versus cyanide concentration (PCC 7420).....	113
Chart 24 Double reciprocal plot (PCC 7420).....	113
Chart 25 Scatchard plot (PCC 7420)	114
Chart 26 k_{obs} values plotted versus the used cyanide concentrations (PCC 8106).....	115
Chart 27 k_{obs} values plotted versus the used cyanide concentrations (PCC 7420).....	117
Chart 28 k_{obs} values of PCC 8106 peroxidase plotted versus the H_2O_2 concentration.....	118
Chart 29 k_{obs} values of PCC 7420 peroxidase plotted versus the H_2O_2 concentration.....	120

Index of Tables

Tab. 1 Parameters for the ClustalX multiple sequence alignment.....	34
Tab. 2 PCR mixture for amplification of the peroxidase gene	38
Tab. 3 PCR cycles; 3-step protocol	39
Tab. 4 Restriction cut.	41
Tab. 5 Mixture for dephosphorylation of pET-21a (+) vector	42
Tab. 6 Ligation	43
Tab. 7 Components of nutrition media used during electroporation.	44
Tab. 8 Mixture for PCR screening	45
Tab. 9 Cycling parameters for PCR screening.....	46
Tab. 10 Mixtures for Bgl II digestion	48
Tab. 11 Required components for expression screening.....	50
Tab. 12 Preparation of sample for SDS-PAGE	51
Tab. 13 Components of Coomassie staining	52
Tab. 14 Components and equipment for large scale expression	56
Tab. 15 Equipment and used solutions for MCAC	58
Tab. 16 Summarized setting for all CD measurements.....	66
Tab. 17 Components of iodination activity assay	67
Tab. 18 Components of MCD bromination activity assay.....	68
Tab. 19 Components of MCD chlorination activity assay	69
Tab. 20 Mixture of the ABTS activity assay.	70
Tab. 21 Mixture of the guaiacol activity assay	71
Tab. 22 Mixture of the tyrosine activity assay	71
Tab. 23 Adjustments in the FL Solutions F-7000 software.....	72
Tab. 24 Amino acid composition of peroxidases.....	86
Tab. 25 Summary of the calculated and predicted protein parameters.	86
Tab. 26 Colony count of incubated LB-agar _{Amp} plates after electroporation.	88
Tab. 27 Contents of secondary structure based on CD spectroscopy.....	97
Tab. 28 Specific iodination activities	100
Tab. 29 Specific bromination activities.....	102
Tab. 30 Specific chlorination activities	103
Tab. 31 Specific ABTS activities.....	105
Tab. 32 Specific guaiacol activities	106
Tab. 33 Specific tyrosine activities.....	107
Tab. 34 Δ Absorption and CN ⁻ concentrations PCC 8106.....	109
Tab. 35 Δ Absorption and CN ⁻ concentrations PCC 7420	112

1. Introduction

Inflammation is the response of vascularized tissue damage. It is a complex response set in motion in any human tissue by virtually any injury due to any cause. It is an attempt to restore homeostasis. In the early history of *Homo sapiens*, when life spans were relatively short and our ancestors were likely to die from infectious disease and trauma, the ability to fight off pathogens and heal wounds was even more critical for the survival of the species than it is today. The inflammatory response is still critical for these purposes. However, now that we are living longer, we have come to realize that inflammation is a double-edged sword. The same inflammatory processes that are so effective at clearing pathogens and repairing damaged skin are the cause of most human pathology today. Atherosclerosis, autoimmune disease, pulmonary fibrosis, asthma and many other common human afflictions are all conditions that result when the inflammatory response is uncontrolled, self-directed, or in the wrong place at the wrong time. These conditions generally affect humans past the traditional breeding age and thus these untoward aspects of inflammation were not selected out during evolution. As a result, there is now far more effort to develop potent anti-inflammatory therapies than there is to develop treatments to boost the inflammatory response [1]

Part of this innate host defense system, are heme peroxidases, iron-containing oxidoreductases. The most common representatives of these metalloproteins, which participate in human host defense, are myeloperoxidase (MPO), eosinophil peroxidase (EPO), lactoperoxidase (LPO) and thyroid peroxidase (TPO)¹. Because of this physiological importance the functionality of mammalian peroxidases is investigated since nearly a century.

1.1 Heme peroxidases superfamily

Although non heme peroxidases, for example, thiol peroxidases represented by thioredoxins, peroxiredoxins, and glutathione peroxidases are widespread in both prokaryotes and eukaryotes, the most abundant peroxidases in all living forms are probably those containing the prosthetic heme group [7]. This work is focused entirely on the heme peroxidases. The majority of currently known heme peroxidases are members of two superfamilies that are ubiquitous in all kingdoms

¹ Responsible for the iodination reaction of the thyroid gland hormones thyroxine (T₄) and triiodthyronine (T₃).

of life. Both superfamilies arose independently, thus their primary structure and tertiary structures and even the nature of prosthetic group differ greatly [7].

The two superfamilies, are the peroxidase-cyclooxygenase (formerly: animal peroxidases) and the peroxidase-catalase superfamily (formerly: non-animal or bacterial, fungal and plant peroxidases). Additionally in three families (DyP-type², heme-haloperoxidases and di-haem peroxidases), are found [8].

This work is focusing on peroxidases of the peroxidase-cyclooxygenase superfamily, which is divided into seven distinct subfamilies that diverged from a common ancestor. Figure 1 shows the phylogenetic tree of the peroxidase-cyclooxygenase superfamily, containing the 7 subfamilies.

All gene sequences used in this work, were collected from public databases (Uniprot, NCBI and Peroxibase). In the Peroxibase the intron splicing of eukaryotic genomic sequences is already taken into account and consequently the current 475 sequences (April 2011), of the peroxidase-cyclooxygenase superfamily, formed the basis for the subsequent analysis according to Zamocky M. et al. [7]

² dye decolorizing peroxidase

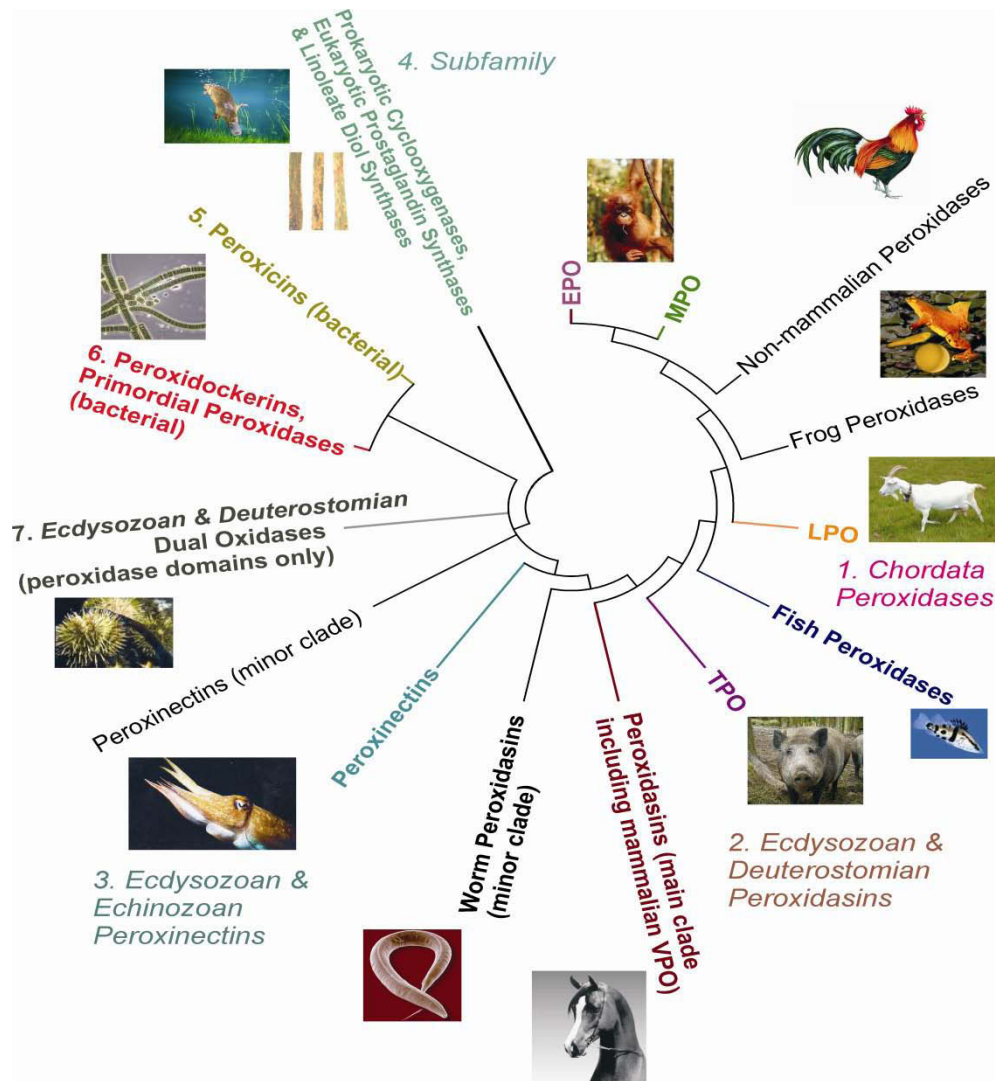


Figure 1. The seven subfamilies of the peroxidase-cyclooxygenase superfamily. 1. Chordata peroxidases 2. Ecdysozoan & Deuterostomian peroxidases 3. Ecdysozoan & Echinozoan peroxinectins 4. Prokaryotic cyclooxygenases and prostaglandin synthases 5. Peroxicins 6. Peroxidockerins, primordial peroxidases 7. Ecdysozoan & Deuterostomian dual oxidases. Zamocky M. et al. [7]

The subfamily of chordata peroxidases is represented by mammalian peroxidases like MPOs, EPOs and LPOs. For example some bird peroxidases are closely related to the LPO branch. The primary translation product of these enzymes contains a signal peptide, a propeptide, and a peroxidase domain, shown in Figure 2 (A). From mammalian MPO, EPO, and LPO it is known that in mature soluble proteins both the signal and the propeptide has been removed by proteolytic processing. Clearly segregated from the now described main clades are frog peroxidases, with having been reported to possess a ribonuclease activity, and the branch of fish peroxidases. A well resolved clade, distantly related with MPO, EPO, and LPO, contains enzymes homologous to mammalian TPOs. Here interestingly related enzymes from

invertebrates are found, which are well separated from mammalian membrane-anchored proteins that are known to be expressed and function in thyroid glands. At the origin of subfamily of chordata peroxidases a marine ancestor of vertebrates is found, which is the closest phylogenetic neighbor of peroxidasins but does not contain the immunoglobulin motif of this subfamily (Fig. 2 (B)) [7].

The second subfamily is represented by peroxidasins. Peroxidasins are found in invertebrates and vertebrates including mammals. The first peroxidasin was found in *Drosophila* and was described as a protein combining peroxidase and extracellular matrix motifs. The multidomain proteins contain a signal peptide, several leucine-rich regions, followed by immunoglobulin-like domains, a linking region, the peroxidase domain, and a C-terminal Willebrand type C protein interaction domain (Fig. 2 (B)). The peroxidase domains of peroxidasins are well separated from other subfamilies. The profile of phylogenetic tree suggest that vertebrate peroxidases probably evolved from a primitive peroxidasin ancestor by duplication of the peroxidase domain and loss of the residual protein part containing the leucine-rich and immunoglobulin-like motifs [7].

The third subfamily is formed by peroxinectins of predominantly *Ecdyzoan* origin. The first peroxinectin was detected in crayfish blood in 1988 and described as a cell adhesion molecule with a peroxidase domain and an integrin-binding motif (Fig. 2 (C)). Two main peroxinectin clades are discernible namely arthropod and worm peroxinectins. So far, no sequences from vertebrate's peroxinectins are known suggesting that this evolutionary line represents an impasse of evolution. Among *Deuterostomia* only a minor subclade of *Echinozoa* peroxinectins exists, but this group is very distantly related with any known sequence of vertebrate peroxidases of this superfamily. In invertebrate genomes, duplicated or multiplied variants of peroxinectin genes are found most probably as a result of repeated gene duplication [7].

The fourth subfamily is comprised of cyclooxygenases. This subfamily and the fifth subfamily diverged from each other very early in history of the peroxidase-cyclooxygenase superfamily representing one of the major streams of evolution. The primary translation product of cyclooxygenases consists of an N-terminal signal peptide followed by an epidermal growth factor domain, a membrane-binding domain and the globular catalytic peroxidase domain (Fig. 2 (D)). The cyclooxygenase genes evolved partially as paralogs in vertebrates that fulfill different physiological roles. The subfamily of cyclooxygenases is divided into two main clades. One clade is containing human paralogs that are directly connected with putative bacterial cyclooxygenases; the second clade is spread mainly among plant and fungal gnomes [7].

The fifth clade is represented by bacterial peroxicins that were formed early in the evolution as a distinct clade. A high portion of currently known members is formed by extremely long pseudo genes (up to 3300 amino acids), where the peroxidase domain or at least some motifs can be repeated several time. This is probably a relic of imperfect gene duplication(s) and intensive mutations. Moreover, these large fusion proteins contain hemolysin-type toxin and Ca^{2+} -binding motifs (Fig. 2 (E)) that could indicate a role in defense of bacteria possessing this multidomain protein against other bacteria of the same environment that lack such a gene. Thus in analogy with bacteriocins, that are proteinaceous toxins produced by bacteria to inhibit the growth of similar or closely related strains. None of the fifth subfamily members has an experimentally verified physiological function.

The sixth clade is represented by peroxidockerins of mixed origin. These multidomain proteins are composed of a transmembrane domain, a sequence motif characteristic for planctomycete extracellular proteins, two dockerin type I repeats and the peroxidase domain (Fig. 2 (F)). Obvious gene transfers are revealed in the peculiar distribution of clades in this subfamily with closest neighborhood to prokaryotic and eukaryotic peroxidase genes. This could indicate either a lateral gene transfer or an endosymbiotic event. The physiological function remains to be elucidated [7]. The subfamily of peroxidockerins is of closer interest for this work. Each of two cyanobacterial organisms *Microcoleus chthonoplastes* (PCC³ 7420) and *Lyngbya sp.* (PCC 8106), possess a peroxidase sequence in the genome with high similarities to mammalian peroxidases. Especially the presumably for peroxidases essential amino acids in the active site are almost identical, which is remarkable, because the peroxidockerin subfamily is, according to Figure 1, at the origin of the peroxidase-cyclooxygenase superfamily. Consequently these two completely unknown peroxidases lend themselves to investigate their functional features compared to the well known mammalian peroxidases.

The seventh and last subfamily is formed by eukaryotic dual oxidases. Dual oxidases are multidomain proteins with an N-terminal peroxidase domain linked with a C-terminal reductase domain by a cytoplasmatic bridge with two EF hands (Fig. 2 (G)). The peroxidase domains of dual oxidases were segregated early in the evolution of this superfamily and were further differentiated within this subfamily. [7]

Figure 2 shows a schematic view of the now described domain structures of the 7 subfamilies.

³ Pasteur Culture Collection

(A) **Chordata peroxidases:** Lactoperoxidase from *Homo sapiens*; HsLPO 712aa



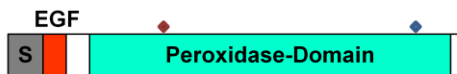
(B) **Peroxidasins:** Peroxidasin from *Homo sapiens*; HsPxd01 1479 aa



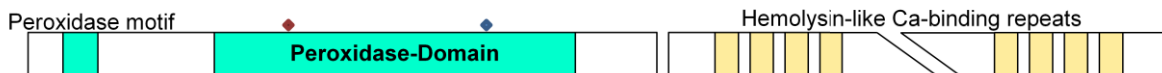
(C) **Peroxiectins:** Peroxiectin-Ovoperoxidase from *Hemicentrotus pulcherrimus* (sea urchin); HpuPxt01 814 aa



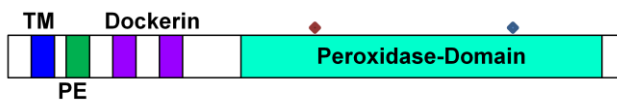
(D) **Cyclooxygenases:** Prostaglandin-Endoperoxide Synthase 1 (*Homo sapiens*); HsPGHS01 599 aa



(E) **Bacterial Peroxins:** Peroxin from *Mesorhizobium sp.*; MspPxc01 2950 aa



(F) **Bacterial Peroxidockerins:** Peroxidockerin from *Rhodospirellula baltica*; RbaPxDo01 779 aa



(G) **Dual oxidases:** Dual oxidase from *Lytechinus variegatus* (green sea urchin); LyaDuOx01 1625 aa

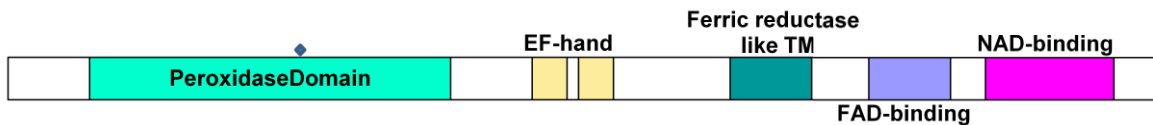


Figure 2. Schematic view of the domain structures of seven typical representatives of the peroxidase-cyclooxygenase superfamily. Abbreviations: S, signal peptide; PP, propeptide; LRR, leucine-rich repeats; I-Set, immunoglobulin I-set domain; VWC, von Willebrand factor type C domain; IBM, integrin-binding motif; EGF, epidermal growth factor like domain; TM, transmembrane helices; PE, planctomycete extracellular motif; EF-hand, EF-hand calcium binding domain; The red rhombus indicates position of distal and the blue rhombus of proximal histidine. Zamocky et al [7].

1.2 *Microcoleus chthonoplastes* (PCC 7420) and *Lyngbya sp.* (PCC 8106)

As mentioned above a comprehensive amino acid sequence alignment done by M. Zamocky revealed a remarkable result. Two peroxidase sequences labeled in Figure 3 showed high similarities to the mammalian peroxidases LPO, EPO, and MPO; furthermore these two sequences are at the phylogenetic origin of the peroxidockerin subfamily.

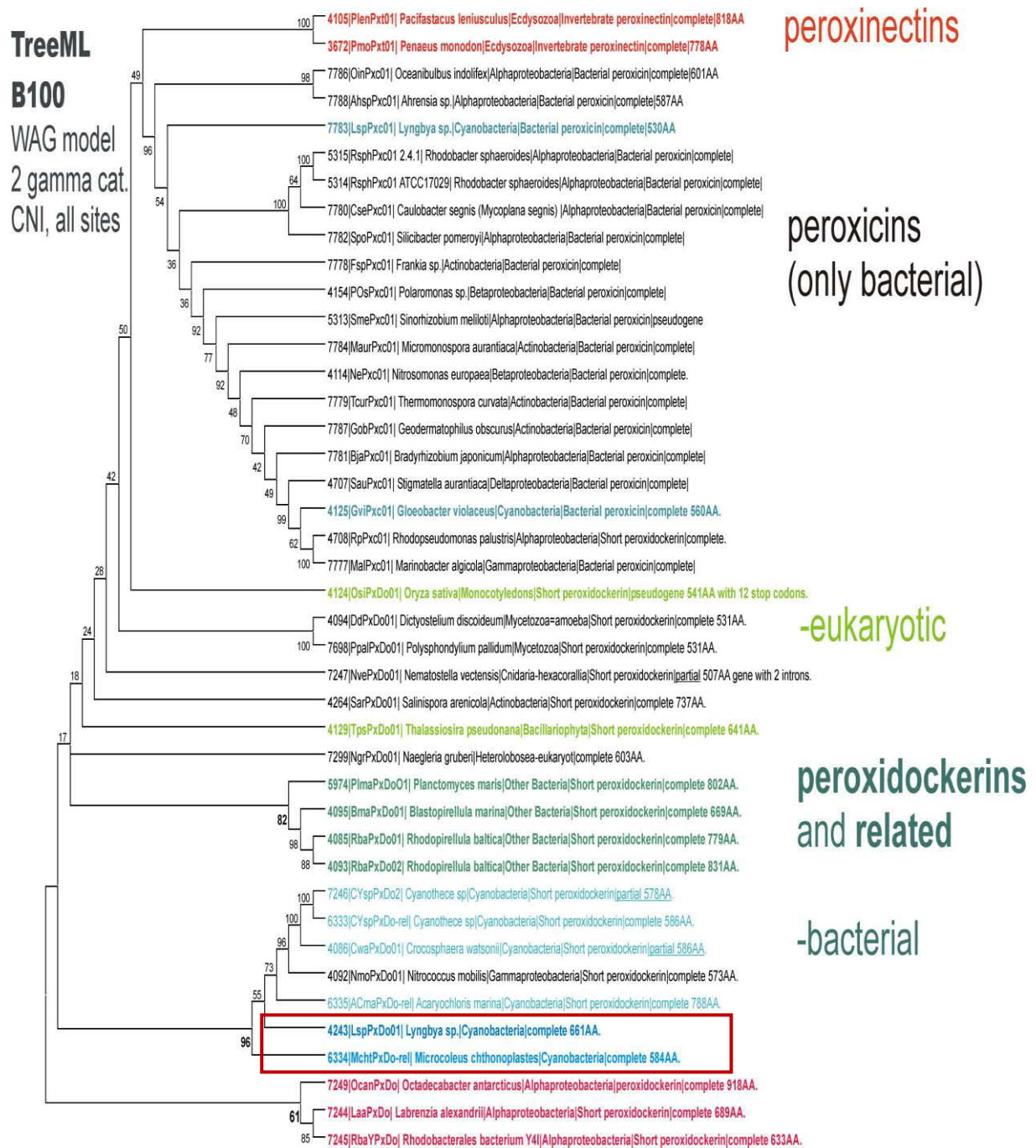


Figure 3. Enlargement of the phylogenetic origin of the cyclooxygenase-peroxidase superfamily; labeled are the two peroxidockerin sequences of *Lyngbya* sp. and *M. chthonoplastes*.

The two peroxidase sequences originate from the two cyanobacterial strains *Microcoleus chthonoplastes* (PCC 7420) and *Lyngbya* sp. (PCC 8106). Cyanobacteria exist probably for more than 3.5 billion years on this earth, thus being actually one of the oldest life forms. Their ability to perform oxygenic photosynthesis is thought to have converted the early reducing atmosphere into an oxidizing one, which dramatically changed the composition of life forms on earth. Cyanobacteria can be found in almost every conceivable environment, from oceans to

fresh water to bare rock to soil. Figure 4 shows where the two organisms *Microcoleus chthonoplastes* (PCC 7420) and *Lyngbya sp.* (PCC 8106) were isolated.

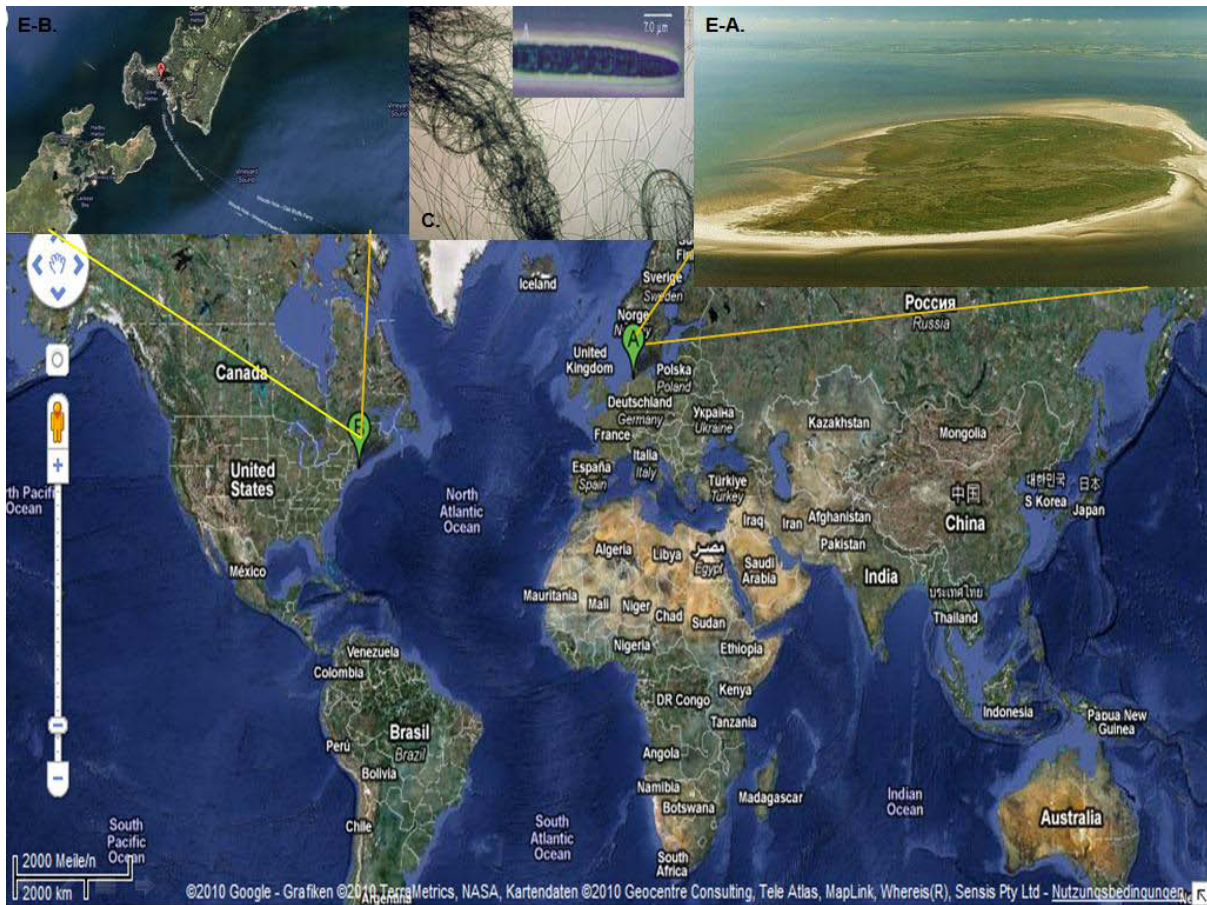


Figure 4. Overview of the habitat of the two cyanobacteria A. Mellum, North sea, Germany; E-A is an aerial photo of the island Mellum location of *Lyngbya sp.* (PCC8106) ; B Woods Hole, Massachusetts; E-B is an enlargement performed via Google maps of the location of *Microcoleus chthonoplastes* (PCC 7420) ; C shows a 40- and 100-fold enlargement of *Microcoleus chthonoplastes*

Both organisms were isolated from cyanobacterial mats, which are benthic prokaryotic communities that are commonly found in coastal environments such as salt marshes, sand flats, or mangroves. Due to grazing by benthic invertebrates and the unstable environment, they are frequently destroyed and do not mature into thick mats in these places [24]. Under more extreme conditions created by high temperature or salinity, high sulfide concentrations, or extreme pH, the mats may sometimes accrete over many years in a seasonal growth pattern. The thick laminated mats or stromatolites which are thereby formed are found today only in scattered environments such as hypersaline lakes and lagoons, hot springs, and sulfur springs. The cyanobacterial mats are characterized by a high primary productivity and rapid recycling of organic matter. Cyanobacteria, which are usually the dominant mat forming organisms, are oxygenic phototrophs. Yet, many strains have the ability to perform anoxygenic photosynthesis with H_2S (or HS^- when solved in water) as an electron donor. Many cyanobacteria can switch totally or partly from a normal green plant-type oxygenic photosynthesis to a bacterial-type

anoxic photosynthesis when the ambient sulfide concentration becomes sufficiently high. Especially for a *Microcoleus chthonoplastes* strain this was observed by B. B. Jørgensen et al [24]. The transition from a sulfide- to an oxygen-dominated environment, which in modern mats can take place through a diurnal cycle, must have occurred as part of the early evolution of the biosphere [24].

Large areas of the upper intertidal of the southern part of the North Sea are covered by mats of cyanobacteria. From these colored, laminated ecosystems the Pasteur culture collection has isolated *Lyngbya sp. (PCC 8106)*. The mats consist of several vertically stratified microbial communities. Under a thin layer of white fine-sand, a 1 mm to 2 mm thick mat of cyanobacteria exists. Sometimes a pink layer of phototrophic purple sulfur bacteria develops directly underneath the cyanobacterial mat, followed by a black zone of sulfate reducing bacteria. Presumably, the cyanobacteria account for most, if not all, of the input of organic carbon in these mat sediments. In view of the very dense populations of cyanobacteria and the fact that seawater usually contains very low amounts of combined nitrogen, nitrogen fixation should play a key role in the development of such mats. Nitrogenase, the enzyme responsible for nitrogen fixation, is very sensitive to molecular oxygen. Therefore cyanobacteria, as aerobic and oxygenic phototrophic organisms, need mechanisms to protect this enzyme against oxygen. Thus far it has generally been accepted that only those cyanobacteria able to form specialized cells, called heterocysts, are able to maintain nitrogenase activity in an aerobic environment [23.] In accordance to the respective data sheet of the Pasteur Culture Collection *Lyngbya sp. (PCC 8106)* shows N₂ fixation only under anaerobic conditions.

Microcoleus chthonoplastes (PCC 7420) was affiliated into Pasteur Culture collection 1974 from Woods Hole Woods, Massachusetts, USA from a salt marsh in the coastal region. The species is easily recognizable by its occurrence in bundles of trichomes, enveloped by a common polysaccharide sheath, although this property may be lost in culture, which has sometimes led to the misidentification of cultured isolates of similar morphological opportunists. Fixation of atmospheric dinitrogen is a property of all cyanobacterial mats that have been investigated so far, however various pure culture studies with different true *M. chthonoplastes* strains did not reveal nitrogenase activity, even under strictly anaerobic conditions [22].

1.3 Human peroxidases myeloperoxidase, lactoperoxidase, and eosinophil peroxidase

The aim of this work was to compare the mammalian peroxidases with the two already mentioned cyanobacterial peroxidases. For this purpose the three major mammalian peroxidases myeloperoxidase (MPO), eosinophil peroxidase (EPO), and lactoperoxidase (LPO) are described shortly below.

Myeloperoxidase (MPO)

Myeloperoxidase is a key component of the antimicrobial armory of neutrophilic polymorphonuclear leukocytes (neutrophils), the major effector cells of the innate immune system. These cells provide the front line of defense against invading microbes and are primed to generate or to release a battery of materials that enable the rapid killing of such species. This is accomplished by engulfing and ingestion of foreign organisms. A phagolysosomal compartment is formed into which materials stored in intracellular granules of the neutrophils are released. Figure 5 shows a schematic view of the even described lysis of invading microbes.

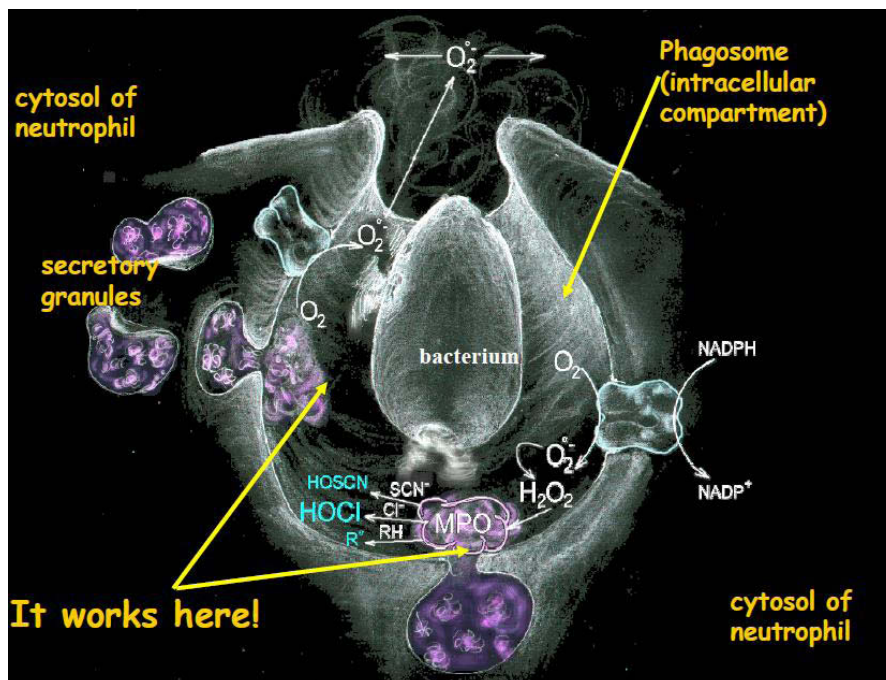


Figure 5. The picture shows schematically the release of MPO into the phagosome, the formation of H₂O₂ by NADPH-oxidase and the main antimicrobial agents.

Neutrophils possess at least three types of intracellular granules [9]. Cytochemical studies dating back to the early 1900s suggested already the presence of a peroxidase in the cytoplasmic granules of mature granulocytes, and subsequent studies indicated its presence entirely in the azurophilic (primary) granules of these cells [5]. The other two major forms of granules do not appear to contain significant peroxidase activity. The lysosomes-like azurophilic granules contain multiple components including serine proteases, lysosomal hydrolases, and MPO [9]. The intensely green iron containing protein was then originally isolated from canine pus and purulent fluid of patients with tuberculous empyema [6]. MPO is present in human neutrophils, at concentrations no less than 1-2% of the dry weight of the cells [5]. The granule proteins are tightly packed inside the granule and are associated with a matrix-like material consisting of polyanionic glycosaminoglycans. The highly cationic granule proteins are believed to bind to this matrix material in a conformation or state that renders them inactive [9]. During neutrophil activation a degranulation process starts. The membrane of the cytoplasmic granules fuse with that of the developing phagosome, the common membrane then ruptures, and the contents, including MPO, of the granules are discharged with great force into the phagosome [5]. Most of the MPO remains within the phagosome but the enzyme can also be released extracellularly by leakage before complete closure of the developing phagosome or in response to stimulation by an antibody/complement coated surface too large to be ingested. Coincident with the segregation of the azurophilic granules into the phagolysosomal compartment, an NADPH oxidase is assembled on the internal membrane surface, with this acting as a source of superoxide radicals ($O_2^{\cdot-}$) and because of subsequent spontaneous or catalyzed dismutation of $O_2^{\cdot-}$ to hydrogen peroxide (H_2O_2). H_2O_2 is an essential cofactor for the functionality of peroxidases [4]. MPO is a strongly basic protein with an isoelectric point of 9.16⁴ and thus binds avidly to negatively charged surfaces like biological membranes. MPO, when released, can be inactivated by products of the respiratory burst or be cleared from the extracellular fluid by uptake by macrophages through reaction with a mannose receptor. Further, the uptake of microorganisms coated with extracellularly released MPO or EPO may arm the macrophages, resulting in an associated increased destruction of the ingested organisms [4].

MPO synthesis is initiated in the promyelocyte stage of neutrophil development and terminates at the beginning of the myelocyte stage, at which time the MPO-containing azurophilic granules are distributed to daughter cells, where they intermingle with the newly formed peroxidase negative, specific (secondary) granules. The MPO containing granules in the mature human neutrophils are heterogeneously by density and morphology [5]. In addition to the synthesis of MPO by promyelocytes that become neutrophils, monocyte precursor cells also synthesize this

⁴ Computed with ExPASy ProtParam tool for 1CXP (PDB accession code) Myeloperoxidase amino acid sequence

enzyme during their maturation in the bone marrow. This synthesis usually ceases after this stage of cell development, so circulating monocytes do not actively synthesize the enzyme. The subsequent maturation of monocyte cells within tissues into macrophages is likewise associated with a loss of MPO, thus fully matured macrophages contain little or no active enzyme. A re-initiation of MPO synthesis may occur in macrophages under some circumstances and may give rise to the significant amounts of MPO detected extracellularly in atherosclerotic lesions [9, 10, 11]. MPO is a cationic 146 kDa with a single disulfide bridge between symmetric-related halves (73 kDa), each of which contains two polypeptides of 14.5 and 58.5 kDa, the latter being glycosylated. The small polypeptide is composed of 106 and the large of 467 amino acids. Additionally there are five intra-chain disulfides in the large polypeptide and one in the small [12]. Figure 6 shows a schematic view of MPO.

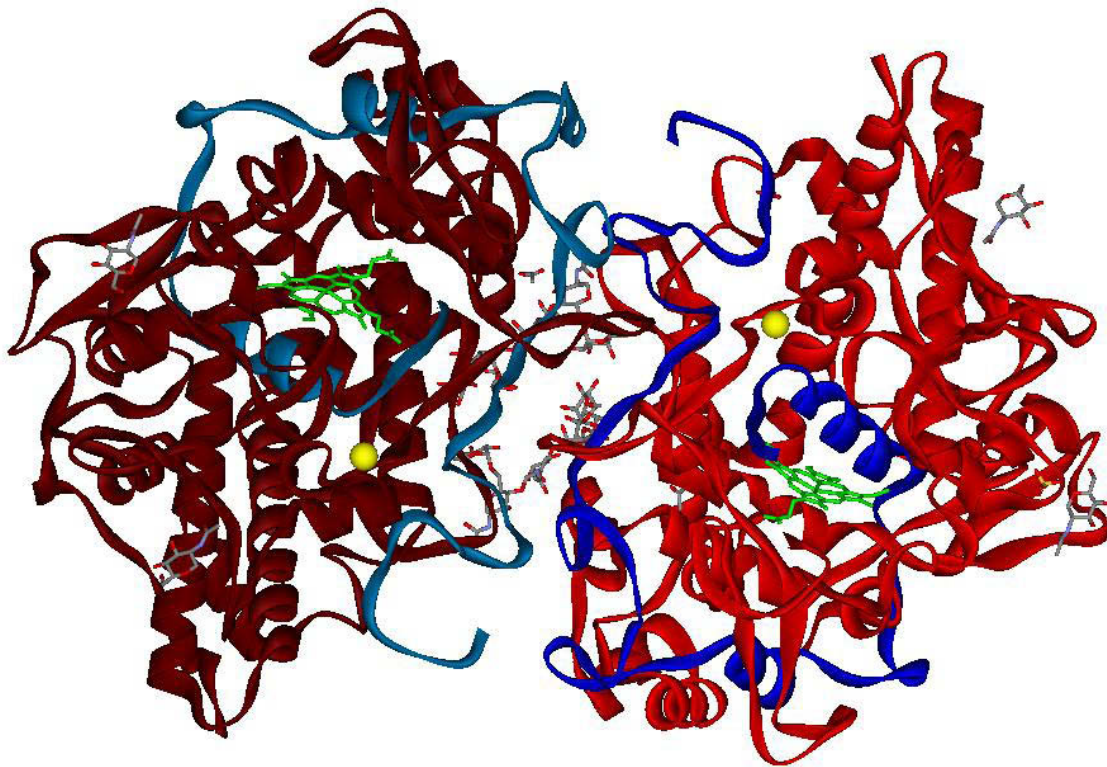


Figure 6 Schematic view of the structure of mature homodimeric human MPO. Protein Data Base (PDB) accession code 1CXP. Each subunit is composed of a light chain (blue) and a heavy chain (red) and contains one modified heme group (green). In addition the calcium ions (yellow spheres) and the glycosylation sites are shown, particularly rich along the dyad interface. This Figure was constructed with the PDB ViewerLite50.

Eosinophil peroxidase (EPO)

EPO is the major granule protein of eosinophils, which are specialized human phagocytic cells that eliminate parasites and related organisms. Eosinophilic refers to the staining with the fluorescent red dye eosin, which is an acidic dye, thus, the structure being stained is basic. In

contrast to the neutrophils, which phagocytose their target organism and subsequently release MPO primarily into the phagolysosomal compartment, eosinophils are forced by the larger size of their parasitic targets to exocytose their granule contents onto the parasite surface to which they are attached [9]. Consequently eosinophils are specialized human phagocytes that play a critical beneficial role to eliminate tissue-invasive parasites. The predominant components of the eosinophils-specific granule are in order of relative abundance, eosinophil peroxidase (EPO) 40%, major basic protein, eosinophil cationic protein, and eosinophil derived neurotoxin. These granule proteins share in common a pronounced cationicity ($pI \sim 10$) that endows them, especially major basic protein, with membrane-perturbant properties that disrupt lipid bilayers and thereby mediate nonspecific cytotoxicity. Given the unusually robust eosinophil NADPH oxidase system that generates 3-10 as much superoxide anion and H_2O_2 as neutrophils, the EPO/ H_2O_2 system has formidable oxidant generating, and therefore cytotoxic, potential [3]. The primary translation product of human eosinophil peroxidase is a protein of 715 amino acids. EPO is a highly cationic glycoprotein that is synthesized as a 80 kDa single chain precursor that undergoes also proteolytic processing during intracellular transport to originate the mature protein, a 69.8 kDa monomer composed of a 57.9 kDa heavy chain and a 11.9 kDa light chain resembling the arrangement of MPO monomer [12]. EPO shares a 70% amino acid homology with MPO [9].

Lactoperoxidase (LPO)

In contrast to the EPO and MPO human lactoperoxidase is secreted by certain glands, like mammary, salivary, and lachrymal glands. As a consequence peroxidase activity is found in human exocrine secretions including tears, milk, and saliva as well as vaginal fluid. Salivary lactoperoxidase is often referred as an important part of mucosal innate defense system. This is supported by observation that hLPO is secreted already at the early childhood, i.e. at similar levels to adults. In contrast, hMPO is present in whole saliva at very low levels before all teeth are fully erupted allowing leakage of polymorphonuclear leukocytes into the oral milieu. Figure 7 shows a schematic view of bovine LPO.

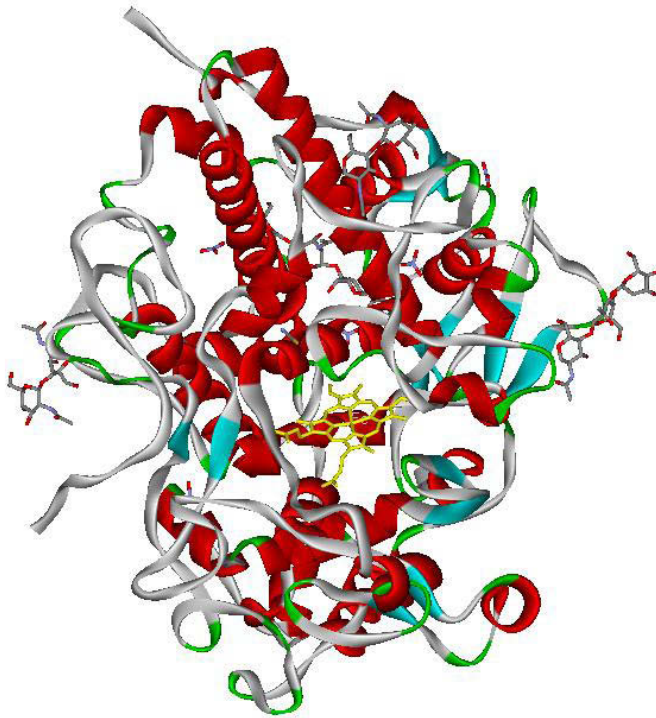


Figure 7. Schematic view of bovine LPO. PDB accession code 3BXI. α -helices are pictured red, β -sheets light blue. Also glycosylation sites and the heme group (labeled yellow) are shown. This Figure was constructed with the PDB ViewerLite50.

By incubating saliva with enamel powder, it has been detected that peroxidases are capable of binding irreversible to human dental enamel in an enzymatic active conformation. In vitro peroxidase-mediated reactions, assessed by consumption of H_2O_2 , are even enhanced on dental enamel surfaces compared to human whole saliva. Peroxidase activity has been detected also in dental plaque and in salivary pellicles formed on denture based materials [2]. Lactoperoxidase also provide an antimicrobial system in milk and vaginal fluid. Thereby microorganisms like lactobacilli, which generate large amounts of H_2O_2 , support the activity against microorganisms that do not produce H_2O_2 themselves [5].

The gene which is coded for the 78.5 kDa hLPO monomer is located on human chromosome 17. The gene for LPO is orientated tail to tail with the hMPO gene and they are only separated with only 2.5 kb. Together with the hEPO gene, these peroxidases form a gene cluster spanning a region of 90 kb. In addition, the three peroxidases have very similar intron exon structure, suggesting that the genes have arisen from the amplification of a common ancestral gene in the locus. No similarity has been found in the promoter region of hLPO and the other peroxidases, which is in accordance to the different expression patterns of these proteins. On the amino acid level hLPO gene product shares about 51% homology with the two other human peroxidases MPO and EPO, while the homology with thyroid peroxidase is only 41% [2, 32]. Bovine LPO and human LPO exhibit a similarity of 83% at the amino acid level [32].

Cyanobacterial Peroxidases

As mentioned before the physiological function of the two cyanobacterial peroxidases from *Microcoleus chthonoplastes* (PCC 7420) and *Lyngbya sp.* (PCC 8106) remains to be elucidated. Both organisms live in coastal areas (cp. section 1.3), thus they are forced with completely other environmental conditions than for example humans at least at cellular levels. It is obvious that the defense against foreign organisms, which could be accomplished by an efficient peroxidase system, is a helpful feature for a life form in evolution. But in contrast to humans, cyanobacteria are able to produce oxygen by means of photosynthesis; hence the cyanobacterial peroxidases could be a part of the scavenging system for reactive oxygen species like H_2O_2 and $\text{O}_2^{\bullet-}$.

According to Peroxibase the peroxidase of the strain PCC 7420 is composed of 584 amino acids, whereas the PCC 8106 peroxidase shows a length of 661 aa. Despite the two cyanobacterial peroxidases sequences are members of the peroxidockerin family, both lack in characteristically domains like transmembrane helices, planctomycete extracellular motifs, or dockerins. A posttranslational processing of the two enzymes is not described till yet.

1.4 Active site of mammalian peroxidases

The common feature of all heme peroxidases is that their active sites contain very similar prosthetic groups. For nearly all known plant peroxidases and catalase-peroxidases the prosthetic group is a ferri-protoporphyrin IX shown in Figure 8. Ferri-protoporphyrin IX is made up of four pyrrole rings joined by methene bridges with iron (III) centering the molecule.

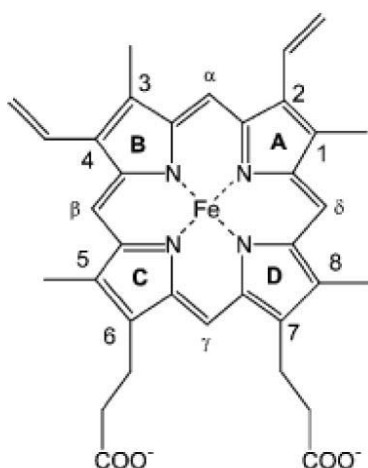


Figure 8. Ferri-Protoporphyrin IX

Two hydrogen atoms attached to pyrrole nitrogens have been displaced by the iron. Therefore the net charge on the heme with a four coordinated iron (III) is +1. There are eight side chains in ferri-protoporphyrin IX as follows: Four methyl groups (position 1, 3, 5 and 8), two vinyl groups (2 and 4) and two propionate groups (6 and 7). The carbon atoms of the methene bridges are labeled α , β , γ and δ . In peroxidases the iron is coordinated to the four pyrrole nitrogen atoms; the fifth coordination position is located on the *proximal* side of the heme and is occupied by the imidazole side-chain of a histidine residue. The sixth coordination position in the resting enzyme is occupied by a weakly bound water molecule (high spin state, $S = 5/2$) and is generally called the *distal* side of the heme [29].

In the following section the amino acids known as essential for mammalian peroxidases in the heme surrounding area are described in detail. Results of Zamocky's [7] work showed a high homology between the two above mentioned cyanobacterial peroxidases and the mammalian peroxidases. Due to the unknown structure of peroxidockerin peroxidases, the active site residues are explained on the basis of the well known structure of MPO and LPO.

The heme group in MPO is a derivative of protoporphyrin IX in which the methyl groups on pyrrole rings A and C have been modified in hydroxymethyl groups to allow formation of ester linkages with the carboxyl groups of Glu242 of the heavy and Asp94 of the light polypeptide. In addition the β -carbon of the vinyl group on pyrrole ring A forms a covalent bond with the sulfur atom of Met243. Due to this linkage the heme porphyrin ring is considerably distorted from planarity [12]. The heme to protein linkages are described in detail by Zederbauer et al. [28]. The heme group is located at the bottom of a deep crevice which hinders access of most compounds to the iron atom, with this being restricted to H_2O_2 and small anions. [27]

Figure 9 A shows the prosthetic heme group and important amino acids in the active site including the calcium binding site of bovine lactoperoxidase (Protein Data Bank accession-code 3XBI). In Figure 9 B the MPO unique Met-linkage and the consequential distortion of the heme group is pictured. Exactly the same residues are in LPO, EPO and MPO responsible for calcium binding (not shown in Figure 9 B).

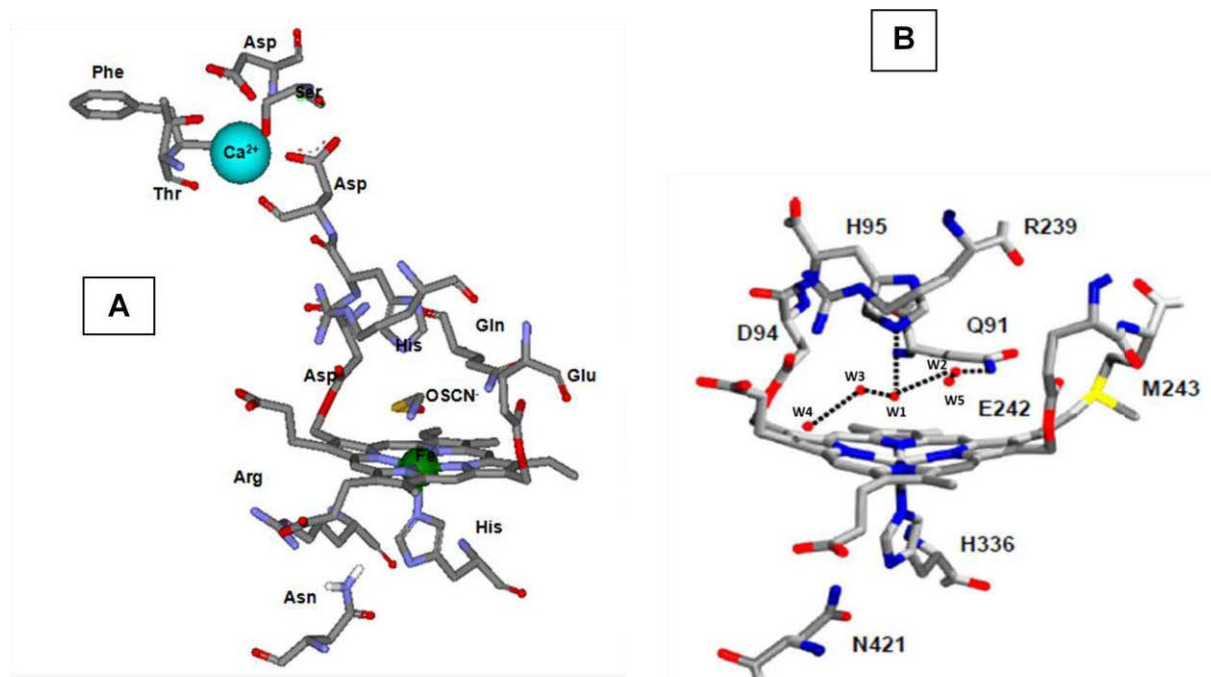


Figure 9. Active site residues of (A) bovine LPO and (B) human MPO. The Figures were constructed using the coordinates deposited in the Protein Data Bank; accession code for (A) 3XBI and for (B) 1CXB. Figure A shows additionally the involved residues in calcium binding site and the position of the substrate OSCN. Figure B pictures the distortion of the heme group by the additive Met234-heme linkage and accessory the positions of 5 water molecules (W1-W5) completing the hydrogen bond chain in the distal cavity of MPO.

Beside the essential residues for the covalent heme-protein linkage (Asp-5-hydroxymethyl group ring C and Glu-1-hydroxymethyl group pyrrole ring A) there are further highly conserved amino acids in the active site of mammalian heme peroxidases. At first on the distal side of the heme there is a glutamine (Gln, Q) found (in Figure B labeled as Q91), which is involved in maintenance of the distal hydrogen bond network and in halide binding. The glutamine is usually not found in the distal cavity of the (archaeal) bacterial, fungal and plant heme peroxidase superfamily [7].

In mammalian peroxidases the highly conserved motive “D-H-D” is found. In addition to the already described aspartate (Asp94 MPO numbering) which is involved in the ester bond formation between heme group and protein, this motif includes the distal histidine (His95

according Figure 9 B) and the calcium ligand aspartate (Asp96 MPO numbering) [7]. The distal arginine supports the distal histidine in its catalytic function; both have critical roles in the binding/orientation/activation of H_2O_2 in the distal pocket. The distal heme cavity is occupied by the side chains of Gln91, His95, and Arg239 (all MPO numbering), together with five water molecules (W1–W5; shown in fig 9 B). Each of these three side chains is hydrogen bonded to a distinct water molecule, whereas a fourth water molecule is hydrogen bonded to the heme pyrrole ring C propionate. Additional hydrogen bonding occurs between these water molecules (Figure 9 B). The fifth water molecule (W5) is hydrogen bonded to W2 and possibly also weakly to W3. The distal His95 is hydrogen bonded to W1, which is positioned approximately mid-way between its N_ϵ and the heme iron [27]. In MPO the N_δ of His95 is hydrogen bonded to a buried water molecule, which is linked by His250 to a succession of four additional buried water molecules forming a chain of hydrogen bonds leading to the surface of the protein. Such a chain could presumably also function to conduct protons away from the distal histidine and thereby ensure that the N_ϵ is free to accept a proton from peroxide [27].

The distal histidine's nearby aspartate (D96 in MPO; shown in Figure 9 A) act as ligand for calcium binding together with a highly conserved loop of eight residues (Leu-Thr-Ser-Phe-Val-Asp-Ala-Ser)[7]. The calcium ion has typical pentagonal bipyramidal coordination to the ligands. The hydroxyl oxygen of the serine and the peptide carbonyl oxygen of the phenylalanine provide the axial ligands, whereas the other five ligands (Asp carboxyl oxygen and peptide carbonyl oxygen, Thr hydroxyl and peptide carbonyl oxygen, and Asp carboxyl oxygen) are arranged approximately co-planar. The ligands in the calcium binding site are shown in Figure 9 A [12].

In heme enzymes belonging to the peroxidase-cyclooxygenase superfamily the proximal histidine is in close interaction with a fully conserved asparagine (Figures 9 A and 9 B). Carpena et al. describe that in mammalian peroxidases the NH_2 group of the asparagine (Asn421 MPO numbering) is orientated toward the unprotonated N^δ of the proximal histidine, whereas its carbonyl group interacts with the positively charged guanidinium group of arginine (Arg333 unembodied in Figure 9 B). The deprotonated anionic histidine strengthens the iron-imidazole bond, and in addition it stabilizes higher oxidation states, an effect that is very important especially in MPO because it is known to form transiently catalytically active redox intermediates with very positive reduction potentials. Carpena et al. show the importance of the close His-Asn-Arg interaction in maintenance of proximal and distal heme cavity architecture, and of the redox properties, by means of a MPO mutant (Asn421Asp). Both halogenation and peroxidase activity were significantly decreased because of this mutation. [13].

1.5 Reaction pathways of peroxidases

Due to stopped-flow measurements performed in this work the different reaction pathways of heme peroxidases are described subsequently. Figure 10 shows the general reaction scheme of human peroxidases. The formation of each Compound comes along with a shift or/and decay of characteristic absorption maxima. These spectral changes enable a detailed analysis of Compound formation kinetics and resemble from heme enzyme to heme enzyme. The main effects of Compound formation are described in detail by Furtmüller et al. [12]. In the subsequent chapter only the reaction pathways and the redox states at each Compound of the heme iron according to Figure 10 are described.

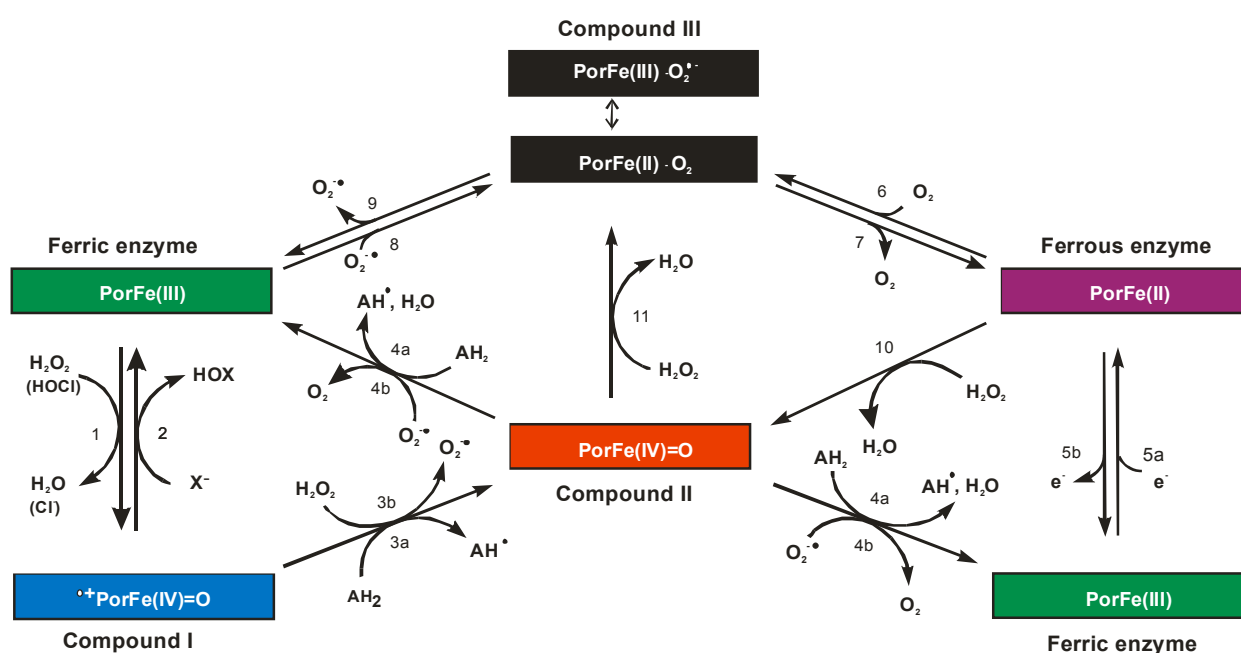


Figure 10 General reaction scheme of peroxidases. In the first step H_2O_2 is used for Compound I formation (reaction 1). Compound I is two oxidizing equivalents above the native enzyme with a porphyrin π -cation with an oxy-ferryl ($^{*+}\text{PorFe(IV)=O}$) center. Compound I can react with halides (X^-) reducing the enzyme back to the ferric state (reaction 2, halogenation activity). In the peroxidase reaction, Compound I is transformed in the first one-electron reduction to Compound II that contains an oxy-ferryl PorFe(IV)=O center. Reaction 3a shows a reduction via organic substrates and 3b via superoxide radical formation from H_2O_2 . Reaction 4a shows the second one electron reduction by organic substrates to the ferric form of the enzyme. Addition of high superoxide concentrations leads directly from ferric enzyme to Compound III according reaction 8. Dissociation of superoxide leads to the resting form of the enzyme again (reaction 9). Dissociation of molecular oxygen from Compound III leads to the ferrous form of enzyme with a PorFe(II) center (reaction 7). Reaction 6 shows the appropriate rereaction to Compound III. The difference between the ferrous and the ferric form of enzyme is one electron (cp. reaction 5a and 5b). The ferrous form of peroxidases can also cleave hydrogen peroxide heterolytically forming water and Compound II (reaction 10). Compound III has also shown to be formed by the H_2O_2 mediated transition of Compound II (reaction 11)

[12.] Both peroxidase and halogenation cycle starts by reaction of the Fe (III) form of the peroxidase with hydrogen peroxide to form Compound I, which contains two oxidizing

equivalents more than the resting enzyme. As mentioned before the conserved distal histidine in mammalian peroxidases plays the principal role as both acceptor of the proton from one oxygen and donor to the other, while the distal arginine modulates the ionization of the distal histidine by decreasing the pK_a of the imidazole N^{δ2} as well as polarize the O-O bond to promote nucleophilic attack at the heme and subsequent heterolytic cleavage. One oxygen leaves as water whereas one remains coordinated to the iron (Fig.10 reaction 1). One electron is removed from the iron to give the oxy-ferryl (Fe (IV) =O) intermediate, and a second electron is removed from the porphyrin to give a porphyrin π -cation radical (^{•+}Por). MPO requires at least a 10-fold excess of hydrogen peroxide to complete the formation of Compound I, which is in contrast to LPO, EPO, and TPO where Compound I can be formed by equimolar H₂O₂ concentrations. In catalases a second molecule of H₂O₂ is used as a reducing agent for Compound I. This two electron reduction completes the cycle forming the ferric enzyme and molecular oxygen. Formation of Compound I by H₂O₂ is a bimolecular reaction and for all mammalian peroxidases the k_{app} values are reported to be within $(1.1-5.6) \times 10^7 \text{ M}^{-1}\text{s}^{-1}$ at pH 7.0. Besides H₂O₂ peroxyacetic acid, ethyl hydroperoxide, cumene hydroperoxide and 3-chloroperoxybenzoic acid have been shown to mediate Compound I formation (Fig. 10, reaction 1). In addition hypochlorous acid can be used to oxidize ferric mammalian peroxidases to Compound I [12].

In the halogenation cycle the halide (X⁻) is oxidized (two-electron oxidation) by Compound I to the corresponding hypohalous acid (HOX), as shown in Figure 10. Generally, the ease of oxidation of halide ions is of the following order $\text{I}^- > \text{Br}^- > \text{Cl}^-$. The oxidation of the so called pseudohalide SCN⁻ is comparable to that of iodide. All heme peroxidases can oxidize iodide, but only MPO Compound I is able to oxidize chloride at pH 7 at reasonable rates. In MPO the positively charged sulfonium ion linkage to the vinyl group attached to the pyrrole ring A is located adjacent to the substrate binding site and enhances the electron deficiency in Compound I (Cp. Fig 9 B). This fact leads to a higher standard reduction potential of Compound I and that is the reason why two-electron oxidations of MPO Compound I are thermodynamically more favorable than in EPO and LPO [12].

In the peroxidase cycle Compound I is reduced by two successive one-electron steps via Compound II (Fig 10 reactions 3a, 4a). In these one electron oxidation reactions numerous organic substrates (AH) are oxidized to their corresponding radicals (A[•]). Compound II is inactive as halide ion oxidant. The obvious natural two electron substrates tyrosine and ascorbate exhibit similar reactivities toward Compound I and II of EPO and MPO. The rates of oxidation of substrates by Compound II of MPO and LPO are also similar and strongly

constrained by the nature of the substrates. The standard reduction potential of each LPO and MPO Compound (except Compound III) is described in detail by Furtmüller et al [12].

Several authors suggest that MPO exhibits a catalase activity [14, 15]. However, experimental evidence against a two-electron oxidation of H_2O_2 by MPO Compound I was brought by Furtmüller et al [16, 17]. Addition of H_2O_2 to preformed Compound I (by either peroxyacetic acid or hypochlorous acid) leads directly to Compound II (PorFe (IV) =O) according to Figure 10. Jantschko et al [18, 19, 20] observed that in the absence of one-electron donors human peroxidases release molecular oxygen at low rates. An alternative cycle involving ferrous peroxidase, Compound II and Compound III (Figure 10) has been reported to be responsible for this pseudo catalytic reactivity. The ferrous enzyme can also cleave hydrogen peroxide heterolytically forming water and Compound II (Fig 10 reaction 10). Alternatively, the Fe (II) form of peroxidases can bind dioxygen and form Compound III (Fig 10 reaction 6 and 7), which is a ferrous-dioxy/ferric-superoxide complex similar to oxymyoglobin and oxyhemoglobin. Compound III has been shown to be formed in stimulated neutrophils (12). Compound III can be formed by the fast addition of superoxide that is for example released in high concentrations in the beginning of phagocytosis to the ferric form of the peroxidase (Fig 10 reaction 8 and 9) or by H_2O_2 mediated transition of Compound II to Compound III (Fig 10 reaction 11). The latter reaction is very slow and seems to be the rate-limiting step in the pseudo catalytic cycle of human peroxidases [12].

1.6 Co-substrate hydrogen peroxide, H_2O_2

Finally several natural sources for the most important co-substrate H_2O_2 for peroxidases are mentioned.

The process of phagocytosis and degranulation by phagocytes is associated with increased metabolic activity. This metabolic activity includes a boost of oxygen consumption and consequently an increase of H_2O_2 formation, which is a product of the respiratory burst. Hydrogen peroxide is only produced in sublethal levels in the human body, thus it's not the sole responsible substrate for the antimicrobial heme peroxidase system [5].

A main source for H_2O_2 is the neutrophil NADPH oxidase for the MPO system and similarly the eosinophil NADPH oxidase for the EPO system, which is unusually robust and generates 3 - 10 as much superoxide anions and H_2O_2 than that of neutrophils [3]. The initial product of the

NADPH oxidase is the superoxide radical $O_2^{\bullet-}$ which dismutates into O_2 and H_2O_2 as mentioned before. A NAD(P)H oxidase is also present in vascular cells, which may serve as source of reactive oxygen species (ROS) in or adjacent to the vessel wall. This is of interest MPO and EPO released in the bloodstream. Further sources of hydrogen peroxide in mammals are the mitochondrial electron transport systems in a variety of cell types. Both cyanobacterial strains *M. chthonoplastes* (PCC 7420) as well as *Lyngbya sp.* (PCC 8106) are capable to produce oxygen via photosynthesis. Hence besides respiration in oxygenic photosynthesis various reactive oxygen species, such as superoxide radical, hydrogen peroxide and the hydroxyl radical (OH^{\bullet}), are generated as a result of the photosynthetic transport of electrons [36].

Additionally certain soluble enzyme systems can form H_2O_2 , some via an $O_2^{\bullet-}$ intermediate and others, without the generation of detectable amounts of $O_2^{\bullet-}$. For example, xanthine oxidase and amine oxidases form $O_2^{\bullet-}$ and H_2O_2 , whereas glucose oxidase forms H_2O_2 without an apparent $O_2^{\bullet-}$ intermediate [5].

The main sources of H_2O_2 for lactoperoxidase are certain microorganism, namely those designated as lactic acid bacteria. These microorganisms, which include strains of *streptococci*, *pneumococci*, and *lactobacilli*, lack heme and thus do not use the cytochrome system for terminal oxidations. Rather flavoproteins are used, which convert oxygen to H_2O_2 . These organisms also lack a heme catalase and thus do not efficiently degrade H_2O_2 , which accumulates in the medium [5]. These H_2O_2 producing lactic acid bacteria are found in the human milk, saliva, vaginal fluid as well as in the colon [5]. In the oral cavity to take it as example, the most potential producers of H_2O_2 are *Streptococcus sanguis* and *Str. mitis*. In human whole saliva the estimated hydrogen peroxide concentration is in the range from 8 to 14 μM [3].

2. Aim of work

The result of a comprehensive sequence alignment (Zamocky et al. [7]) showed a high similarity between the two cyanobacterial peroxidases from *Lyngbya sp.* (PCC 8106) and *Microcoleus chthonoplastes* (PCC 7420) especially to lactoperoxidase, eosinophil peroxidase and myeloperoxidase. The aim of this work was to characterize these two completely unknown peroxidases in detail and to gain as much as possible information about the properties of the enzyme during 10 month of work.

At first a detailed sequence alignment between the two peroxidases and the mammalian peroxidases was performed, analyzing the presence, or absence of known essential amino acid residues and their existence in the cyanobacterial peroxidases. Additionally several protein parameters of the two peroxidases were computed to deliver a first estimation of the enzyme characteristics and possible purification options.

Subsequently, the wild type peroxidase of *Microcoleus chthonoplastes* (PCC 7420) was cloned. Therefore the corresponding genes were isolated from the cyanobacterial organism. The cloning steps are described in this work. The PCC 7420 peroxidase DNA segment was cloned in a pET-21a (+) vector and overexpressed in *Escherichia coli* BL21 Star (DE3). The peroxidase of *Lyngbya sp.* (PCC 8106) was already cloned in the same expression system before this work had started.

A further part of this work was the improvement of the enzyme purification. Overexpression of the recombinant proteins was performed with different growing media and different chromatographic steps were probed. In Material and Methods only the most effective expression and purification systems are mentioned.

The two peroxidases were purified by metal-chelat affinity chromatography (MCAC) charged with Zn^{2+} (and Ni^{2+}) ions and analyzed by UV-Vis-, circular dichroism (CD)- and stopped-flow spectroscopy. The emphasis respective stopped-flow spectroscopy was placed on the kinetics of hydrogen peroxide and cyanide binding. The peroxidase activities were determined spectrophotometrically and fluorimetrically and compared with human myeloperoxidase and bovine lactoperoxidase.

The new peroxidases were probed for the most common substrates known to be converted by the mammalian peroxidases MPO, LPO, and EPO. As two-electron donors the halides chloride,

bromide, iodide and as one-electron donors ABTS, guaiacol and tyrosine were tested. Kinetic parameters and pH optima were elucidated.

3. Material and Methods

3.1. Sequence analysis and protein parameter prediction of *Microcoleus chthonoplastes* (PCC 7420) and *Lyngbya sp.* (PCC8106) peroxidases.

The following two (putative) peroxidase amino acid sequences of *Microcoleus chthonoplastes* (PCC 7420) and *Lyngbya sp.* (PCC 8106) were taken directly from the NCBI data base.

Microcoleus chthonoplastes (PCC 7420) peroxidase amino acid sequence (584 aa)

MTAHKIRQTLTLLTSFATLGFVSLPAQAIEFRSIDGSNNLDNPTWGEAEIELIRLLEPDYSDEISAPAG
MNRPNPRAISNAIASQSESLPNPFHASDWLWQWGQFVDHDLTDPPEGAEPLPIIVPENDLTFTPGSEI
PFNRNVAAPGTGTDSSNPRQQVNAITAYIDGSNVYGS DIERANFLRTGDSGKLKTSAGNLLIFNTANLPN
ANPFGVDAEDLFIAGDVR SNEQIGLTA VHTLFVREHNRLADEIAADPTTSQKAADAGLSVDDYIYQTTRRI
VSAQIQAITYNEFLPLLLGEG AIDPYSGYDET VNP S ISNEFSTAAYRVGHTMLPSELQRINNDGTSAGSISL
RDSFFKPQEITDNGIDSLLLGLASQKAQTIDAFIVDDVRNFLFPAGNGGLDLAAVNIQRGRDHGLPSYNE
ARQALGLGGYTSFDQITSDAEIAQRFRDIYGT TDGQDNIDLVDLWIGGIAEDAYNGGMV GELFNVIISDQF
QRLQDGD RFFYLADQDLLNLVPDIGDTRLSDIIVRNTDITTIQDN AFIVAKDVPEPSALFGLFLIGVFGGTL
GQLRQRQSTNKGHSQSI

Lyngbya sp (PCC 8106) peroxidase amino acid sequence (661 aa)

MQNNGNGNGNGNGSSKSGSNDVYENNSRRQAYDLTSLEQTPLSEIQGLAIAKNPDWYKIQVSP
GTTSLVDLQFTHADGNIDLFLHNANGNEIASSTSQTNNESINFDSPTAGVYYIKVKSIGKPGNSYDLVW
DDIVPIEFRSIEGLNNNLVNPDWGTPDSQLIRLSESAYNDEISEPRGGDPSSLVSPREVSNTIFDQSESIPN
ETGVSDWFWQWQGFIDHMDLTPGTSGESFNISVPLGDPSFDPFNSGTQEIPLTRSIYDFDTGIDSPREQ
INEITAYIDGSNVYGS DSERAEALRTNDGTGKLKTSVSESGEVLLPFNTDGLDNDNPFGIANDSIFVAGDV
RANEQVGLTATHTLFVREHNRLADDIATRLDNGDAELLDLFAESGLSEGDFIYESARRIVGAEIQAITYNE
FVPLLVGSNALDGYDGYNVTVDSGISNEFSTA AFRFGHTMLSPTLQNGTNEGLSLRDTFFNPDLVVEGG
VDSLLLGLASQEAQEVDTQVIDDVRNFLFGAPGSGGLDLVSLNIQRGRDHGLPSYTEVREELGLDPITNF
GEITSDPIVQAQLESAYTDVDNIDLWVGGLAEDHVNGSLFGETFQVIVVDQFTRLRDGDRFYYENDNLLS
VLAPDVAETTLSDVIVANSAISSIQSNAFLV

3.1.1. Sequence alignment of the two peroxidockerin sequences with selected mammalian peroxidases.

Multiple sequence alignment of the 6 selected heme enzymes was conducted with Clustal X [30]. The selected sequences were the two cyanobacterial peroxidases, the human peroxidases hMPO, hLPO, hEPO, and additionally *bovine* LPO (bLPO). The parameters for the multiple sequence alignment are listed in Table 1.

Tab. 1 Parameters for the ClustalX multiple sequence alignment.

Gap opening penalty	10
Gap separation distance	4
Gap extension penalty	0.2
Delay divergent sequences	30%
Protein weight matrix	Gonnet series

The output was depicted with Genedoc [31] according 4.1.1.

3.1.2 Protein parameter prediction

All parameters were computed via the tools provided on the ExPASy Proteomics Server. Therefore the isoelectric point (pI), the molecular weight (M_w), the amino acid composition, the secondary structure, the extinction coefficient at 280 nm were computed and predicted. Additionally a signal peptide prediction was performed with the aid of the cbs SignalP 3.0 Server from the technical university of Denmark. The secondary structure was predicted via the PSIPRED protein structure prediction server from the Bloomsbury Centre of Bioinformatics and all other parameters were computed with the ProtParam tool on the ExPASy Proteomics Server. For these purposes it was only necessary to insert the two cyanobacterial sequences (according 3.1) in the respectively user-friendly software.

3.2 Cloning of the *Microcoleus chthonoplastes* (PCC 7420) peroxidase.

For this purpose the cyanobacterial strain *Microcoleus chthonoplastes* (PCC 7420) was ordered from the Pasteur culture collection. The peroxidase gene was amplified out of the organism's genome DNA, prepared and inserted into the pET-21a (+) vector shown in Figure 11.

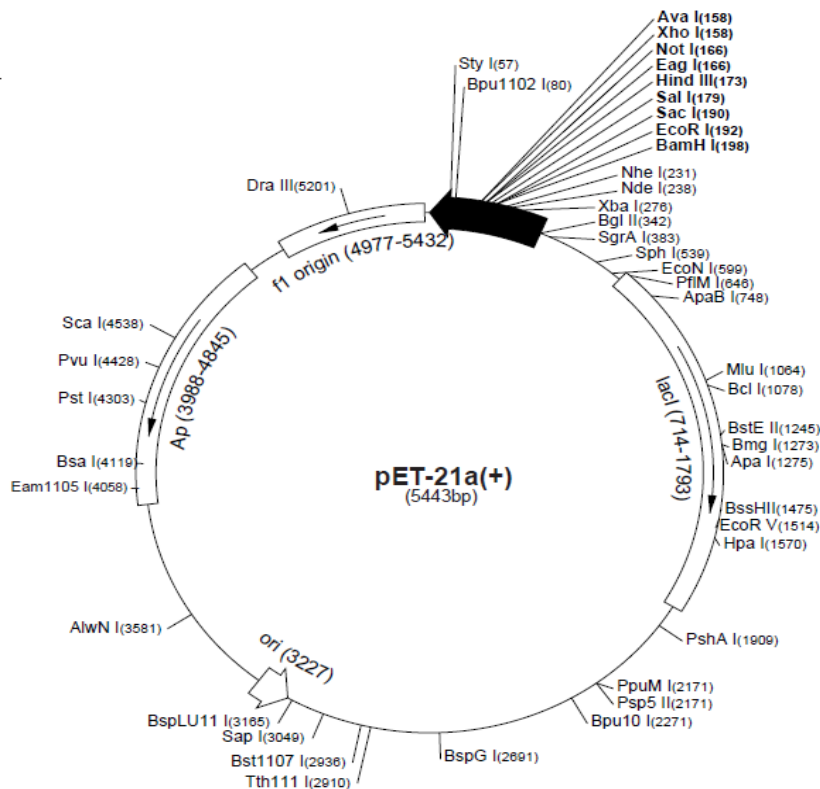


Figure 11 shows the pET-21a (+) expression vector with multiple restriction sites labeled. The pET-21a (+) sequence landmarks are: T7 promoter (311-327 bp); T7 transcription start (310 bp); T7•Tag coding sequence (207-239 bp); multiple cloning sites (Bam H I - Xho I (158-203 bp)); His•Tag coding sequence (140-157 bp); T7 terminator (26-72 bp); *lacI* coding sequence (714-1793 bp); pBR322 origin (3227 bp); *bla* coding sequence (ampicillin resistance (3988-4845 bp)); *f1* origin (4977-5432 bp) [Novagen]

The used pET expression system is pictured in Figure 12.

In the T7 expression system the expression vector including the target gene (in this work the cyanobacterial peroxidase gene) is under control of the strong and inducible bacteriophage T7 promoter. The genome of the host cell provides the T7 RNA polymerase gene which is under control of the *lac* promoter, therefore T7 RNA polymerase and consequently the target gene can only be transcribed and translated after induction with lactose or IPTG. IPTG (the presented inductor in Figure 12) binds to the polymerase like lactose via the galactosyl group, but in contrast to lactose the sulfur bond of IPTG is not hydrolysable, therefore it's not metabolized by the host cell. In this work the used inductor was lactose. According to Figure 12, the *E. coli* expression strain BL21 Star (DE3) did not have the pLys (E or S) plasmid, containing the T7 lysosome. The permanently expressed base level of active T7 RNA polymerase was accepted.

Summing up, *Escherichia coli* host strain BL21 Star (DE3) carrying the pET-21a(+) plasmid containing the wild type peroxidase gene of *M. chthonoplastes* (PCC 7420) was used as final expression system, whereas the *E. coli* strain TOP 10 served for plasmid preparation.

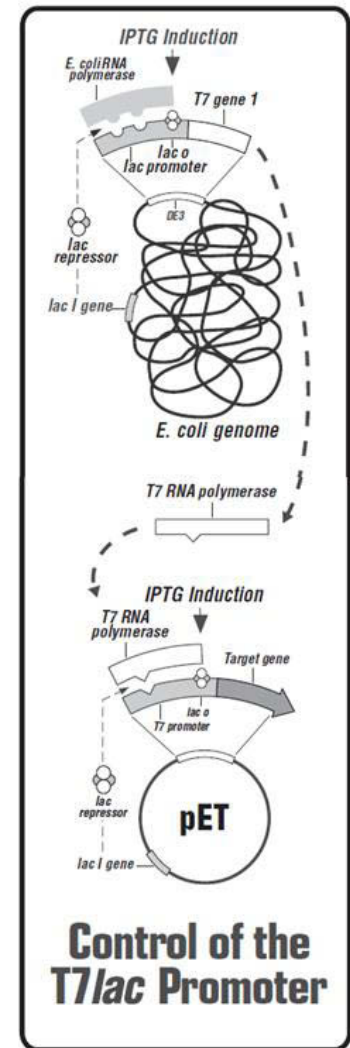


Figure 12. Schematic view of the pET expression system using *E. coli* as host cell. [Novagen]

3.2.1. Amplification of peroxidase gene DNA and preparation of vector DNA

A specific piece of DNA can be amplified by using PCR (polymerase chain reaction). This is achieved by mixing denatured DNA with thermostable DNA-polymerase, two short oligonucleotides (primers) and essential molecules like nucleotides (dNTPs). The primers hybridize with single stranded DNA and function as initiation points for the DNA-polymerase, which synthesizes the complementary DNA strands. Hybridization can only occur when single strands DNA is available, therefore the template DNA has to be denatured (usually by heating)

in a first step. The used DNA-polymerase has to be thermostable. The following steps are performed during one PCR- cycle:

- 1) Denaturation of double-stranded DNA
- 2) Annealing of primers to the single-stranded DNA
- 3) Elongation (synthesis of complementary DNA strands)

In this work these steps were repeated 30 times.

3.2.1.1 Primer design for amplification of the cyanobacterial peroxidase gene DNA from genomic DNA

The adequate forward and reverse primers were constructed with the software “gene runner” and ordered from the company genXpress. The primers were designed with regard to the proper restriction enzymes therefore the primers had to contain the respective restriction sites of NdeI and XhoI (labeled *violet*).

5'-primer 1 containing NdeI restriction site:

5'-AAGGGAATTCCA/TATGACTGCTCACAAAATC-3' (31mer, GC=38.7%, Tm=71.9°C)

3'-primer 1 containing XhoI restriction site:

5'-TAACGACCGC/TCGAGTATTGATTGGGAATG-3' (30mer, GC=46.6%, Tm=75.5°C)

Figure 13 underlines the choice of the two restriction enzymes Nde I and Xho I. The restriction site of Nde I exhibits the ATG start codon and the restriction site of Xho I in the primer should delete the stop codon of the peroxidase sequence to incorporate the His•Tag coding sequence of the vector. The restriction site of Xho I within the multiple cloning site is adjacent to the His•Tag coding sequence which minimizes nonsense DNA. Additionally no restriction sites inside of the peroxidase sequence were found for both enzymes.



Figure 13. pET-21a-d (+) cloning/expression region. Labeled red are the recognition sites of the two for the vector preparation used restriction enzymes NdeI and XhoI. [Novagen]

3.2.1.2 Amplification of the cyanobacterial peroxidase gene DNA from genomic DNA by using polymerase chain reaction (PCR)

Amplification of the peroxidase gene DNA using *Microcoleus chthonoplastes* (PCC 7420) cell culture was performed via Phusion Hotstart PCR. Thereby the 10 min long initial denaturation and the subsequent disruption of the cells should enable a successful cloning of the peroxidase gene from a cell culture. 1.5 mL was gathered from the *M. chthonoplastes* (PCC 7420) cell culture, centrifuged 5 min at 8000 rpm. The supernatant was discarded and the cell pellet was the template for the polymerase chain reaction.

The mixtures for the two PCR approaches (one with HF-Buffer, one with GC-Buffer) were prepared in 100 µl PCR tubes, as described in Table 2. Additionally negative controls including all components except the template were mixed. The DNA polymerase was Phusion® Hot Start from the company Finnzymes and as a consequence all following concentrations and PCR cycling parameters were in dependence on the Phusion® Hot Start data sheet.

Tab. 2 PCR mixture for amplification of the peroxidase gene from genomic DNA of *M. chthonoplastes* (PCC 7420).

Component	PCC7420Perox1	HF_blank	PCC7420Perox2	GC_blank	Final conc.
H ₂ O	31 µL	33.5 µL	31 µL	33.5 µL	-
5x Phusion Buffer X	10 µL HF	10 µL HF	10 µL GC	10 µL GC	1x
10 mM dNTPs	1 µL	1 µL	1 µL	1 µL	200 µM
5' primer 1 (10 µM)	2.5 µL	2.5 µL	2.5 µL	2.5 µL	0.5 µM
3' primer 1 (10 µM)	2.5 µL	2.5 µL	2.5 µL	2.5 µL	0.5 µM
PCC 7420 Template	2.5 µL	2.5 µL	2.5 µL	2.5 µL	-

DNA					
Phusion® Hot Start DNA polymerase (2 U/μL)	0.5 μL	0.5 μL	0.5 μL	0.5 μL	0.02 U/μL
Final volume	50 μL	50 μL	50 μL	50 μL	-

Phusion® Hot Start DNA polymerase is an Mg^{2+} dependent enzyme, therefore each buffer (GC, HF) contains 7.5 mM $MgCl_2$.

The PCR was performed in a thermocycler. 30 cycles containing the following steps (Table 3) were carried out. The initial denaturation was intercepted after 5 and after 10 minutes. After 5 min the samples were stirred carefully to prevent agglutination of the cell pellet and after 10 minutes at the end of the initial denaturation the DNA polymerase was added. The extension time was set to 1 min 20 s according to the peroxidase gene size (1752 bp).

Tab. 3 PCR cycles; 3-step protocol

Cycling step	Temperature	Time	Cycles
Initial denaturation	98°C	10 min	1
Denaturation	98°C	10 s	30
Annealing	75°C	30 s	
Extension	72°C	1 min 20 s	
Final extension	72°C	10 min	1
	4°C	hold	

The PCR products were investigated by agarose gel electrophoresis and purified with the help of the GFX™ PCR DNA and Gel Band purification kit. In general to gain more peroxidase DNA fragments optionally an additionally PCR out of purified PCR product can be performed.

3.2.1.3. Agarose gel electrophoresis (E-Gel®, Sybr® safe)

Agarose gel electrophoresis is used for analytical as well as for preparative purposes. The principle of this method is based on the anionic nature of DNA in solution and on the migration of negatively charged molecules toward the positive pole in an electric field. The polymerization degree of the agarose gel, which acts like a strainer, determines how fast the molecules can move through. Thereby the pore size of the polymerized agarose is suitable for separation of DNA molecules. In general small DNA molecules can move faster than bigger ones, so the DNA

can finally be separated by size. For visualizing the DNA, the gel was stained with Sybr® safe and analyzed by ultraviolet light.

In this work all agarose gel electrophoresis that served for DNA analysis were performed with the Invitrogen E-Gel® system of precast 1.2% agarose gels containing Sybr® safe.

Therefore 10 µL of each of the four above described PCR products were filled into the gel pockets. The used marker was from Fermentas #SM0311 (cp. 4.2.1). Electrophoresis ran 30 min.

3.2.1.4 GFX™ PCR DNA and gel band purification

The GFX™ PCR DNA and gel band purification kit is used for isolation and concentration of PCR products and DNA fragments of 0.1 - 48 kbp from solution and from agarose gel slices. In this case the cyanobacterial peroxidase DNA fragments were purified from the PCR “soup” containing cell fragments with genomic DNA and cell proteins. The purification kit uses a chaotropic agent which denatures proteins and promotes the binding of double stranded DNA to a glass fiber matrix. Furthermore this acetate containing “Capture buffer” dissolves agarose. While the DNA is captured to the Microspin™ column, proteins, salts, and other contaminants are washed away with “Wash buffer”, which contains ethanol that additionally dries the matrix prior to elution. The purified DNA can be recovered by eluting with sterile RO water or with a low ionic strength buffer. The purification was performed analog to following steps.

- The GFX Microspin™ column was placed in a 2 mL collection tube.
- 500 µL of Capture buffer were added to each column.
- Up to (100 µL) DNA containing solution was transferred to the column and mixed carefully by pipetting the sample up and down several times.
- The column was centrifuged in a micro centrifuge at 16000 g for 1 minute.
- The flow-through was discarded.
- 500 µL of Wash buffer were added to the column and again centrifuged at 16000 g for 1 minute.
- The collection tube was discarded, secured that no ethanol is left and the column was transferred to a fresh 1.5 mL micro centrifuge tube.

- 50 μL of sterile RO water were added directly to the top of the glass fiber matrix of the GFX Microspin™ column.
- The sample was incubated at room temperature for 1 minute and then centrifuged for 1 minute at 16000 g to recover the purified DNA.

3.2.2. Plasmid preparation

The cyanobacterial peroxidase gene DNA was inserted into the pET-21a (+) vector. Therefore both insert and vector were cut with the restriction enzymes NdeI and XhoI. Subsequently the 5'-phosphate residues were removed from the linearized vector with the aid of CIAP and afterwards insert and vector were ligated with the DNA Ligase T4. The finished plasmid was electroporated into *E.coli* TOP 10 cells.

3.2.2.1 Restriction cuts of peroxidase gene DNA and pET-21a (+) vector

Due to the circumstance that NdeI and XhoI require the same Buffer (Buffer 4 from New England Biolabs NEB), it was possible to perform the respective restriction cuts within one digestion approach. PCC 7420 peroxidase DNA insert and pET-21a (+) vector were cut parallel according to Table 4.

Tab. 4 Restriction cut approaches for PCC 7420 peroxidase gene Insert and pET-21a (+) vector.

Component	Insert approach	vector approach
Sterile RO water	8.5 μL	53 μL
pET-21a(+) vector	-	30 μL
PCC 7420 peroxidase gene from GC-Buffer PCR	33 μL	-
10 x NEB Buffer 4	5 μL	10 μL
100 x BSA (NEB)	0.5 μL	1 μL
NdeI (20 U/ μL) NEB	1.5 μL	3 μL
XhoI (20 U/ μL) NEB	1.5 μL	3 μL
Total volume	50 μL	100 μL

Both approaches were incubated at 37°C for 2 hours and afterwards GFX™ PCR DNA and Gel Band purification kit purified analog to 3.2.1.4.

3.2.2.2. Removal of 5'-phosphate residues from vector pET-21a (+) with CIAP

Calf intestinal alkaline phosphatase (CIAP) catalyzes the hydrolysis of 5'-phosphate groups from DNA, RNA, and ribo- and deoxyribonucleoside triphosphates. This enzyme is used to prevent self ligation of linearized cloning vehicle DNA by removing phosphate groups from both 5'-termini of the double strand. This fact enables a rough electrophoretic control if the vector cut were successful because of the different moving ranges of circularized and linear DNA. The in Table 5 listed mixture was incubated at 37°C for 30 minutes.

Tab. 5 Mixture for dephosphorylation of pET-21a (+) vector

Component	Vector approach
Sterile RO water	4 µL
pET-21a(+)	40 µL
10 x CIAP NEB Buffer 3	5 µL
CIAP enzyme (NEB; 10 U/µL)	1 µL

After the first 30 minutes incubation, there was additionally 1 µL CIAP enzyme solution added and again incubated for 30 minutes at 37°C. Then the Vector solution was purified by using the GFX™ PCR DNA and Gel Band purification kit analog 3.2.1.4 again.

The electrophoretic incubation was again performed with the E-Gel® / Sybr® safe system as described in 3.2.1.3.

3.2.2.3 Ligation

DNA Ligase catalyzes the formation of a phosphodiester bond between a 3'-OH and a 5'-P-terminus of double stranded DNA. The molar ratio of insert to vector should be around 3:1. Therefore the DNA concentrations of the purified insert and vector solutions were roughly estimated over the DNA band intensity according to the corresponding agarose gel

electrophoresis (4.2.2; Fig 24). The needed volumes of insert and vector DNA (Table 6) were a consequence of this estimation. The used ligase was the T4 DNA Ligase from New England Biolabs.

Tab. 6 Ligation approach of PCC 7420 peroxidase insert with linearized pET-21a (+) vector.

Component	Volume
PCC 7420 peroxidase Insert	9 μ L
Linearized pET-21a(+) Vector	6.9 μ L
10 x Ligase buffer (NEB)	2 μ L
T4 DNA Ligase (NEB; 2000 U/ μ L)	1 μ L
Sterile RO water	1.1 μ L
Total volume	20 μ L

As control for the background level of self-ligated vectors an additional ligation approach with T4 DNA Ligase and linearized pET-21a (+) vector without PCC 7420 peroxidase insert was performed. This vector control also served as confirmation of a successful dephosphorylation. Each ligation mixture was put on ice for 30 min and afterwards incubated 2 hours at 22°C.

3.2.2.4. Electroporation

The expected result of the ligation approach was a plasmid (vector + insert) with 7195 base pairs. For transferring such large DNA fragments into *E. coli* cells, electroporation is used. Thereby a strong electric pulse, for instance 2500 V, creates pores in the bacterial cell wall, where the plasmid DNA is able to access into the cells. The working steps for this procedure are described below. The electroporation was performed with electrocompetent TOP 10 *E. coli* cells.

- 15 μ L of the two ligation mixtures (pET-21a (+)/peroxidase and vector control) were transferred into prepared electroporation cuvettes together with 80 μ L of electrocompetent TOP 10 *E. coli* cells. The cuvettes were cooled on ice until electroporation.
- 1 mL sterile SOC-medium per electroporation were pipetted into 1.5 mL Eppendorf tubes and kept warm at 37°C.
- Electroporation was performed with the help of the Biorad MicroPulser™ Electroporator immediately after mixing the electrocompetent cells with the ligation mixtures in the cuvettes.
- The voltage was set to 2500 V at the electroporator.

- After electroporation, the cells were transferred into Eppendorf tubes containing the tempered SOC-medium and incubated at 37°C for 30 minutes.
- 200 µL and about 900 µL (remaining content of Eppendorf tube) of each tube were finally plated on selective LB-agar_{Amp} plates and incubated for 12 hours at 37°C.

Only successfully transformed cells or cells with a recircularized vector should grow on selective LB-agar_{Amp}. Table 7 shows the composition of the used media for the electroporation.

Tab. 7 Components of nutrition media used during electroporation.

LB-Medium (Agar)	SOC-Medium
5 g peptone	20 g peptone
5 g sodium chloride	5 g yeast extract
2.5 g yeast extract	0.58 g sodium chloride
7.5 g Bacto-agar	0.19 g potassium chloride
RO water added to 500 mL -->autoclaved	2.03 g MgCl ₂ • 6H ₂ O
	3.96 g glucose • H ₂ O
	2.46 g MgSO ₄ • 7H ₂ O
	RO water added to 1000 mL --> autoclaved
Ampicillin stock solution	
100 mg sodiumampicillin solved in 1 mL RO water; sterile filtrated and stored at -20°C	
Ampicillin was used in concentrations of	
100 µg/mL media	

3.3 Screening for colonies

The colonies grown on the plates had to be screened for containing correctly prepared plasmids. First a PCR screening, followed by a restriction screening was carried out, in order to check whether the transformed cells contained the cyanobacterial peroxidase insert.

3.3.1. PCR screening

PCR screening allows the selection of clones that had incorporated a pET-21a(+) vector containing the *M. chthonoplastes* (PCC 7420) peroxidase gene as insert by using the flanking primer of the DNA fragments. The following two primers were used.

PCC7420perox-sequ01for:

5'-TCACAAAATCCGTCAAAC-3' (18mer, T_m=57.48°C, GC=38.89%)

PCC7420perox-sequ06rev:

5'-AATGTCCTTTGTTGGTG-3' (17mer, T_m=54.49°C, GC=41.18%)

Both primers were also used for sequencing that was performed in this work. 18 colonies were chosen from the LB-Agar_{Amp} plate and were resuspended in 50 µL sterile RO water.

2 µL of the respective suspension was transferred to a new LB_{Amp} agar plate to create a master plate for further use. The order of the 18 colonies was according to Figure 14 and the plate was incubated over night at 37°C.

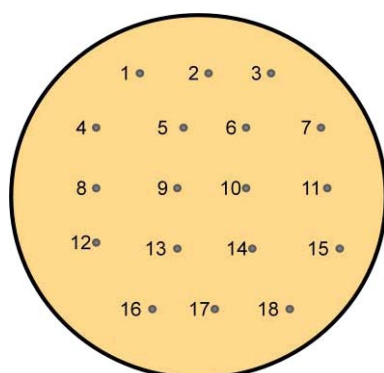


Figure 14. Master plate for PCR screening containing 18 colonies

10 µL of each of the 18 bacterial suspensions were taken for the 20 µL PCR approach. Table 8 shows the mixture of the PCR tubes. For the PCR screening the DNA polymerase needed not to be as accurate as the Phusion® Hot Start DNA polymerase, that was the reason why the much cheaper HotMaster™ Taq DNA polymerase (5 Prime) was used. Concentrations of the mixture and PCR cycling parameters were adopted from the HotMaster™ Taq DNA polymerase manual.

Tab. 8 Mixture for PCR screening

Component	Volume
Sterile RO water	6.6 µL
10x HotMaster™ Taq Buffer with 25 mM Mg ²⁺	2 µL
10 mM dNTP mix	0.4 µL
Primer A <u>PCC7420perox-sequ01for</u>	0.4 µL
Primer B <u>PCC7420perox-sequ06rev</u>	0.4 µL

Colony suspension (1-18) as template	10 μ L
HotMaster™ <i>Taq</i> DNA Polymerase (5 U/ μ L)	0.2 μ L
Total Volume	20 μ L

Additionally a positive and a negative control were performed. For the positive control ((+)contr.) 9.5 μ L sterile RO water and 0.5 μ L PCC 7420 peroxidase insert were added to the mixture analog Table 8 instead of colony suspension, whereas for the negative control ((-)contr.) 10 μ L sterile RO water were used instead of colony suspension. Table 9 shows the PCR cycling parameters during the PCR screening.

Tab. 9 Cycling parameters for PCR screening

Cycling step	Temperature	Time	Cycles
Initial denaturation	94°C	2 min	1
Denaturation	94°C	20 s	30
Annealing	57°C	15 s	
Extension	65°C	2 min	
Final extension	60°C	10 min	1
	4°C	hold	

For electrophoresis the E-Gel® / Sybr® safe system analog description 3.2.1.3 was used.

3.3.2 Plasmid amplification and purification

For the subsequent screening methods it was necessary to amplify the ligated plasmids. Therefore 3 mL of sterile LB media were transformed in each of 5 test tubes together with 3 μ L of ampicillin. Afterwards the test tubes were inoculated with one pipette tip of colonies 9, 13, 14, 17, and 18. The five test tubes were incubated at 37°C and shaken with 180 rpm for 12 hours.

The following plasmid purification was carried out using the GFX™ plasmidPrep Mini Spin kid. The cells were suspended in an isotonic solution containing RNase I and 10 mM EDTA (Solution 1), before the cells were lysed by alkali treatment and SDS (Solution 2), which also denatured chromosomal DNA and proteins. That following the pH of the lysate was neutralized with an acetate solution containing a high concentration of a chaotropic salt (Solution 3), which also promoted the binding of plasmid DNA to the glass matrix. The Matrix-bound DNA was washed with an ethanolic buffer to remove salts and other residual contaminants. This buffer

also dried the matrix before elution with sterile RO water. The pipetting steps are listed subsequently.

- 1.5 mL of each overnight culture were transferred to 1.5 mL micro centrifuge tubes and centrifuged at 16000 g for 1 min.
- The supernatants were discarded and the tubes were refilled with the remaining 1.5 mL of the overnight cultures and again centrifuged at 16000 g for 1 min.
- The supernatant was removed carefully and the pellet was resuspended completely in 175 μ L Solution 1.
- 175 μ L of Solution 2 were added and the tube was gently inverted to mix the suspension. The bacterial suspension became clear as soon as lysis occurred. The sample should not be left in this solution for more than a few minutes after the Solution 2 was added.
- 350 μ L of Solution 3 were added to solve flocculent precipitation by inverting the tube gently.
- Cell debris was pelleted by centrifuging the sample for 5 min at 16000 g.
- Afterwards the supernatant (~700 μ L) was transferred into a GFX™ plasmid mini column placed in a new collection tube and incubated for 1 minute at room temperature.
- Centrifuged at 16000 g for 1 min, then flow-through was discarded.
- 400 μ L of Wash Buffer were added to the column and removed again by centrifugation at 16000 g for 2 min. Flow-through was discarded together with the collection tube and attention was paid that no Wash Buffer was left on the column.
- The GFX™ column was transferred to a new micro centrifuge tube and 50 μ L of sterile RO water were added directly on the top of the GFX™ column glass fiber matrix.
- Afterwards incubation for 1 minute at room temperature.

The obtained plasmid solutions were the basis for the further screening methods and the procedure of section 3.2.3.2 was optionally repeated whenever more plasmid solution was needed.

3.3.3 Restriction screening

According to the results of PCR screening (4.3.1) the clones 9, 13, 14, 17, and 18 were chosen for further analysis. These clones seemed to contain plasmids that exhibit presumably an insert of correct size (~1750 bp), but the PCR screening did not elucidate if the plasmid was present completely and if the insert was incorporated in the right direction. The restriction screening allows the confirmation of these two facts with the aid of restriction digestion. The required restriction enzyme for the screening had to cut the plasmid at least once within the vector and once within the insert. To assess the direction of the incorporated insert, it is necessary that the restriction site of the enzyme is not midway of the insert DNA. By means of the software Generunner the restriction enzyme BglII was chosen with following recognition site.

5'...A'GATCT...3'

In Table 10 the components for the restriction screening are listed.

Tab. 10 Mixtures for Bgl II digestion

Component	Volume
Sterile RO water	16 µL
10x NEB Buffer 3	2.5 µL
Bgl II NEB (10 U/µL)	1.5 µL
PCC 7420 peroxidase Plasmid 9, 13, 14, 17, 18	5 µL
Total Volume	25 µL

The five mixtures were incubated for 2 h at 37°C and afterwards inspected by agarose gel electrophoresis.

3.3.4 Expression screening

For protein the protein overexpression the designated *E. coli* strain was BL21 Star (DE3). Therefore the plasmid containing PCC 7420 peroxidase (Clon 14) was electroporated into the even mentioned host strain. The electroporation was performed as described in 3.2.2.4.

After 30 min incubation at 37°C, 1 mL of the colonies containing SOC medium was divided and transferred to LB-agar_{amp} master plates. Collectively 4 plates were inoculated, with 20 µL, 100 µL, 200 µL, and the remaining ~700 µL of SOC culture. The plates were incubated at 37°C over night.

Afterwards 5 single colonies were taken from the plate inoculated with 20 μ L SOC culture, each resuspended in 50 μ L sterile RO water. These 50 μ L suspensions were again divided. With 2 μ L of each colony suspension an LB_{amp}- medium master plate was generated according to Figure 15.

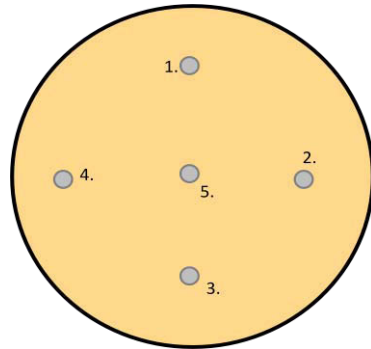


Figure 15 Scheme of master plate for expression screening.

The remaining parts of the 50 μ L colony suspensions were the inocula for each with 2.5 mL LB_{amp} medium filled 10 mL sterile test tubes.

Both approaches were incubated at 37°C for 12 hours and the test tubes were additionally shaken at 180 rpm.

After incubation the master plate was sealed with parafilm and stored at 4°C, whereas 200 μ L of each of the 5 incubated test tubes were taken as inocula for 20 mL M9ZB_{amp} (100 mL Erlenmeyer flasks).

These flasks were then incubated for 4 hours at 37°C.

After incubation 200 μ L of a hemin solution (5 mg/mL) were added to get a final concentration of 50 μ g/mL. After 30 minutes the expression was induced with 20 μ L of 1 M IPTG solution.

The expression was carried out for 12 hours at 16°C and 180 rpm.

After the 12 hours to each Erlenmeyer flask 5 mL of digestion solution were added and the cells were disrupted afterwards by using sonification.

The cultures were transferred to Falcon tubes and centrifuged with 4000 rpm for 10 minutes.

The supernatants were aspirated and stored in fresh Falcon tubes, and the pellet was resuspended in 1 mL sterile RO water. Subsequently both supernatant and pellet were investigated by means of SDS-PAGE (3.2.3.5).

Tab. 11 Required components for expression screening.

<p>M9ZB_{amp} medium</p> <p>800 mL solution A 100 mL solution B 50 mL solution C 1 mL solution D</p> <p>Solution A</p> <p>20 g peptone 10 g yeast extract 5 g NaCl 1 g NH₄Cl Filled up to 800 mL with RO water --> autoclaved</p> <p>Solution B</p> <p>12 g KH₂PO₄ 24 g Na₂HPO₄ Filled up to 400 mL with RO water --> autoclaved</p> <p>Solution C</p> <p>16 g Glucose Filled up to 400 mL with RO water --> autoclaved</p> <p>Solution D</p> <p>12.3 g MgSO₄ • 7 H₂O 2x LB medium 40 g peptone20 g yeast extract5 g NaCl1 g NH₄Cl</p> <p>LB medium</p> <p>20 g peptone 5 g sodium chloride 10 g yeast extract 1 g ammonium chloride RO water added to 1000 mL --> autoclaved</p>	<p>Lysis buffer</p> <p>2 mL 1,0 M Tris/HCl pH 8,0 (50 mM) 160 µL 0,5 M EDTA pH 8,0 (2 mM) 40 µL Triton X-100 (0.1%)200 µL 200 mM PMSF (1 mM)(200 µL 1 mM Pepstatin (5 µM)) Filled up to 40 mL with RO water</p> <p>1 mM Pepstatin A: 5 mg in 5,54 mL methanol</p> <p>200 mM PMSF: 34,8 mg in 1 mL isopropanol</p> <p>5 mg/mL bovine heminchloride solution (7,67 mM) prepared in the following way 100 mg bovine heminchloride Solved in 800 µl 0,5 M NaOH and 20 mL RO water added Then 300 µL 1 M HCl Afterwards adjusted to pH 9-10 with 0.5 M NaOH To enable a convenient pH measurement it is recommended to solve the heminchloride by gentle shaking (optionally on a shaker) to avoid abundant foam formation.</p> <p>1 M IPTG solution 2.38 g IPTG solved in 10 mL RO water</p>
--	---

3.3.5 Sodium dodecyl sulfate polyacrylamide-gel-electrophoresis (SDS-PAGE)

Many biomolecules carrying a charge can move in an electric field. The mobility of the ions depends on charge, size, and shape. In contrast to the above mentioned agarose gel electrophoresis which is usually used for large DNA molecules, the polyacrylamide gel possesses excellent features for separation of proteins. Moreover, the pore size can be controlled by choosing various concentrations of acrylamide and methylenebisacrylamide (as cross linking reagent) at the time of polymerization. Furthermore using this gel for separation of proteins with similar charges but different shapes and sizes can be achieved with high reproducibility.

Sodium dodecyl sulfate (SDS) is an anionic organosulfate consisting of a 12-carbon tail attached to a sulfate group, giving the material amphiphilic properties. The carbon tail binds to hydrophobic groups of proteins and due to the negatively charged sulfate group all proteins are charged negatively. Under saturated conditions (about 1.4 g SDS is bound per gram protein) all proteins are loaded with certain amount of negative charges per units of mass, which accomplish the high reproducibility. Therefore, in most cases the mobility of the protein-SDS-complex through the molecular sieve of the gel is proportional to the logarithm (\log_{10}) of the relative mass (M_r).

In this work for all protein separation applications the precast system NuPAGE® Novex 12% Bis-Tris Gel 1.0 mm, 15 well, from Invitrogen was used. The crosslinker concentration for the NuPAGE® Novex® Pre-Cast Gel ranges from 3.8–5% depending on the range of application. The procedure of electrophoresis was performed according to the by Invitrogen provided manual of NuPAGE® Novex® Bis-Tris Mini Gels.

Supernatant and pellet of the five colonies were investigated via SDS-PAGE. Collectively 10 micro centrifuge tubes were prepared according to Table 12.

Tab. 12 Preparation of sample for SDS-PAGE

Reagent	Volume
Sample	2.5 μ L
NuPAGE® LDS Sample Buffer (4x)	2.5 μ L
Deionized Water	5 μ L
Total Volume	10 μ L

The samples were heated at 70°C for 10 minutes and afterwards loaded on the gel. Due to the expected protein size (~ 60 kDa for monomer) the corresponding running buffer (MOPS) to the NuPAGE® Electrophoresis System was used. The elected protein marker was Mark 12™ Unstained Standard from Invitrogen which was used in all SDS-PAGE applications in this work.

The gel was run at constant 200 V and max. 125 mA. The used equipment was the XCell SureLock™ Mini-Cell (1500 V) from Invitrogen

After electrophoresis the gel was taken out of the plastic cover, rinsed with RO water and incubated in staining solution at room temperature for 30 minutes on a shaker. Finally, after washing with RO water the gel was treated with destaining solution for ~1 hour whereat the destaining solution were changed every 20 minutes. This procedure was done until bands could be visualized with a clear background. Table 13 shows the composition of staining and destaining solution.

Tab. 13 Components of coomassie staining

Staining solution	Destaining solution
0.1% (^w / _v) Coomassie Blue R-250	40% (^v / _v) methanol
40% (^v / _v) methanol	10% (^v / _v) acetic acid
10% (^v / _v) acetic acid	50% (^v / _v) RO water
50% (^v / _v) RO water	

3.3.6. DNA-Sequencing

According to the results of expression screening (4.3.3) *E. coli* clone 14/5 was selected and the plasmid consisting of pET 21a (+) vector containing the PCC 7420 peroxidase gene was isolated and purified as described in section 3.2.3.2 with the aid of the GFX™ plasmidPrep Mini Spin kit. The sequencing was performed by AGOWA GmbH, which is a member of the LGC group. The chosen Barcode Sequencing Service of LGC Genomics is an automated and standardized ABI 3730xl sequencing run with a read length up to 1000 nt. Therefore collectively 6 Primers were designed (3 forward and 3 reverse) in order to cover the whole 1752 bp long DNA insert and to get overlapping sequence fragments as option to control the accuracy.

10 µL of purified Plasmid DNA solution containing about 40 ng/µL template DNA were send together with the 6 sequencing primers listed below.

PCC7420perox-sequ01for:

5'-TCACAAAATCCGTCAAAC-3' (18mer, Tm=57.48°C, GC=38.89%)

PCC7420perox-sequ02rev:

5'-TACCCGCACTGGTTTTG-3' (17mer, Tm=61.2°C, GC=52.9%)

PCC7420perox-sequ03for:

5'-TACGCACAGGAGACAG-3' (16mer, Tm=54.1°C, GC=56.2%)

PCC7420perox-sequ041rev:

5'-AAGAGGAAATTGCGAAC-3' (17mer, Tm=55.7°C, GC=41.2%)

PCC7420perox-sequ05for:

5'-TGTTGCAATTTCTC-3' (16mer, Tm=55.9°C, GC=43.8%)

PCC7420perox-sequ06rev:

5'-AATGTCCTTTGTTGGTG-3' (17mer, Tm=54.49°C, GC=41.18%)

3.3.7 Cryoculture of sequenced clone

A frozen stock of *E. coli* clone 14/5 containing the pET 21a (+) vector + PCC 7420 peroxidase gene insert was prepared for storing the clone for a longer period.

- 5 mL LB_{amp} medium were inoculated with a colony from the master plate (Figure 15) and grown over night at 37°C and 180 rpm.
- 500 µL of the incubated cell culture were filled into a cryotube and 500 µL of sterile 30% glycerol were added.
- The tubes were frozen at -80°C.

3.4 Large-scale expression and purification of the two cyanobacterial peroxidases from PCC 7420 and PCC 8106

Besides *E. coli* clone 14/5 containing *Microcoleus chthonoplastes* PCC 7420 peroxidase an already screened and sequenced *E. coli* clone containing *Lyngbya sp.* PCC 8106 peroxidase

was used for large-scale expression, purification and enzyme characterization. In contrast to the expression screening both large scale expressions were induced with lactose instead of IPTG.

3.4.1 Expression of cyanobacterial peroxidases in *E. coli* BL21 (DE3) Star

During the overexpression cells containing the PCC 7420 peroxidase gene grew on 2x LB medium, whereas cells containing the PCC 8106 peroxidase gene grew on M9ZB medium. Apart from that both cell types were treated in the same manner as described below.

- *E. coli* BL21 (DE3) Star cells containing the cyanobacterial peroxidases were incubated in 12 mL LB_{amp} medium at 37°C and shaken at 180 rpm.
- Cell cultures containing the PCC 7420 peroxidase were used as inoculums for 1 L 2x LB_{amp}-medium and cell cultures containing the PCC 8106 peroxidase were used as inoculums for 1 L M9ZB_{amp} medium.
- 1 L inoculated growing medium was divided into two 2 L Erlenmeyer flasks and incubated at 37°C and 180 rpm until the optical density at 600 nm (OD₆₀₀) reached a value between 0.9 and 1.2 (after 3-4 hours).
- After reaching this value as component for the active site of the enzyme, 10 mL bovine hemin solution (5 mg/mL) were added to facilitate the incorporation of heme into the protein.
- Then the expression of both peroxidases was induced with 50 mL of a 10% (^w/_v) lactose solution (final concentration 5 g/L)
- The cells were grown over night at 16°C with shaking at 180 rpm to slow down the metabolism and avoid the formation of inclusion bodies.
- The cells were harvested by centrifugation at 4000 rpm and 16°C for 6 min (Sorvall RC6 PLUS; SLA-3000 Rotor)
- The supernatant was discarded and the pellet was resuspended and transferred into 50 mL Falcon tubes and stored at least one night at -80°C.

3.4.2 Cell lysis and metal-chelate-affinity-chromatography (MCAC)

3.4.2.1 Cell lysis and sample preparation

- The cell pellet of 1000 mL *E. coli* culture was thawed and resuspended in 40 mL lysis buffer.
- The cell suspension was cooled on ice during the lysis by ultrasonic treatment (50% pulse; 2x 1 min; stage 6 micro tip limit; cp. Figure 16) and then centrifuged at 15000 rpm at 4°C for 20 min (Sorvall RC6 PLUS ,SS-34 Rotor)

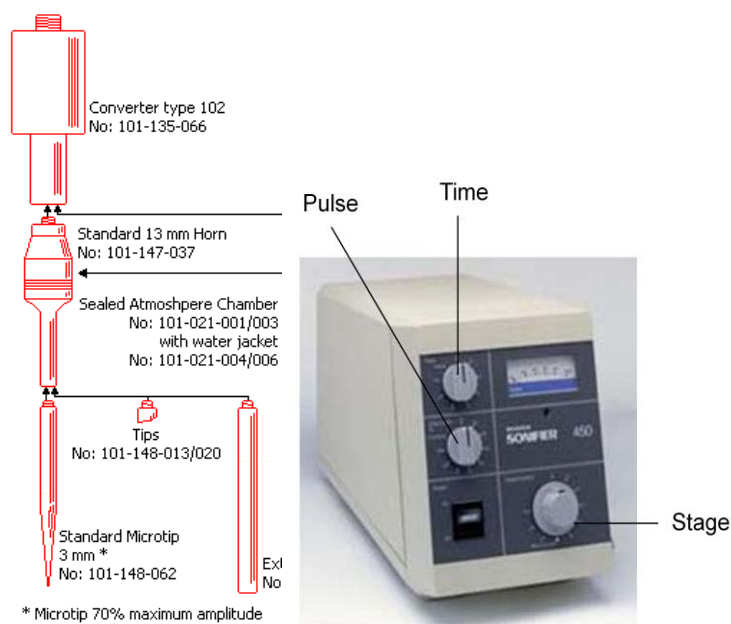


Figure 16 Components of the Sonifier II W-250

- The supernatant containing the soluble enzyme was transferred into a measuring jar and diluted 1:2 with deionized water. After dilution 1/3 of the volume 4 M NaCl (final NaCl concentration 1 M) and 1/50 of the volume 1 M imidazole (final imidazole concentration 20 mM) was added.
- The solution was mixed gently to create as less foam as possible and filtrated with the force of underpressure through a Nalgene filter funnel (filter pore size 0.45 µm). The solution was degassed by remaining in the vacuum flask until no air bubbles were left.
- Afterwards the pH was controlled (pH 7.2-7.3) and the sample was applied to the column.

The used components for large scaled expression, cell lysis and sample preparation are listed in Table 14.

Tab. 14 Components and equipment for large scale expression and sample preparation for MCAC

<p>M9ZB_{amp} medium (analog Table 11)</p> <p>Lysis buffer (analog Table 11)</p> <p>2x LB medium 40 g peptone 20 g yeast extract 5 g sodium chloride 1g ammonium chloride</p> <p>Lactose solution (10% (w/v)) 50 g lactose solved (Ultrasonic bath) in 500 mL RO water --> autoclaved</p> <p>1 M Imidazole: 6,81 g imidazole (1,0 M) 5,85 g NaCl (1,0 M) Filled up to 100 mL with 67 mM PP-buffer. pH 7,0, control pH</p>	<p>Membrane vacuum pump (Vacuumbrand CVC 2)</p> <p>Nalgene filter funnel 315-0047 with clamp</p> <p>Millipore-Filter HVLP04700 (Pore size 0,45 µm)</p> <p>Sonifier II W-250</p> <p>4 M NaCl (in 67 mM PP buffer. pH 7,2- 7,3): 93,6 g NaCl 4,38 g Na₂HPO₄·7H₂O 1,41 g KH₂PO₄</p> <p>Filled up to 400 mL with RO water, control pH, recommended storage at room temperature</p> <p>pH-Meter (Radiometer Copenhagen)</p> <p>Bovine heminchloride solution (analog Table 11)</p>
---	---

3.4.2.2 Metal chelate affinity chromatography (MCAC)

MCAC utilizes the strong interaction between certain amino acid residues in proteins, notably histidines, and metal ions that are immobilized on an adsorbent matrix. In this work sepharose with iminodiacetic acid ligands was used (Figure 17).

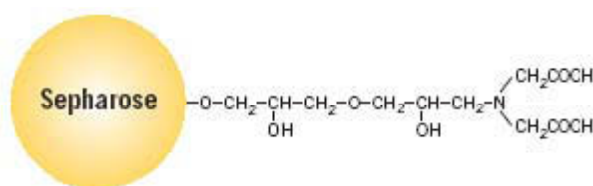


Figure 17. Sepharose with iminodiacetic acid. Matrix of the MCAC

The adsorbent consists of a metal ion complexing agent attached to the matrix in such a way that when the metal ions are introduced, they are complexed leaving part of the coordination sphere free, or rather, occupied by water molecules. These metals are then searching for

alternative ligands to complete their coordination, and residues of proteins may be suitable. In particular it has been found that surface histidine residues, and to a lesser extent cysteines and tryptophans, are mainly responsible for the interactions. There are many different metal ions that can be used; the most widely used are Zn^{2+} , Ni^{2+} , Cu^{2+} and more recently Fe^{3+} has found uses for phosphoproteins. The His•Tag has been C-terminally fused to the peroxidase genes and binds to the metal ions by complex forming. Only uncharged histidines will coordinate with the metal ion, so the pH for adsorption should be above 7.0.

In this work for the PCC 7420 peroxidase Zn^{2+} ions were used whereas the PCC 8106 peroxidase was complexed with Ni^{2+} ions which have a higher affinity to the his₆-tag. Each buffer and solution was treated in an ultrasonic bath for about 10 minutes.

- The used column had a diameter of 1.6 cm and an area of 2.0 cm.
- A small volume of degassed water was injected into the column from the bottom side by using a syringe and the base of the column was adjusted.
- New gel (Chelating Sepharose fast flow; Pharmacia Biotech) kept in 20% ethanol was filled air bubble free into the column until the gel bed had a length of ~ 10-12 cm.
- After complete sedimentation of the gel in the column, it was closed on the top, and water was pumped through by a connected peristaltic pump. The bed was further compressed at this point and the space between the bed surface and the adapter was 0.5-1 cm.
- The column was washed with 50 mL of RO water at a flow rate of 2 mL/min to remove the ethanol.
- The gel was charged with 30-40 mL of $ZnCl_2$ (5 mg/mL) solution for purification of PCC 7420 peroxidase. For the purification of the PCC 8106 peroxidase the gel was charged with $NiCl_2$ (5 mg/mL) solution until the whole gel bed was colored constant light blue. The metal ion charging was performed at a flow rate of 1 mL/min.
- The excess of metal ions was washed out with 50 mL of RO water and afterwards the column was rinsed with 50 mL 1 M NaCl (in 67 mM P. pH 7.2-7.3) with 2 mL/min.
- The prepared sample was loaded at a flow rate of 1 or 1.5 mL/min. At this point fractions were started to be collected (Fraction size 6-9 mL)
- The column was washed with 20 mM imidazole (1 M NaCl in 67 mM P. pH 7.2-7.3) solution (2 mL/min) until the flowthrough was completely clear with no coloration. (Up to 200 mL) (Fraction size 4-6 mL)

- The bound proteins were eluted with 100 mL of a 20-500 imidazole buffer gradient. The gradient mixer contained 50 mL of 20 mM imidazole and 50 mL of 500 mM imidazole. The flow rate was adjusted to 1-1.5 mL/min. (Fraction size 1.5-3 mL).
- Fractions showing a discernible red brown color were investigated UV/VIS spectroscopically and electrophoretically by using NuPAGE® Novex® Bis-Tris Mini Gels as described in 3.2.3.5. At the PCC 7420 purification all colored fractions were able to be pooled. In contrast it was necessary to investigate all of the red brown colored PCC 8106 peroxidase fractions spectroscopically and electrophoretically and only selected fractions were pooled. Results of these electrophoretical analyses are not shown.
- After elution of the protein, the column was washed with 50 mL of 50 mM EDTA to remove the metal ions and rinsed with 50 mL RO water (each at 2 mL/min).
- Then the column was washed with 50 mL of 1 M NaOH (2 mL/min)
- Finally the column was rinsed with approximately 1000 mL RO water until the flowthrough had a pH of 7.
- Usually the gel was then white and clean. When this was not the case the last two steps (NaOH; water) were repeated.
- If the column was not used again immediately, 50 mL of 20% ethanol were applied on the column for long term storage.

Tab. 15 Equipment and used solutions for MCAC

<p>4 M NaCl (in 67 mM PP buffer. pH 7.2- 7.3) analog Table 13</p> <p>1 M Imidazole analog Table 14</p> <p>67 mM PP buffer pH 7.2-7.3 21.9 g Na₂HPO₄ x 7 H₂O 7.044 g KH₂PO₄ RO water added to 2000 mL (pH was tested and adjusted)</p> <p>1 M NaCl (in 67 mM PP buffer. pH 7.2- 7.3) 125 mL 4 M NaCl (in 67 mM PP buffer. pH 7.2- 7.3) 375 mL 67 mM PP buffer pH 7.2-7.3</p>	<p>20 mM Imidazole (pH 7.0) 1.36 g imidazole 58.5 g NaCl 10.95 Na₂HPO₄ x 7 H₂O 3.52 g KH₂PO₄ RO water added to 1000 mL (pH was tested and adjusted)</p> <p>500 mM Imidazole (pH 7.0) 34.04 g imidazole 58.5 g NaCl 10.95 Na₂HPO₄ x 7 H₂O 3.52 g KH₂PO₄</p>
--	--

<p>50 mM EDTA (pH 8.0) 17.6 g NaCl (300 mM) 17.32 g Na₂HPO₄ • 7 H₂O 0.28 g KH₂PO₄ 18.6 g Na₂EDTA (50 mM) Filled up to 1000 mL with RO water pH was tested and adjusted</p> <p>20% Ethanol 208.3 mL 96% ethanol 791.6 mL RO water</p> <p>5 mg/mL ZnCl₂ 2.5 g ZnCl₂ For dilution a few drops of 1 M HCl necessary, then filled up to 500 mL with RO water</p> <p>5 mg/mL NiCl₂ 2.5 g NiCl₂ Solved in 500 mL RO water</p>	<p>RO water added to 1000 mL (pH was tested and adjusted)</p> <p>Chelating Sepharose Fast Flow (Pharmacia Biotech) in 20% ethanol Capacity 30 μmol Zn²⁺ or Ni²⁺/mL</p> <p>Ultrasonic bath Bandelin Sonorex Super RK 510 H</p> <p>Gradient mixer BioRad type 385 Gradient Former Capacity 30-100 mL</p> <p>Column with stamp (Pharmacia) d=16 mm; A=20.1 mm; l=30 cm; V=60 mL</p> <p>Fraction collector (Pharmacia Biotech) LKB 2111 Multirac</p> <p>Peristaltic pump Pharmacia Peristaltic Pump P-1; i. d. 3.1 mm</p>
--	---

3.4.3. Ultrafiltration and desalting of the protein

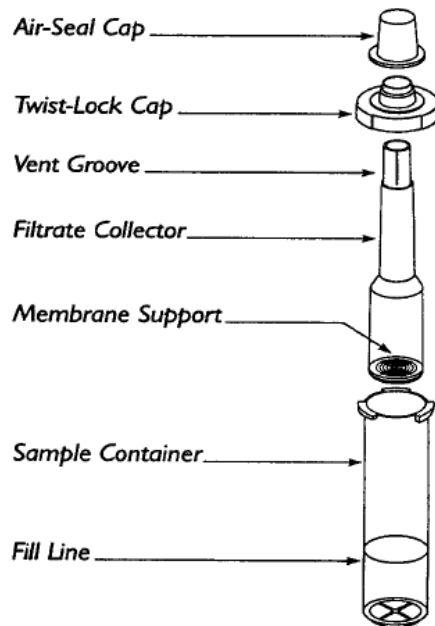


Figure 18. Amico Centriprep

The selected fractions after MCAC were pooled and afterwards concentrated with Amicon Centripreps to reduce the sample volume. Centriprep devices consist of a sample container with a twist-lock cap, a filtrate collector containing a low adsorptive cellulose membrane, plus an air-seal cap for sample isolation. Based on the principle of ultrafiltration the membrane of the centriprep let pass smaller molecules like water, found after centrifugation in the filtrate collector, while bigger components (protein) are retained in the sample container (Figure 19) [29]. Due to the molecular weight of the two cyanobacterial peroxidases Amicon centriprep-30 with an exclusion size of 50 kDa was used.

Amicon Centripreps- were filled up to the fill line (~15 mL) with pooled protein solution and subsequently centrifuged at 2500 rpm at 4°C for 20 min (Sorvall RC6 PLUS, SLA-1500)

The content of the filtrate collector was discarded and the centrifugation step was repeated 3 times.

Due to agglutination of recombinant protein it was not possible to perform more than collectively 4 centrifugation runs.

To remove the high amounts of NaCl and imidazole the sample was desalted afterwards.

3.4.3.1 Desalting of proteins with PD-10 columns

PD-10 Desalting Columns contain 8.3 mL Sephadex G-25 Medium (bed high 5 cm), which allows rapid group separation of high molecular weight substances from low molecular weight substances. These columns are used for desalting; buffer exchange and sample clean up. Thereby molecules larger than the largest pores in the Sephadex matrix are excluded from the

matrix and are eluted first in or just after void volume. The exclusion limit (M_r , for globular proteins) for PD-10 Desalting Columns is 5000 Da. The Sephadex G-25 medium is held within two sintered polyethylene frits with a pore size of 50-150 μm to protect the gel from running dry under gravitational buffer flow. They are capable of handling sample volumes up to 2.5 mL. The columns were washed with RO water before and after each application. The washing of the column and the following steps were performed at a temperature of 4°C.

- The top and bottom cap of the column were removed, the column storage solution poured away and the sealed end of the column tip was cut at notch.
- The column was equilibrated with approximately 25 mL of 10 mM phosphate buffer (pH 7.0).
- 2 mL of the concentrated sample applied to the column.
- After the sample has entered the packed bed completely it was eluted with 3.5 mL of 10 mM phosphate buffer (pH 7.0). The first eluted 1.2-1.5 mL were discarded and the remaining 2 mL were the desalted protein solution. The adherence of the even described volumes was necessary for the case of protein solution with weak coloring.
- Afterwards the column was washed with 25 mL RO water.

Optionally the eluted sample could be concentrated again as described in 3.3.3.1.

Finally the protein solutions of both cyanobacterial peroxidases were investigated by using electrophoresis according to 3.2.3.5 and the spectral features were characterized. Results are shown in 4.4.1.

The purified proteins were aliquoted in 2 mL and stored at -80°C.

3.5 Spectroscopic characterization of cyanobacterial peroxidases.

3.5.1 Determination of protein concentration by UV-Vis spectroscopy

For all further purposes it was necessary to know the enzyme concentration. Therefore the frozen protein solution was thawed and UV-Vis spectra (wavelength range 200-800 nm) were recorded on a diode array spectrometer. The protein concentration was calculated using Lambert-Beer's law and the absorption at 412 nm (Soret peak of heme).

$$A_{412 \text{ nm}} = c \cdot \epsilon_{412 \text{ nm}} \cdot d \quad (1)$$

$\epsilon_{412 \text{ nm}}$ is the molar extinction coefficient at 412 nm. The real value of the coefficient was not measured for the cyanobacterial enzymes in this work. It was estimated to be $10^5 \text{M}^{-1} \text{cm}^{-1}$ in accordance to the extinction coefficients of the mammalian peroxidases.

c concentration (mol/L)

$A_{412 \text{ nm}}$ Absorbance at 412 nm

d diameter of the cuvette (1 cm)

Additionally the "Reinheitszahl" was determined by dividing the absorption of the protein solution at 412 nm by the absorption at 280 nm (protein peak).

$$RZ = \frac{A_{412 \text{ nm}}}{A_{280 \text{ nm}}} \quad (2)$$

3.5.2 Circular dichroism (CD) spectroscopy

3.5.2.1 Principles of CD spectroscopy

Electromagnetic waves are periodic changes of electric and magnetic fields in space and time. They propagate at the speed of light. At any point of a light beam the magnetic field is always perpendicular to the electric field. Each wave has magnitude and oscillation properties. The wave magnitude is constant and the direction oscillates causing the electric vector to trace a circle. As the light beam is passed through an optically active sample, the magnitude of waves will be altered as a result of changes in the molar extinction coefficients of the left and right handed polarized light. The electric vector now traces an ellipse instead of a circle as pictured in Figure 19.

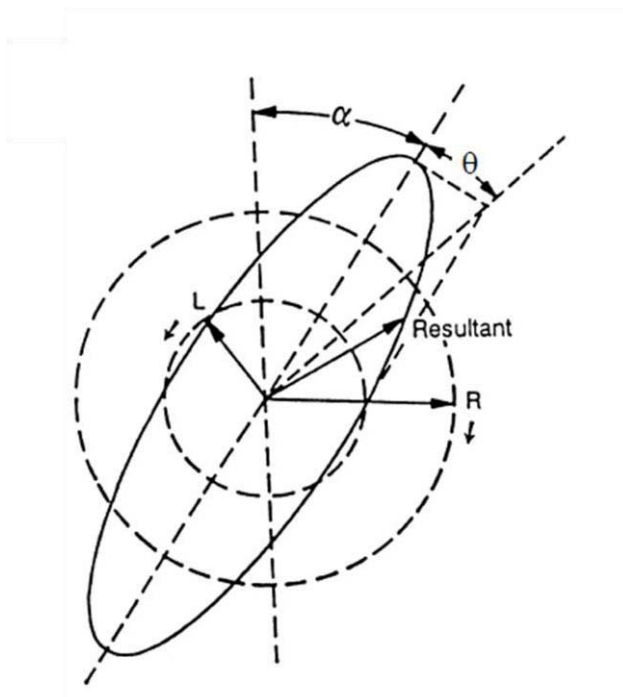


Figure 19 shows the transition from circular polarized light to elliptic form. The angle between the major axis of the ellipse and the plane of the incident polarized light correspond to the optical rotation α . The resultant electric vector that prescribes an ellipse is defined by the ellipticity θ (delta).

Generally circular dichroism (CD) instruments measure in terms of ellipticity, which is directly proportional to the circular dichroism and related to the difference in absorbance by $\theta = 32.98 \Delta A$ (degree or mdeg). ΔA is the difference in absorbance between left and right polarized light. To

remove the dependence on cuvette pathlength and solution concentration, one can use molar ellipticity $[\theta]$ and mean residual molar ellipticity $[\theta]_{MRW}$.

Molar ellipticity $[\theta]$:
$$[\theta] = \frac{\theta}{c \cdot d} \cdot 100 \quad (3)$$

Mean residual molar ellipticity $[\theta]_{MRW} = \frac{[\theta]}{N} \quad (4)$

c concentration of the enzyme (mol/L)

d optical pathlength

N number of amino acids

The factor 100 is due to the use of measure of d in centimeter. Mean residual ellipticity is used only in the far UV range (wavelength 180-250 nm) in the analysis of the overall secondary structure of proteins where the peptide bond is the optically active component. A CD spectrum is obtained when the dichroism is measured as a function of wavelength.

Chiral molecules and chromophores are optically active groups within the protein. Prime candidates are backbone amide bonds and disulphide bonds as well as aromatic side chains such as phenylalanine, tryptophan and thyrosine to a lesser extent. In secondary structure conformations, the backbone and hence the amide bond chiral molecules are arranged in regular organized patterns. CD spectroscopy is extremely sensitive to these patterns and each conformation gives rise to characteristic spectral feature. The direct relationship between protein secondary structure and circular dichroism spectra means that the circular dichroism spectra can be exploited for prediction of protein conformation and to determine α -helix and β -sheet structures in proteins. The common types of secondary structure caused by peptides and proteins show distinctive CD spectra in the far UV (Chart 1).

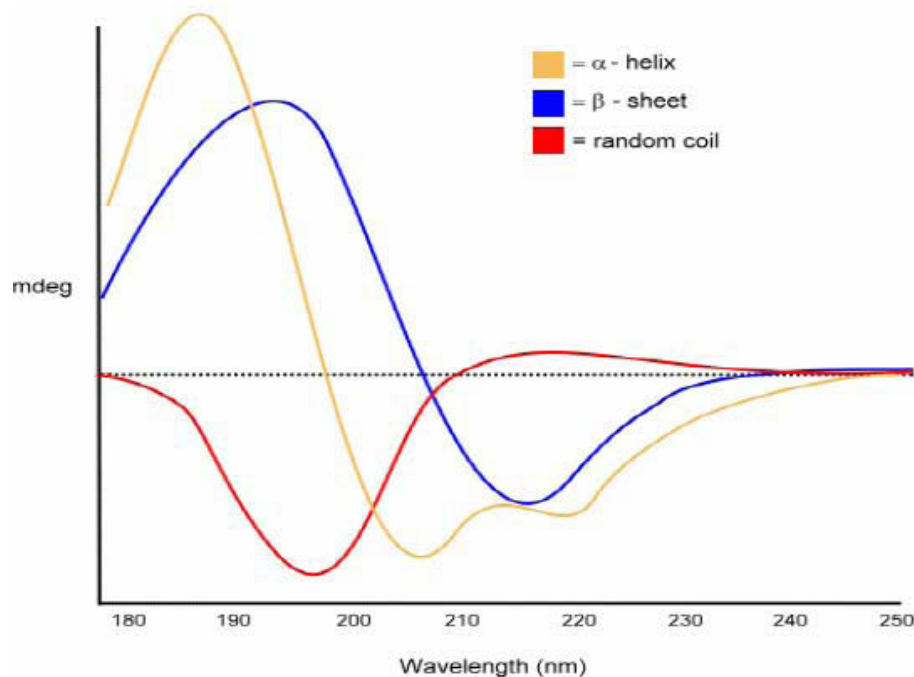
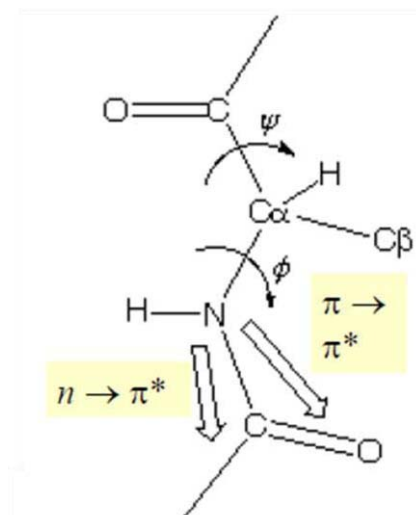


Chart 1 shows the characteristic CD spectra of α -helix, (yellow), β -sheet (blue), and random coil (red) in the far-UV region (180- 250 nm)

Studies of the far UV region (180-250 nm) can be used to assess quantitatively the overall secondary structure content of proteins. In this region the absorbing group is principally the peptide bond. There is a $n \rightarrow \pi^*$ transition, weak in absorption but often strong in CD, centered around 210 nm, and a $\pi \rightarrow \pi^*$ transition near 190 nm, which is strong in both absorption and in CD. The intensity and energy of these transitions depend on the angles Φ (phi) and Ψ (psi). These are two degrees of freedom per residue for the peptide chain and define the conformation of the tertiary structure. Rotation is allowed between the α -carbon and the carbon of peptide bond (denoted by Φ). The CD spectrum of each secondary structure is assumed to be independent of the others and the resulting CD spectrum is a simple summation.



Several factors influence the intensities of near UV CD bands (250-340 nm) deriving from aromatic amino acids. Amongst these are the extent to which the residue is mobile (rigidity of the protein) and the extent to which the aromatic ring interacts with its surroundings. Intense CD bands tend to be observed when the residue is immobilized and when it interacts with neighboring aromatic residues. Because CD bands from individual residual may either be positive or negative and may vary widely in intensity it is often difficult to separate out the contributions of individual aromatic residues in a protein. Near UV CD provides a sensitive fingerprint for the native state of a protein. Beside aromatic amino acid side chains contributions come from disulfide bonds and non-protein cofactors like heme which might absorb in this spectral region. Furthermore the CD bands around the Soret peak (412 nm) were of closer interest for the recombinant cyanobacterial enzymes.

3.5.2.2 Sample preparations and CD measuring settings

Experiments were carried out using the Applied Photophysics Chirascan CD Spectrometer. The two recombinantly produced cyanobacterial enzymes were measured together with bovine LPO and human MPO. Each enzyme solution was diluted until the absorption maximum of the 280 nm protein peak had a value of 0.6 related to a 1 cm cuvette. Measurements of two regions were taken, the far UV- region from 190-290 nm and the near UV/Vis- region from 250-500 nm in order to cover the region of the Soret band (412 nm). The pathlength of the cuvette for the far UV region was 1 mm whereas for the near UV-Vis region a cuvette with a pathlength of 1 cm was used. Table 16 shows the parameters in the Chirascan software used for both regions.

Tab. 16 Summarized setting for all CD measurements.

Settings	190-290 nm	250-500 nm
Pathlength	1 mm	10 mm
Step size	1 nm	1 nm
Bandwidth	2 nm	1 nm
Time per point	8 s	4 s
Repeats	2	2

3.6. Determination of peroxidase and halogenation activities.

The two cyanobacterial peroxidases were tested for conversion of putatively two-electron donors (iodide, bromide and chloride) and one electron donors (ABTS, guaiacol and tyrosine). All activities except the peroxidase activity with tyrosine were measured spectrophotometrically (Hitachi U-3000, ZEISS SPECORD UV VIS S10). The tyrosine activity was measured on a spectrofluorimeter (Hitachi F-4500).

3.6.1 Iodination activity

As described in section 1.5 all heme peroxidase can convert iodide, consequently this substrate was suited to test if the cyanobacterial peroxidases had a halogenation activity. The increase of the secondary product of the halogenation reaction triiodide (I_3^-) was measured spectrometrically at a wavelength of 353 nm ($\epsilon_{353 \text{ nm}} (I_3^-) = 25.5 \text{ M}^{-1}\text{cm}^{-1}$). A pH-profile was recorded. Table 17 shows the components of the iodination activity assay.

Tab. 17 Components of iodination activity assay

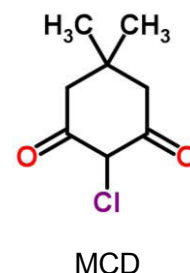
Solution	Sample	Blank
200 mM buffer (phosphate/citrate) pH X ($c_{\text{end}} = 100 \text{ mM}$)	500 μL	500 μL
Cyanobacterial peroxidase sample ($c_{\text{end}} = 25\text{-}50 \text{ nM}$)	50 μL	-
500 mM KI ($c_{\text{end}} = 50 \text{ mM}$)	100 μL	100 μL
1 mM H_2O_2 ($c_{\text{end}} = 0.1 \text{ mM}$)	100 μL	100 μL
RO water	250 μL	300 μL

A baseline at 353 nm was measured and the reaction was started with 50 μL of peroxidase sample.

3.6.2 Bromination activity

Bromide as substrate is more specific than iodide, not all heme peroxidase are able to convert bromide. For mammalian peroxidases bromide is a very important substrate, especially for human EPO it is under physiological conditions the most prominent electron donor.

Monochlorodimedon (MCD) is a substrate often used to study halogenations reactions. Upon brominating or chlorinating (DCD) it loses its absorbance at 290 nm. Rates of peroxidases mediated MCD halogenation were determined from the initial linear part of the time traces followed at 290 nm. ($\epsilon_{290\text{nm}}(\text{MCD}) = 17.7 \text{ mM}^{-1}\text{cm}^{-1}$ [39]). Table 18 shows the components of the bromination activity assay.



Tab. 18 Components of MCD bromination activity assay

Solution	Sample	Blank
200 mM buffer (phosphate/citrate) pH X ($c_{\text{end}} = 100 \text{ mM}$)	500 μL	500 μL
Cyanobacterial peroxidase sample ($c_{\text{end}} = 25\text{-}100 \text{ nM}$)	50 μL	-
1 M KBr ($c_{\text{end}} = 100 \text{ mM}$)	100 μL	100 μL
1 mM MCD (solved in RO water)	100 μL	100 μL
1 mM H_2O_2 ($c_{\text{end}} = 0.1 \text{ mM}$)	100 μL	100 μL
RO water	150 μL	200 μL

A baseline at 290 nm was measured and the reaction was started with 50 μL of peroxidase sample. KBr and MCD were solved by using the ultrasonic bath. Bromination activity of both cyanobacterial peroxidases was measured from pH 7 to pH 3

3.6.3 Chlorination activity

As described in section 1.5 only Compound I of MPO oxidizes chloride at reasonable rates at pH 7. Preliminary tests at several pH values have indicated that PCC 7420 peroxidases showed no or very weak chlorination activity whereas PCC 8106 peroxidase seemed to oxidize chloride at lower pH values. Consequently only the PCC 8106 peroxidase was tested again at several pH values compared to human MPO. The UV absorbing substrate MCD was used again according

to 3.5.2 and the KCl concentration was set to 300 mM. The mixture was prepared according to Table 19.

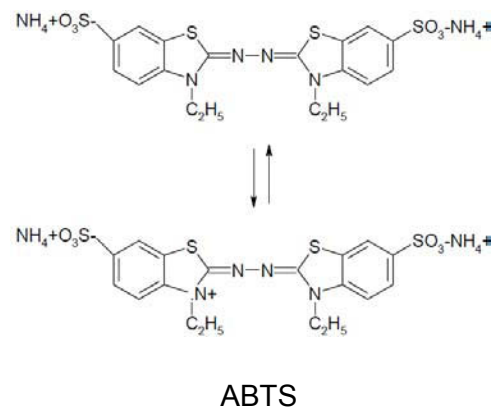
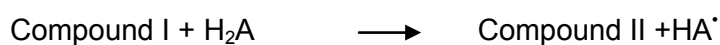
Tab. 19 Components of MCD chlorination activity assay

Solution	Sample	Blank
200 mM buffer (phosphate/citrate) pH X ($c_{\text{end}} = 100 \text{ mM}$)	500 μL	500 μL
Cyanobacterial peroxidase sample ($c_{\text{end}} = 50 \text{ nM}$)	50 μL	-
3 M KCl ($c_{\text{end}} = 300 \text{ mM}$)	100 μL	100 μL
1 mM MCD (solved in RO water)	100 μL	100 μL
1 mM H_2O_2 ($c_{\text{end}} = 0.1 \text{ mM}$)	100 μL	100 μL
RO water	150 μL	200 μL

A baseline at 290 nm was measured and the reaction was started with 50 μL of peroxidase sample. KCl and MCD were solved by using the ultrasonic bath. PCC 8106 peroxidase was measured from pH 7 to pH 3.

3.6.4 ABTS-peroxidase assay

The one electron donor ABTS is converted by peroxidases with the aid of H_2O_2 according to following peroxidase mechanism.



The increase of the oxidation product HA^\bullet was recorded spectrometrically at a wavelength of 414 nm ($\epsilon = 31100 \text{ M}^{-1}\text{cm}^{-1}$) [38].

The mixture for the ABTS activity assay was prepared analog Table 20.

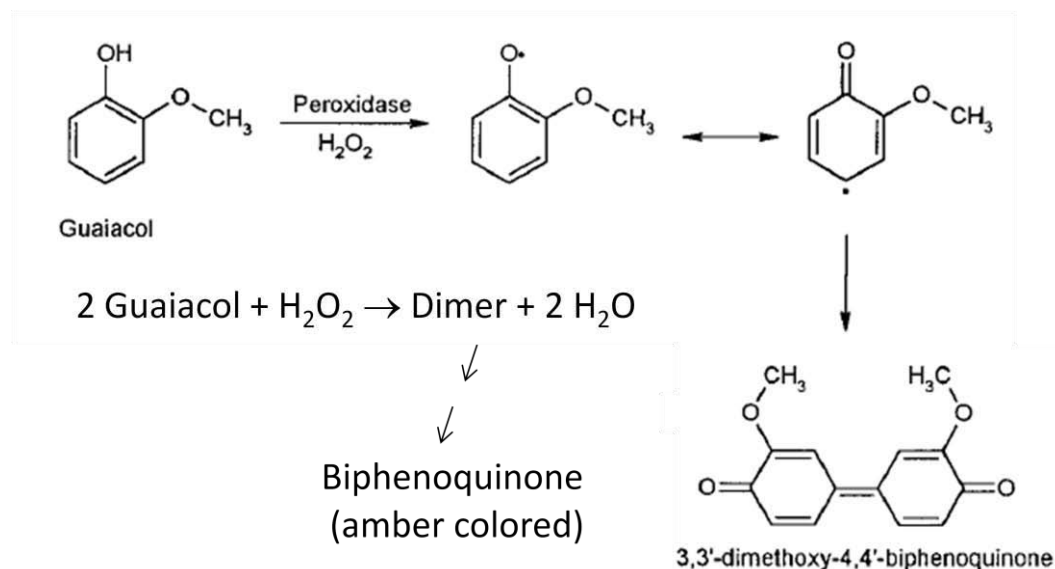
Tab. 20 Mixture of the ABTS activity assay.

Solution	Sample	Blank
200 mM buffer (phosphate/citrate) pH X ($c_{\text{end}} = 100 \text{ mM}$)	500 μL	500 μL
Cyanobacterial peroxidase sample ($c_{\text{end}} = 50\text{-}100 \text{ nM}$)	50 μL	-
10 mM ABTS ($c_{\text{end}} = 1 \text{ mM}$)	100 μL	100 μL
1 mM H_2O_2 ($c_{\text{end}} = 0.1 \text{ mM}$)	100 μL	100 μL
RO water	250 μL	300 μL

A baseline at 414 nm was measured and the peroxidase reaction was started with 50 μL of peroxidase sample. Both cyanobacterial peroxidases were measured from pH 9 to pH 3, additionally ABTS activity of bovine LPO and human MPO were measured at several pH values.

3.6.5 Guaiacol peroxidase assay

The colorimetric assay of peroxidase activity using guaiacol is based on the following reaction scheme proposed by Doerge et al. [37] at which intermediates are not shown. The increase of the subsequently formed colored biphenoquinone ($\epsilon = 26.6 \text{ mM}^{-1}\text{cm}^{-1}$) was measured at 470 nm.



The mixture for the guaiacol activity assay was prepared analog Table 21.

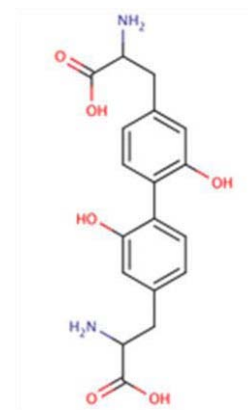
Tab. 21 Mixture of the guaiacol activity assay

Solution	Sample	Blank
200 mM buffer (phosphate/citrate) pH 7 and 5.5 ($c_{\text{end}} = 100 \text{ mM}$)	500 μL	500 μL
Cyanobacterial peroxidase sample ($c_{\text{end}} = 50\text{-}200 \text{ nM}$)	50 μL	-
1 mM Guaiacol ($c_{\text{end}} = 1 \text{ mM}$)	100 μL	100 μL
1 mM H_2O_2 ($c_{\text{end}} = 0.1 \text{ mM}$)	100 μL	100 μL
RO water	150 μL	200 μL

A baseline at 470 nm was measured and the peroxidase reaction was started with 50 μL of peroxidase sample. The two cyanobacterial peroxidases, human MPO, and bovine LPO were measured at the pH values 7.0 and 5.5.

3.6.6. Tyrosine peroxidase assay

Dityrosine formation from tyrosine was followed spectrofluorometrically on a Hitachi F-4500 spectrofluorimeter. The components of the mixture for the tyrosine peroxidase assay are listed in Table 22 and the adjustments in the FL Solutions F-7000 software are listed in Table 23. All parameters were chosen in accordance to Zederbauer et al. [40].



Dityrosine

Tab. 22 Mixture of the tyrosine activity assay

Solution	Sample	Blank
200 mM buffer (phosphate) pH 7 ($c_{\text{end}} = 100 \text{ mM}$)	1000 μL	1000 μL
Cyanobacterial peroxidase sample ($c_{\text{end}} = 50\text{-}200 \text{ nM}$)	50 μL	-
1 mM Tyrosine ($c_{\text{end}} = 200 \text{ }\mu\text{M}$)	400 μL	400 μL
1 mM H_2O_2 ($c_{\text{end}} = 0.1 \text{ mM}$)	200 μL	100 μL
RO water	350 μL	400 μL

The reaction was started with 50 μL of peroxidase sample. The two cyanobacterial peroxidases, human MPO, and bovine LPO were measured at the pH 7.0. Tyrosine is hardly soluble, hence the 1 mM stock solution was solved repeatedly in an ultrasonic bath.

Tab. 23 Adjustments in the FL Solutions F-7000 software

Measure type	Time scan
Data Mode	Fluorescence
Scan time	70 s
Excitation wavelength	325 nm
Emission wavelength	405 nm
Delay time	0.0 s
Excitation slit	2.5 nm
Emission slit	2.5 nm
PMT voltage	700 V
Response	0.5 s
Shutter control	off

3.7 Cyanide Binding

The bimolecular association of a ligand (S Substrate) to an enzyme (E) can be described according to the law of mass action through the association constant K_a or its reciprocal the dissociation constant K_d .



For reactions in which protons (H^+) participate, an apparent equilibrium constant is defined K_{app} , which depends on the pH-value in contrast to the real K_d constant.

$$K_{\text{app}} = K_d [\text{H}^+]$$

When cyanide is added to peroxidase solutions, it diffuses into the distal cavity and coordinates directly to iron (III). Cyanide binds very tightly to iron (III) and convert the protein into a low spin

species ($S = 1/2$). The pH dependency of cyanide binding resembles that of H_2O_2 in Compound I formation, since both require the deprotonation of the distal histidine [29].

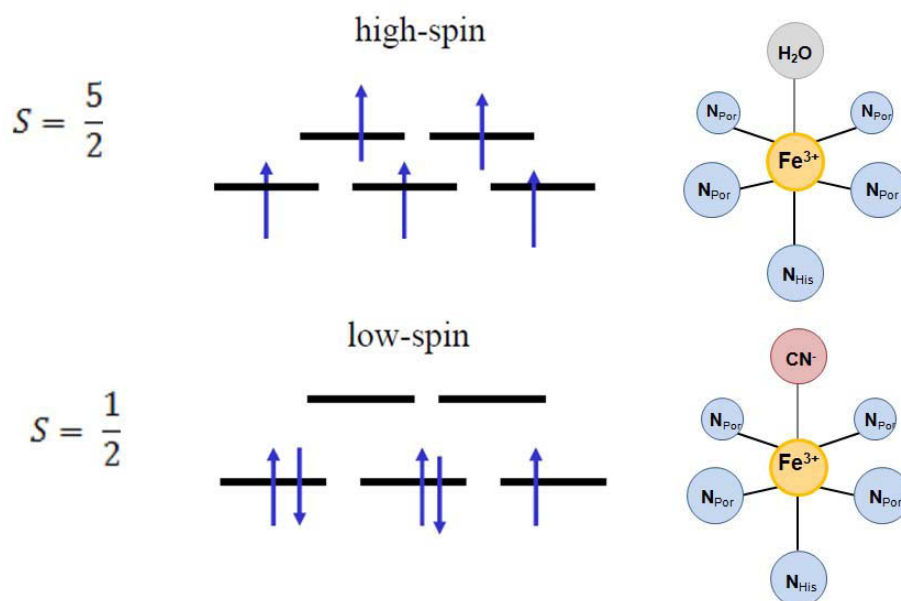


Figure 20. Electron structure of a six coordinated high and low spin complex .

Upon binding of cyanide to peroxidases in its iron (III) high-spin state, the absorption spectrum changes significantly. These spectral changes of the two cyanobacterial peroxidases remained to be investigated. Thereby two methods were used to determine the K_d values for cyanide binding. On the one hand cyanide was step by step added to a peroxidase solution in a cuvette and the spectral changes were followed spectrophotometrically and on the other hand the K_d values were determined by using stopped flow measurement.

3.7.1 Determination of K_d values by using spectrophotometrical cyanide titration

A silica glass cuvette with magnetic stirrer was used. 2 mL peroxidase solution pH 7 (10 mM phosphate buffer) were filled into the cuvette. The first ligand concentration in the cuvette was 50 μM and was raised stepwise with nearly unchanging protein concentration. The change of volume per cyanide addition step should be a minimum (not more than 1 μL), hence two NaCN stock solutions were prepared with concentrations of 100 mM and 1 M. The spectral changes were followed on a ZEISS Specord UV VIS S10. Afterwards difference spectra were calculated

with the aid of the Aspect_Plus software, to find out the wavelength that showed the maximum changes in absorption (ΔA). For the interpretation these changes in absorption were plotted against their originating CN^- concentration. Finally the K_d values were calculated by using the Double Reciprocal Plot and the Scatchard Plot.

3.7.2. Determination of K_d values by using stopped-flow spectroscopy.

While steady-state kinetic methods measure only the rate limiting step of a complex pathway when only one substrate is involved, transient-state kinetic methods are able to provide information about the whole pathway of a complex reaction sequence, as well as the rate of each reaction. The measurement of transient-state kinetics of enzymes requires rapid mixing techniques, which allow measuring the kinetics of a reaction in the millisecond time scale. The stopped-flow method is the most widely used method to study fast reactions. In this work a stopped-flow apparatus, an appropriate computer system and software from Applied Photophysics were used. The reactions were monitored by using a diode-array detector and alternatively a photomultiplier detector. The essentials of a stopped-flow apparatus are shown in Figure 21.

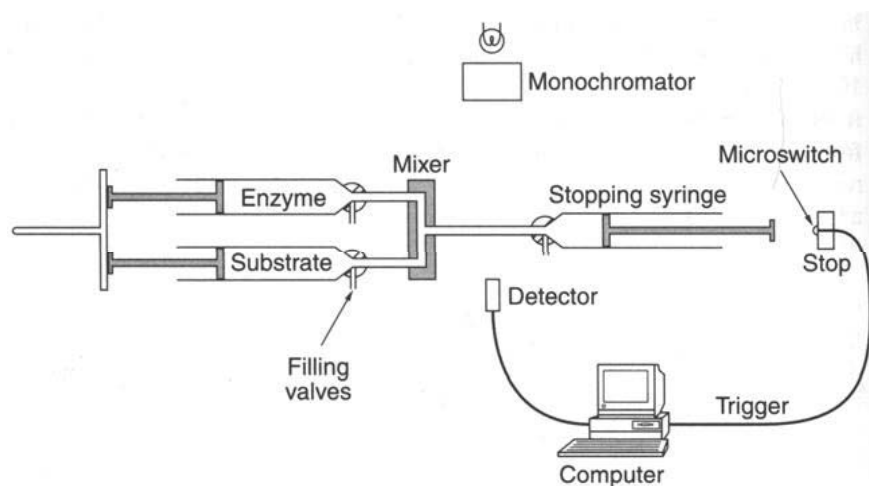


Figure 21. Essentials of a stopped-flow apparatus; Two drive syringes containing the reacting species, a mixing device and observation cell, a stop syringe, a detecting system and a recording system capable of responding very rapidly [29].

The analysis of the reactions was performed with the scanning software from XScan or the Pro-K simulation program from Applied Photophysics.

At stopped flow measurements the reaction is started by pushing the two drive syringes simultaneously. This causes the two reactants to mix, and the mixture is forced to the observation cell and into the stop syringe. A short movement of the stop syringe brings it to a mechanical stop, which prevents further mixing and simultaneously activates the detecting and recording system. The time that inevitably elapses between the first mixing of reactants and the arrival of the mixture in the observation cell is called the dead time of apparatus, and is commonly in the order of 1 ms. Furthermore elimination and prevention of air bubbles are of great importance for rapid mixing experiments.

Generally experiments are performed by mixing a substrate with the enzyme and monitoring the signal as a function of time after mixing. Most experiments are performed with substrate in at least 10-fold molar excess over enzyme so that the concentration of substrate can be assumed to be constant during the time course of the reaction. Correspondingly, the second order reaction of substrate with enzyme is reduced to pseudo first order kinetics. This fact simplifies the kinetics and is really a necessary assumption required to solve explicitly the equations describing the time dependence of the reaction.

For the interpretation the first order rate constant (k_{obs}) is plotted toward the substrate concentration in the diagram. The slope of the resultant straight line corresponds to the second order rate constant (K_{app} or K_{d}) of the reaction.

3.7.2.1 Reaction of cyanobacterial peroxidases with cyanide

Determination of the spectra was accomplished by means of diode array stopped flow apparatus. The enzyme concentration of the cyanobacterial peroxidases was around 2 μM (in 100 mM phosphate buffer pH 7). In both cases a final concentration of 10 mM cyanide was used. The spectral changes were analyzed with the Pro-K simulation program from Applied Photophysics.

The determination of the second order rate constants for formation of the enzyme-cyanide complex was determined for both cyanobacterial enzymes at 426 nm. The cyanide concentrations for the PCC 8106 peroxidase were 50 μM , 100 μM , 250 μM , 400 μM , 500 μM , 600 μM , and 1 mM and the cyanide concentrations for PCC 7420 peroxidase were 500 μM , 1 mM, 2 mM, 5 mM, 10 mM, 25 mM, and 50 mM.

3.8 Reaction of ferric enzymes with H₂O₂

Like cyanide binding, determination of H₂O₂ spectra was performed with the aid of diode array stopped flow apparatus. The enzyme concentration was around 2 μM (in 100 mM phosphate buffer pH 7). In case of the PCC 8106 peroxidase a final H₂O₂ concentration of 5 μM was used and for the PCC 7420 peroxidase a final concentration of 50 mM was chosen. Hydrogen peroxide was applied as substrate to oxidize the enzymes to Compound I and to observe the spectroscopic changes during the pre steady state phase.

The determination of the second order rate constants for formation of the intermediate Compound I was performed by using the conventional mixing mode as described in 3.6.2 and a photomultiplier detector. The PCC 7420 was measured at 408 nm and the used H₂O₂ concentrations were 5 mM, 10 mM, 25 mM, 50 mM, and 100 mM. Compound I formation of PCC 8106 peroxidase was followed at 406 nm with concentrations of 10 μM, 20 μM, 40 μM, 50 μM, 60 μM, 80 μM, and 100 μM. Additionally the increase of the PCC 8106 peroxidase Soret peak at 428 nm was measured at concentration of 50 μM, 100 μM, 150 μM, 200 μM, 300 μM, and 500 μM.

4. Results and Discussion

4.1.1 Peroxidase sequence alignment

Figure 22 shows the result of the multiple sequence alignment. In order to give a better overview about the similarity between the two cyanobacterial and the chosen mammalian peroxidase sequences, the whole amino acid sequence of each peroxidase is pictured in Figure 22. The functions of all labeled amino acids have already been described in section 1.4.

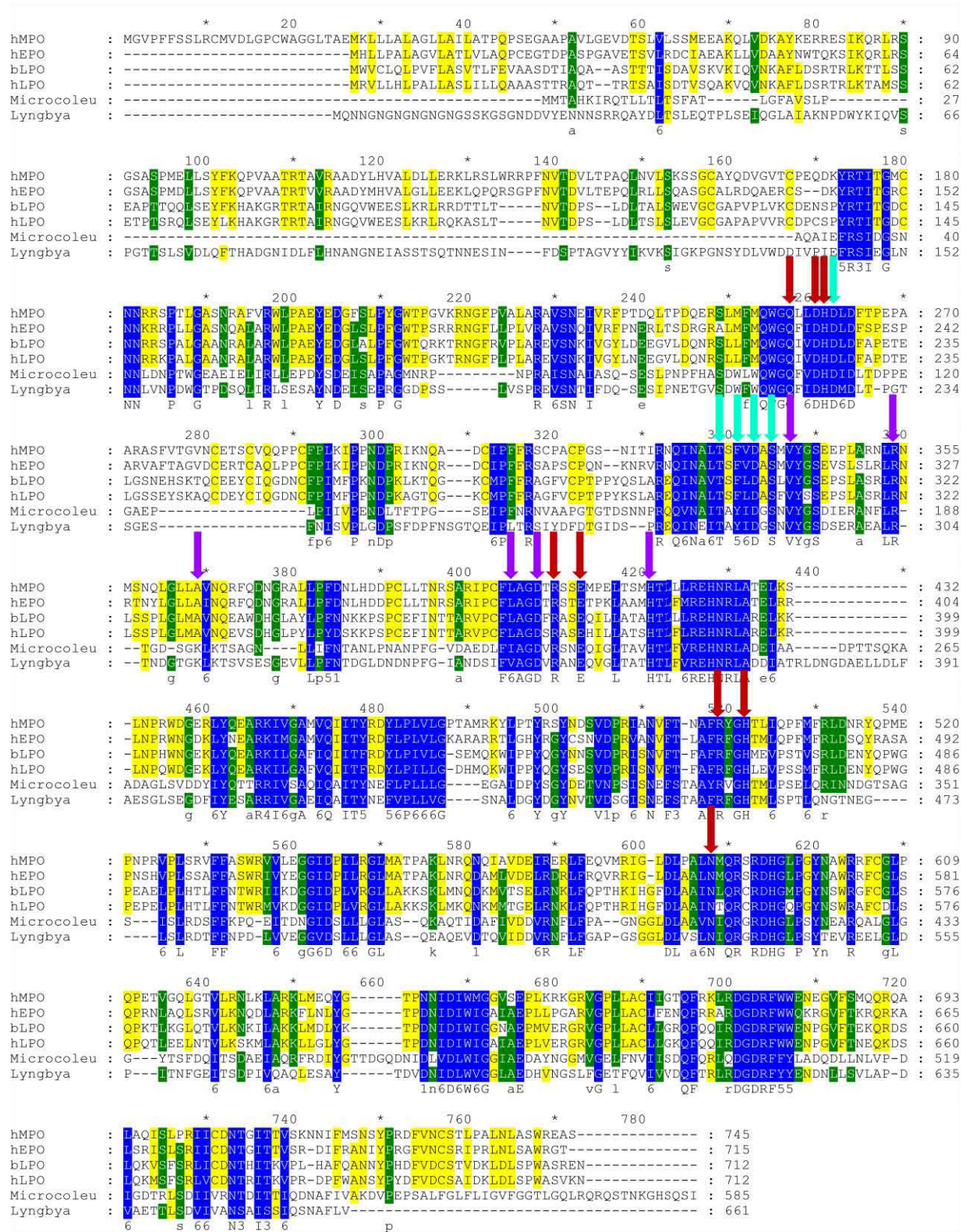


Figure 22. Multiple sequence alignment of the human peroxidases MPO, LPO, and EPO with *Microcoleus chthonoplastes* (PCC 7420) and *Lyngbya sp.* (PCC 8106) peroxidase domains and additionally bovine b, lactoperoxidase were aligned. Labeled with red color are the proximal and distal essential amino acids in mammalian peroxidases. Labeled in blue color is the highly conserved loop containing 4 amino acids providing 5 ligands for Ca²⁺ in the calcium binding site. The other two ligands come from the fifth blue labeled aspartate adjacent to the distal histidine. Labeled in violet color are the six amino acids that are involved beside the distal histidine in MPOs hydrogen bond chain to the surface of the protein proposed by Fiedler et al [27].

For both cyanobacterial peroxidase sequences many highly conserved regions were obtained compared to the mammalian peroxidases. *M. chthonoplastes* (PCC 7420) as well as *Lyngbya sp.* (PCC 8106) show two essential amino acids for the heme to protein linkage, the aspartate and the glutamate such as LPO and EPO. The methionine for the third linkage like in MPO is not present (Figure 22). Also the distal histidine and the adjacent two ligands for the calcium binding site providing aspartate were present. Both cyanobacterial peroxidases also exhibit the distal with histidine interacting arginine. On the proximal heme site all aligned peroxidases possess the three amino acids His, Arg and Asn. At the calcium binding site all residues are identical except the phenylalanine in the mammalian peroxidases is a tyrosine. In contrast to phenylalanine, tyrosine provides one additional hydroxyl group. The catalytic and structural functions of these essential amino acids are already described in section 1.4.

The H-bonding network of MPO includes Val, Leu, Ala, Leu, Asp, and His and is found in the three human peroxidases. This hydrogen bond chain was proposed by Fiedler et al [27] and is not well investigated. In spite of that the alignment showed that this motif had also high similarities. One Leucine in *M. chthonoplastes* (PCC 7420) peroxidase is an isoleucine and in *Lyngbya sp.* (PCC 8106) peroxidase a valine. The Alanin that resides presumably at the edge of the MPO protein which is also present in the other mammalian peroxidases is in the cyanobacterial peroxidases a lysine. The four other residuals are identical among all aligned sequences.

4.1.2. Protein parameters

4.1.2.1 Signal peptide prediction

SignalP 3.0 consists of two different predictors based on Neural Network and Hidden Markov Model algorithms. Detailed information of these two algorithms can be found on the SignalP 3.0 server.

Microcoleus chthonoplastes (PCC 7420) peroxidase sequence:

SignalP Neural Network (NN) prediction:

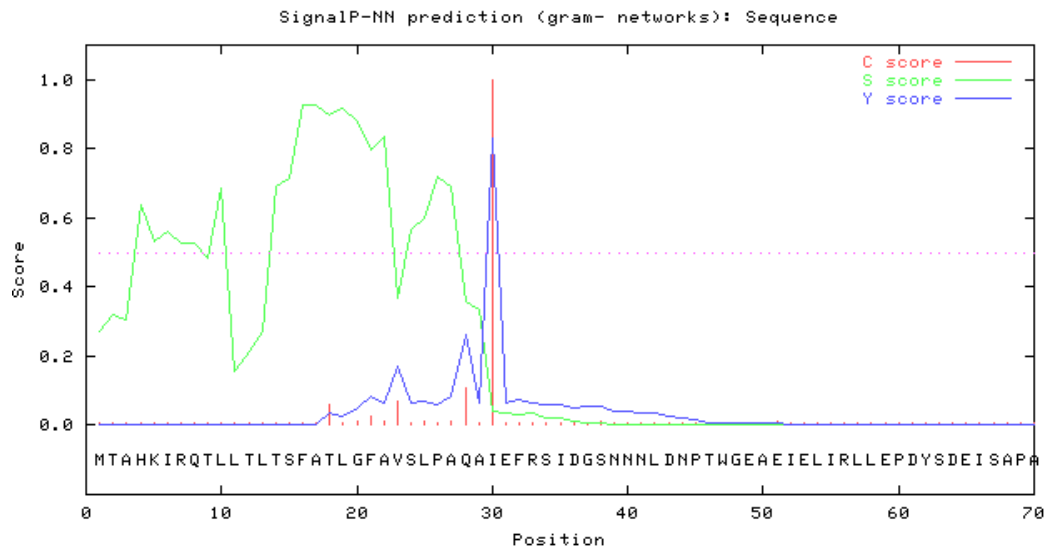


Chart 2. shows the graphical output from SignalP neural network comprising three different scores, C,S and Y. The S-score (green) is reported for every single amino acid position in the submitted *Microcoleus chthonoplastes* (PCC 7420) sequence, with high scores indicating that the corresponding amino acid is part of a signal peptide, and low scores indicating that the amino acid is part of a mature protein. The C-score (red) is the “cleavage site” score. This score is reported for each position of the submitted and should only be significantly high at the cleavage site (of signal peptidase I). In this case the position 30 has the highest value which means the isoleucine on position 30 is the first amino acid of the mature protein. The Y-score is a derivative of the C-score combined with the S-score resulting in a better cleavage site prediction than the raw C-score alone. This is due to the fact that multiple high peaking C-score can be found in one sequence , where only one is the true cleavage site. The cleavage site is assigned from the Y-score where the slope is steep and a significant C-score is found. (cp. SignalP 3.0 Server)

Computed output:

```
# Measure  Position  Value  Cutoff  signal peptide?
max. C     30         0.998  0.52   YES
max. Y     30         0.829  0.33   YES
max. S     17         0.929  0.92   YES
mean S     1-29       0.576  0.49   YES
D          1-29       0.703  0.44   YES
# Most likely cleavage site between pos. 29 and 30: AQA-IE
```

The S-mean is the average of the S-score, ranging from the N-terminal amino acid to the amino acid assigned with the highest Y-max score, thus the S-mean score is calculated for the length of the predicted signal peptide. The *D*-score is introduced in SignalP version 3.0 and is a simple average of the S-mean and Y-max score.

For non-secretory proteins all the scores represented in the SignalP3-NN output should ideally be very low. (cp. SignalP 3.0 Server)

SignalP Hidden Markov Model:

The Hidden Markov Model calculates the probability of whether the submitted sequence contains a signal peptide or not. Therefore this model of signal peptides contains submodels for the N-terminal part (n-region), the hydrophobic region (h-region), and the region around the cleavage site (c-region). For known signal peptides, the model can be used to assign objective boundaries between these three regions [34].

SignalP-HMM result:

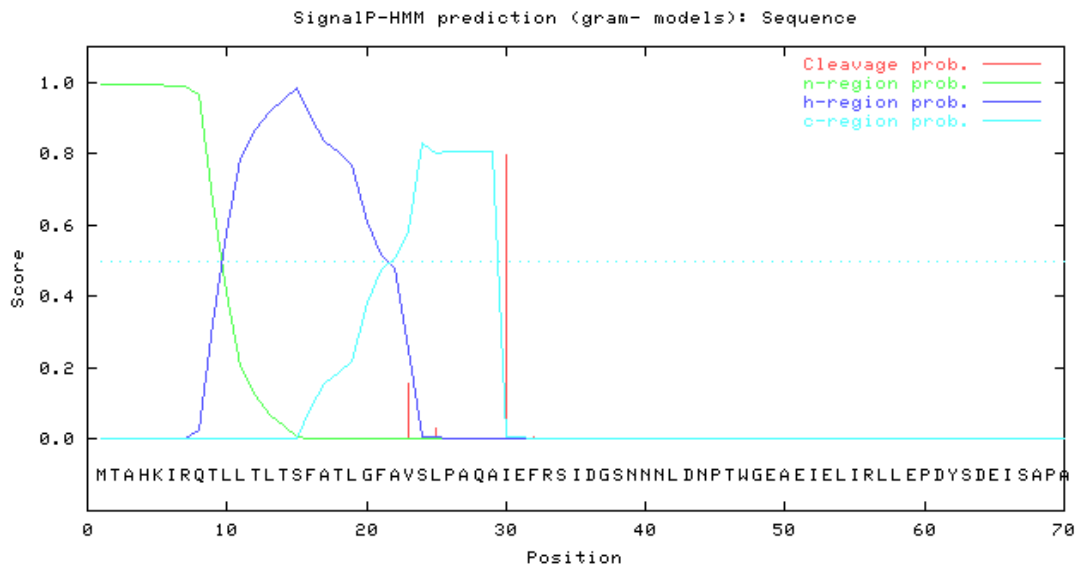


Chart 3. shows the hidden Markov model calculation for signal peptide probability within the first 70 amino acids of the submitted sequence of *Microcoleus chthonoplastes* (PCC 7420). The cleavage site is assigned by a probability score (cleavage prob. (red)) together with scores for the n-region (green), h-region (light blue), and c-region (dark blue). Description according to SignalP 3.0 Server.

Prediction: Signal peptide
 Signal peptide probability: 0.992
 Max cleavage site probability: 0.799 between pos. 29 and 30

The *Microcoleus chthonoplastes* (PCC 7420) peroxidase domain seems to have a signal peptide with a probability of 99.2 % which is with a chance of 79.9 % between the amino acid position 29 and 30. The common structure of signal peptides from various proteins is commonly described as a positively charged n-region, followed by a hydrophobic h-region and a neutral but polar c-region. At the -3 and -1 position (relative to the cleavage point 0) must be small and neutral amino acids for correct cleavage. In prokaryotes alanine is almost exclusively in these two positions [35], which is also the case in *M. chthonoplastes* (PCC 7420) peroxidase sequence. At the position -4 of the cyanobacterial peroxidase resides a proline which is a strong helix breaker and also a typical pattern for a signal peptide cleavage site [33]. In the first few positions of the mature protein (downstream of the cleavage site) the prokaryotes show certain preferences for

Ala, negatively charged (D or E) amino acids, and hydroxyl amino acids (S or T) [35]. According to Charts 2 and 3 within the first 9 amino acids of the mature protein there are two serines, one aspartates as well as one glutamate found.

As a consequence of these results it is assumed that a 29 amino acid long signal peptide was presumably split off from the *M. chthonoplastes* (PCC 7420) peroxidase during protein expression and the molecular weight of the shorter peroxidase formed the basis for calculations in this work.

Lyngbya sp. (PCC 8106)

Similarly *Lyngbya sp.* peroxidase was investigated.

SignalP 3.0 neural network results:

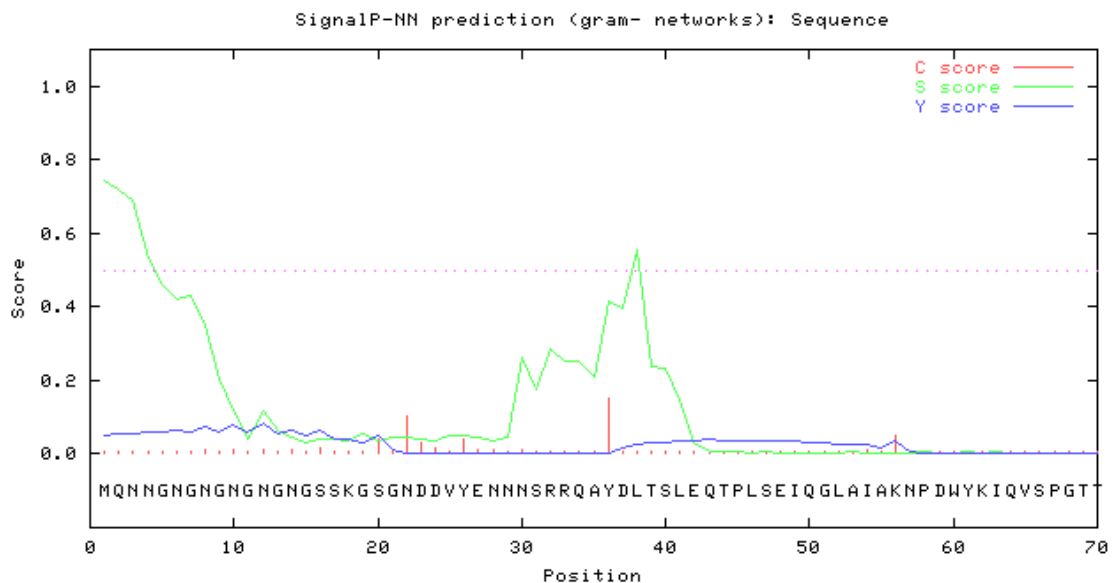


Chart 4. pictures the graphical output from SignalP neural network comprising three different scores, C (red), S (green) and Y (blue). Obviously the *Lyngbya sp.* (PCC 8106) peroxidase domain shows no significant score for a signal peptide within the first 70 amino acids. Score description according to Chart 2.

Computed output

```
>Sequence          length = 70
# Measure  Position  Value  Cutoff  signal peptide?
max. C     36          0.153  0.52   NO
max. Y     12          0.083  0.33   NO
max. S     1           0.742  0.92   NO
mean S     1-11        0.428p  0.49   NO
D         1-11        0.256  0.44   NO
```

SignalP Hidden Markov Model:

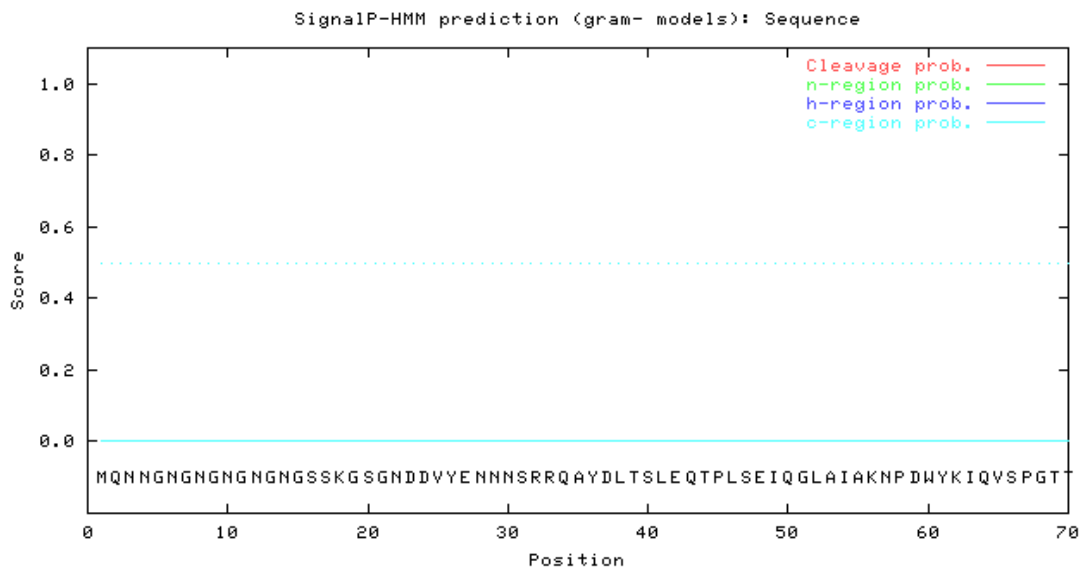


Chart 5. shows the Hidden Markov Model calculation for signal peptide probability within the first 70 amino acids of the submitted sequence of *Lyngbya sp.* (PCC 8106). The cleavage site is assigned by a probability score (cleavage prob. (red)) together with scores for the n-region (green), h-region (light blue), and c-region (dark blue). Description according to SignalP 3.0 Server.

```
>Sequence
Prediction: Non-secretory protein
Signal peptide probability: 0.000
Max cleavage site probability: 0.000 between pos. -1 and 0
```

According to the signal peptide prediction *Lyngbya sp.* PCC 8106 exhibit no cleavage site.

4.1.2.2 Secondary structure prediction

Microcoleus chthonoplastes (PCC 7420):

PsiPred Prediction Results

Key: Conf: Confidence (0=low, 9=high)
Pred: Predicted secondary structure (H=helix (green), E=strand (blue), C=coil)
AA: Target sequence
Amino acids which are predicted with a confidence lower 3 are labeled red.

PSIPRED HFORMAT (PSIPRED V2.6 by David Jones)

Conf: 75268998776531333348899999766775589987646588745568883477458
 Pred: CCHHHHHHHHHHHCCHHHHCC
 AA: MTAHKIRQTLTLTSLFATLGFVAVSLPAQAIEFRSIDGSNNLDNPTWGEAEIELIRLLE
 10 20 30 40 50 60

Conf: 31002756777666888899999872576667887554289999998755542378877
 Pred: CCCCCCCCCCCCCCHHHHHHHHHCCCCCCCCCCCCCHHHHHHHHHHHHHHHHHCCCCC
 AA: PDYSDEISAPAGMNRPNPRAISNAIASQSESLPNPFHASDWLWQWQFVDHDIDLTDPPPE
 70 80 90 100 110 120

Conf: 786356645888877688774012345556688887778022311355602334465899
 Pred: CCCEEEECCCCCCCCCCCCCEEEEECCCCCCCCCCCCCHHHHHCCCCCCECCCCCCCC
 AA: GAELPIIIVPENDLFTFTPGSEIPFNRNVAAPGTGTDSDNNPRQVNAITAYIDGSNVYGS
 130 140 150 160 170 180

Conf: 88856530152111045777788888888754666887000100056433443678988
 Pred: HHHHHHHHCCCCHHHCCCCCCCCCCCCCCCCCCCCCCCCCCCCCCCCCCCCHHHHHH
 AA: IERANFLRTGDSGKLTSAAGNLLIFNTANLPNANPFGVDAEDLFIAGDVRVSNQIGLTAV
 190 200 210 220 230 240

Conf: 89986156799889864686312331024665458999999988786787689766877
 Pred: HHHHHHHHHHHHHHHHHCCCCCHHHHCCCCCHHHHHHHHHHHHHHHHHHHHHHHHH
 AA: HTLVFVREHNRLADEIAADPTTSQKAADAGLSVDDYIYQTTTRRIVSAQIQAITYNEFLPLL
 250 260 270 280 290 300

Conf: 186666766677888887541898876898656507636640155566655432667641
 Pred: CCCCCCCCCCCCCCCCCCEHHHHHHHHHHHHHHHCCCHHHHHCCCCCCCCCCCCHHHHHC
 AA: LGEAIDPYSYDETVNPSISNEFSTAAYRVGHTMLPSELQRINNDGTSAGSISLRDSFF
 310 320 330 340 350 360

Conf: 820022125247887763154643665569889975035676420077876777787078
 Pred: CCHHHHCCCHHHHHHHHHHHCHHHCCCCCHHHHHHHCCCCCCCCCHHHHHHHHHHHHHCC
 AA: KPQEITDNGIDSLLLGLASQKAQTIDAFIVDDVRNFLFPAGNGGLDLAAVNIQRGRDHGL
 370 380 390 400 410 420

Conf: 86889999965898788878718989999998632644546510122211210245678
 Pred: CCHHHHHHHHCCCCCHHHHCCCCHHHHHHHHHHHCCCCCCCCCHHHHHHHHHHHCCCCC
 AA: PSYNEARQALGLGGYTSFDQITSDAEIAQRFRDIYGTTDGQDNIDLVDLWIGGIAEDAYN
 430 440 450 460 470 480

Conf: 87778689999999999772792340268875114588883879898785588553565
 Pred: CCCCCHHHHHHHHHHHHHHHHCHHHCCCCCCCCCHHHHHHHHCCCHHHHHHHCCCCCCCC
 AA: GGMVGELEFNVIISDQFQRLQDGRFFYLADQDLLNLVDPIDGTRLSDIIVRNTDITTIQD
 490 500 510 520 530 540

Conf: 564477789988663560016776656577863002445543459
 Pred: CCCCCCCCCCCCCCCCCCHHHHHHHHHHHHHHHHCCCCCCCCC

4.1.2.3 Extinction coefficient, pI, M_w, and amino acid composition and secondary structure prediction

Amino acid composition

Tab. 24 shows the amino acid composition of *M. chthonoplastes* (PCC 7420) peroxidase (584 aa) and the sequence without predicted signal peptide (555 aa), together with the amino acid composition of *Lyngbya sp.* (PCC 8106).

Amino acid	<i>M. chthonoplastes</i> PCC 7420 584 aa		<i>M. chthonoplastes</i> PCC 7420 555 aa		<i>Lyngbya sp.</i> PCC 8106 661 aa	
Ala (A)	52	8.9%	47	8.5%	36	5.4%
Arg (R)	29	5.0%	28	5.0%	25	3.8%
Asn (N)	40	6.8%	40	7.2%	55	8.3%
Asp (D)	52	8.9%	52	9.4%	62	9.4%
Cys (C)	0	0.0%	0	0.0%	0	0.0%
Gln (Q)	30	5.1%	28	5.0%	25	3.8%
Glu (E)	27	4.6%	27	4.9%	43	6.5%
Gly (G)	49	8.4%	48	8.6%	62	9.4%
His (H)	8	1.4%	7	1.3%	8	1.2%
Ile (I)	48	8.2%	47	8.5%	41	6.2%
Leu (L)	55	9.4%	50	9.0%	59	8.9%
Lys (K)	8	1.4%	7	1.3%	8	1.2%
Met (M)	4	0.7%	3	0.5%	3	0.5%
Phe (F)	29	5.0%	27	4.9%	31	4.7%
Pro (P)	30	5.1%	29	5.2%	28	4.2%
Ser (S)	41	7.0%	39	7.0%	65	9.8%
Thr (T)	38	6.5%	33	5.9%	41	6.2%
Trp (W)	5	0.9%	5	0.9%	7	1.1%
Tyr (Y)	14	2.4%	14	2.5%	18	2.7%
Val (V)	25	4.3%	24	4.3%	44	6.7%

The most obvious detail of the cyanobacterial amino acid composition was that both peroxidases do not have cysteines. As a consequence no cystine disulfide bonds are possible which are an indication for protein stability. In Table 25 the remaining prediction results are summarized.

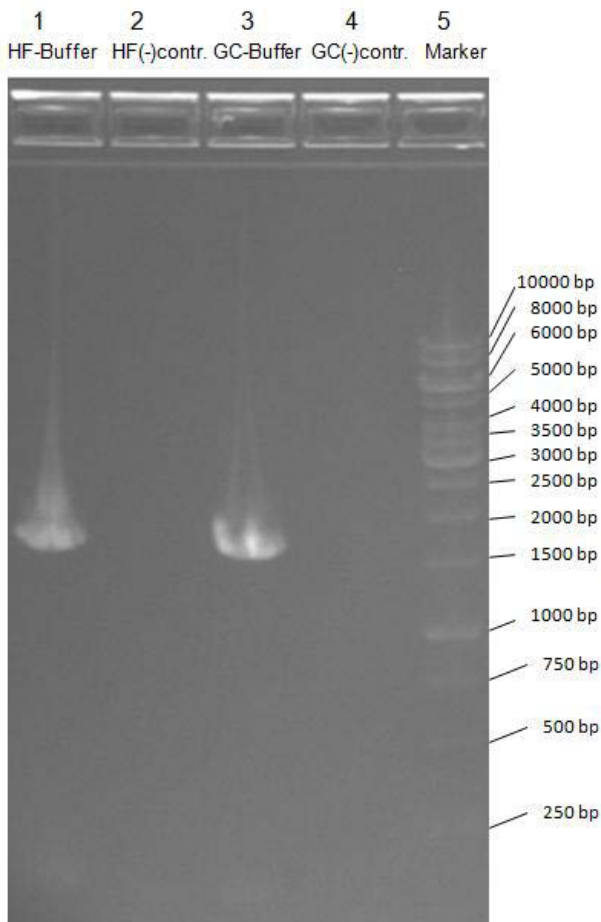
Tab. 25 is a summary of the calculated and predicted protein parameters ext. coefficient, pI, M_w; the α -helix and β -sheet contents. Furthermore the molecular weight including the weight of 6 histidines (His-Tag) and the heme-group are listed.

Parameter	<i>M. chthonoplastes</i> PCC 7420 584 aa	<i>M. chthonoplastes</i> PCC 7420 555 aa	<i>Lyngbya sp.</i> PCC 8106 661 aa
Ext. coefficient Abs 0.1% (=1 g/L)	48360 M ⁻¹ cm ⁻¹ 0.761	48360 M ⁻¹ cm ⁻¹ 0.800	65320 M ⁻¹ cm ⁻¹ 0.911
Theoretical pI	4.31	4.21	4.01
Molecular weight	63508.2 Da	60437.6 Da	71706.8 Da
Molecular weight incl. His-Tag (840.8 Da) and heme-group (650.4 Da)	64999.4 Da	61928 Da	73198 Da
α -helix	43.3%	43.4%	34.6%
β -sheet	2.4%	2.5%	2.9%

In contrast to the mammalian peroxidases, which have relatively high isoelectric points (Cp. introduction 1.3), the cyanobacterial peroxidases are acidic proteins with p/Is of 4.21 and 4.01, respectively.

4.2.1 Agarose gel electrophoresis of PCR product containing amplified peroxidase genes.

The PCR product (Ac. 3.2.1.1) containing the amplified *M. chthonoplastes* (PCC 7420) peroxidase gene DNA was loaded on an agarose gel. The expected DNA fragment should have a length ~ 1770 bp. The used Marker #SM0311 comprises DNA fragments from 250 bp to

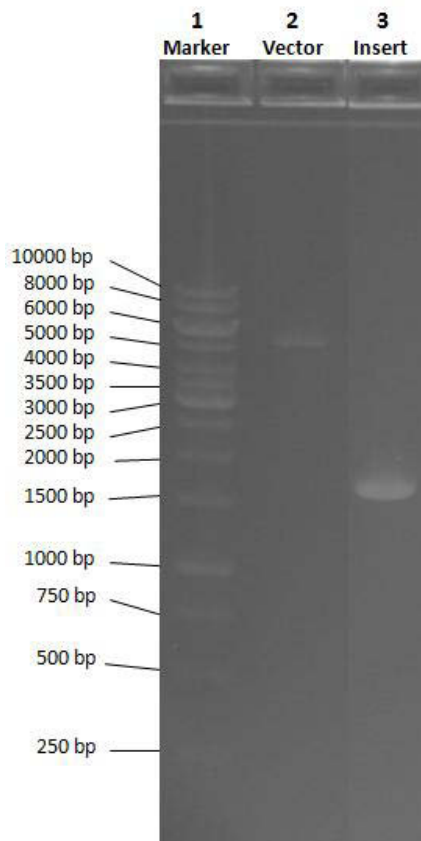


Both PCR products showed a band between the 1500 bp and 2000 bp fragments of the marker. Respective to the calculated DNA fragment size of ~ 1770 bp it seemed that the amplification of the *M. chthonoplastes* (PCC 7420) peroxidase gene was successful. The PCR/GC-Buffer product yield was higher (Figure 24), that was the reason why the product with GC-Buffer was taken for the following cloning step, the vector preparation.

Figure 23. Agarose gel electrophoresis (E-Gel®/ Sybr® safe/1.2% agarose system). Lane 1 shows the result of PCR with PCC 7420 genome as template, performed in HF-Buffer. Lane 2 is the negative (-) control of lane 1, consequently without PCC 7420 genome as template. Lane 3 and 4 also show a PCR with PCC 7420 genome as template and the respectively negative (-) control, but executed in GC-Buffer. Lane 5 is the 1:5 diluted DNA marker #SM0311 from Fermentas. 10 µL of PCR product were filled in all lanes.

4.2.2. Restriction analysis of vector and insert.

The results of the agarose gel electrophoresis is pictured in Figure 24. After the restriction cut



the few “nonsense” base pairs on each side of the insert, originated from the designed primers during the PCR should be removed. Hence a peroxidase insert of exact 1752 bp was expected. These differences of a few base pairs were obviously not observable, but the DNA fragment of lane 3 (Fig. 25) resided in the correct range which allowed to continue the work. The cut of pET-21a (+) vector which should led to an 80 bp (removed fragment between NdeI and XhoI restriction site in the MCS) shorter fragment than the natural vector of 5443 bp. The apparent band (Lane 2, Fig. 25) between the 5000 bp and 6000 bp fragments of the marker indicated a linear DNA fragment with appropriate size. As a consequence these two approaches were used for the ligation during the plasmid preparation.

Figure 24. Agarose gel electrophoresis (E-Gel®/ Sybr® safe/1.2% agarose system). Lane 1 shows the used 1:5 diluted marker from Fermentas #SM0311, lane 2 the NdeI/ XhoI restriction cut and 5’dephosphorylated pET-21a (+) Vector, and lane 3 the NdeI/ XhoI restriction digested *M. chthonoplastes* (PCC 7420) peroxidase gene DNA Insert. For lane 2 and 3 10 µL of digested and GFX™ purified DNA solution were used.

4.2.3. Analysis of LB-agar_{amp} plates.

Altogether 4 plates were incubated, two plates with TOP 10 *E.coli* cells putatively containing the pET-21a (+)/peroxidase plasmid and two plates TOP 10 *E.coli* with only exhibiting the linearized pET-21a (+) vector (vector control). Table 26 summarizes the results.

Tab. 26 Colony count of incubated LB-agar_{Amp} plates after electroporation.

Amount of used cell culture (SOC-Medium)	Cells with ligated plasmids	Cells with linearized pET-21a (+) vector
200 µL	267 colonies	2 colonies
~900 µL	Not countable > 300	22 colonies

The two plates putatively containing the *E. coli* cells with the prepared plasmids showed abundant growth, whereas the plates with incubated cells only containing the linearized pET-21a (+) vector showed sparse growth. Consequently the cells with the plasmids effectively expressed the ampicillin resistance gene which indicates intact plasmids. If the plasmids contained a correctly inserted PCC 7420 peroxidase gene, could not be confirmed at this moment. The following PCR screening which was performed with colonies from the 267 colony plate (Table 10), should give further information about the correct plasmid construction.

4.3.1. PCR Screening

Because of the used primer PCC7420perox-sequ01for and PCC7420perox-sequ06rev which bound within the edges of the PCC 7420 peroxidase insert, a 1733 bp long DNA fragment was expected. Two gels were performed, the first with colonies 1-9 (Figure 25) and the second with colonies 10-18 (Figure 26).

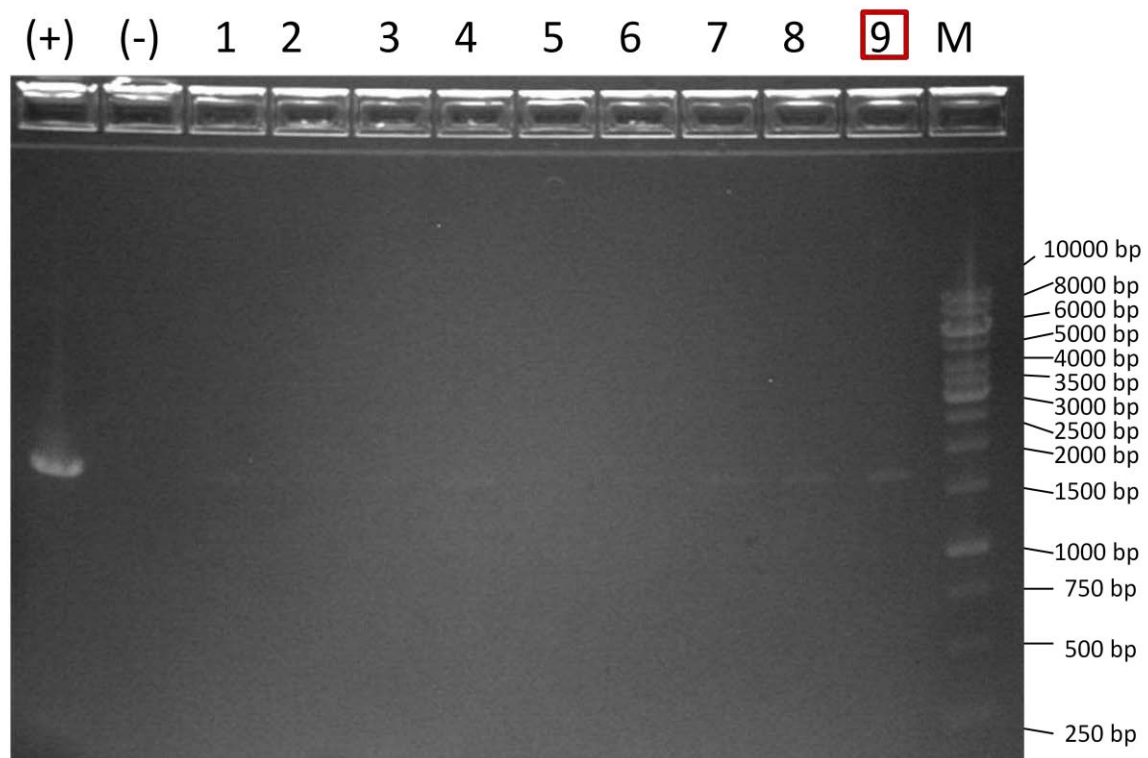


Figure 25. PCR screening; Agarose gel electrophoresis (E-Gel®/ Sybr® safe/1.2% agarose system. (+) shows the positive control, the PCR of the PCC 7420 peroxidase Insert as template. Lane (-) was the negative control, the PCR without template. In lanes 1-9 10 µL PCR product of the colony suspensions 1-9 were filled. M is the used 1:5 diluted marker from Fermentas #SM0311. Labeled red is the lane (9) with the strongest DNA Band.

In the first gel exhibiting the colony suspension 1-9 many lanes showed a DNA fragment with probably the desired size. According to Figure 26 the strongest DNA Band was in lane 9 (labeled red) and consequently the colony number 9 was considered for further analysis.

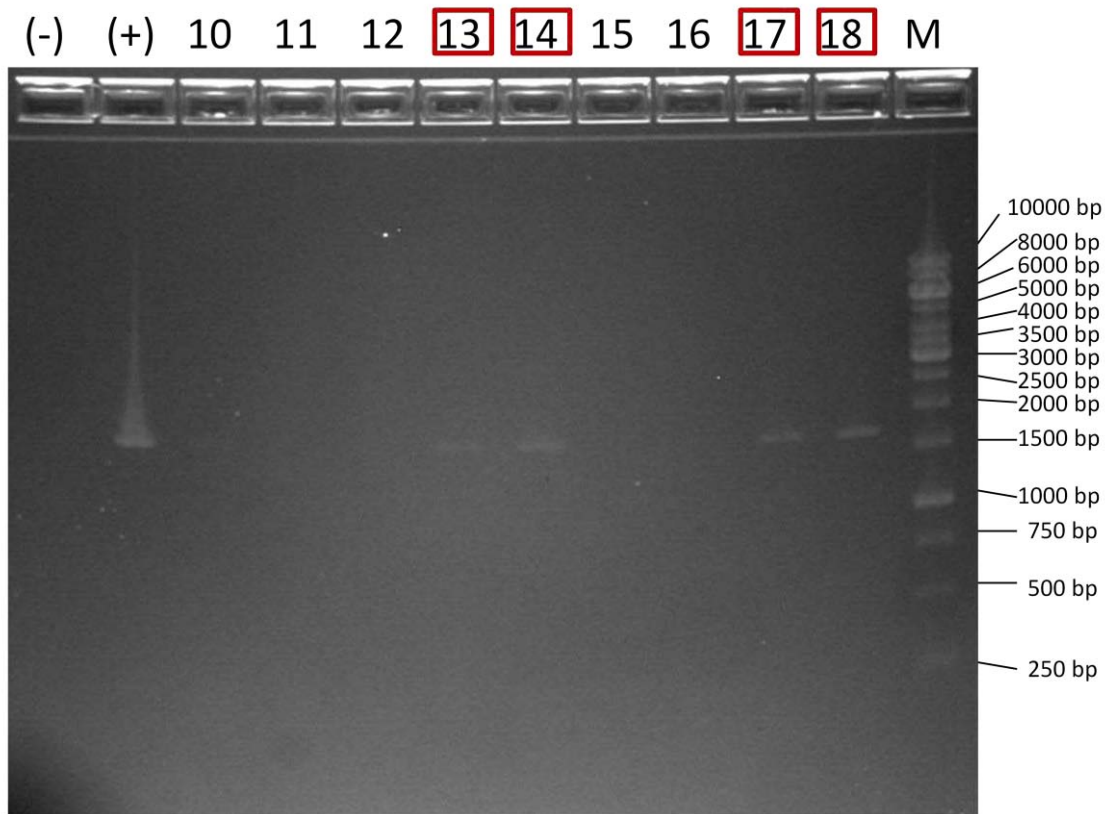


Figure 26 PCR screening; Agarose gel electrophoresis (E-Gel®/ Sybr® safe/1.2% agarose system. (-) was the negative control, the PCR without template. (+) shows the positive control, the PCR of the PCC 7420 peroxidase Insert as template. In lanes 10-18 10 µL PCR product of the colony suspensions 10-18 were filled. M is the used 1:5 diluted marker from Fermentas #SM0311. Labeled red are lanes 13, 14, 17, 18 which manifest a clear DNA band with a size between 1500 and 2000 bp.

Figure 26 displays the result of electrophoresis for the PCR product of colony suspension 10-18. In each of lanes 13,14,17, and 18 a clear DNA fragment with a size between 1500 bp and 2000 bp were observable. Thus colony numbers 13, 14, 17, and 18 were chosen together with number 9 for further analysis by means of restriction screening. The cells of these 5 colonies seemed to exhibit a plasmid containing an insert with correct size.

4.3.2. Restriction screening

The complete plasmid consisting of a 5363 bp vector pET-21a (+) and a 1752 bp PCC 7420 peroxidase DNA insert had a length of 7115 bp. For a complete plasmid two options were possible. If the Insert was incorporated in the right direction the expected sizes for the fragments were due to the restriction sites 770 bp and 6345 bp. In case of a wrong directed insert the expected sizes of the fragments were 1194 bp and 5921 bp. The results of the agarose gel electrophoresis are pictured in Figure 27.

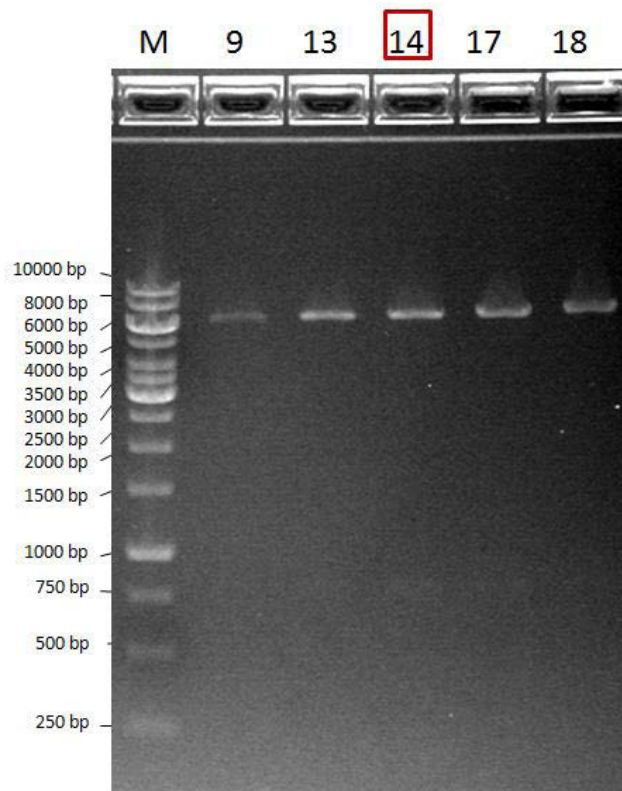
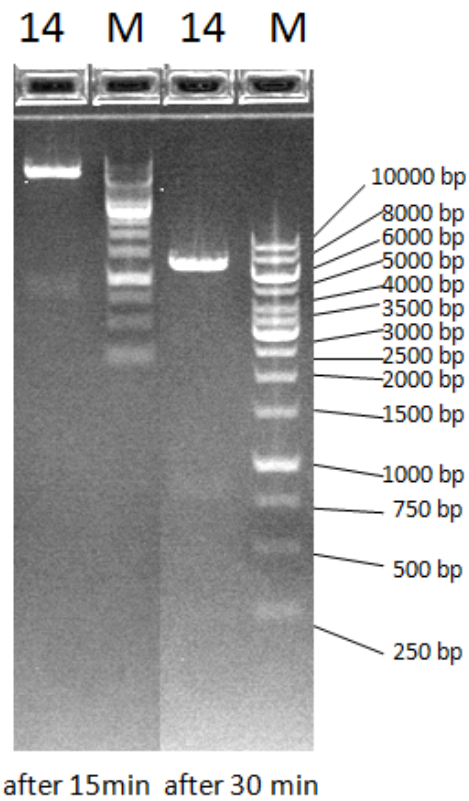


Figure 27 Restriction screening agarose gel electrophoresis (E-Gel®/ Sybr® safe/1.2% agarose system). The Bgl II restriction digestion of colony suspensions 9, 13, 14, 17, 18. In each lane 10 µL restriction digestion product were filled. M is the used 1:5 diluted marker from Fermentas #SM0311. Labeled red is the most clear discernible result.

Compared to Figure 27 all five clones showed a clear DNA fragment above the 6000 bp fragment of the DNA marker. In general it is hard to distinguish between large DNA fragments, thus it was hard to confirm the observable fragment as the expected 6345 bp fragment. On the other hand it should be much easier to confirm the 770 bp fragment compared to the 750 bp fragment of the DNA marker and in fact such a fragment was hardly observable for the clones 13, 14, 17. Clone 14 showed the best result and that was the reason why a further agarose gel electrophoresis (Figure 28) was performed.



In Figure 29 the expected 770 bp DNA fragment is better visible than in Figure 28, consequently the plasmid containing the PCC 7420 peroxidase gene insert and the pET-21a (+) vector of clone 14 was taken for further analysis.

Figure 28 shows the electrophoretical confirmation of restriction screening for clone 14 after 15 min and 30 min running time. Apart from that all conditions were the same as in Figure 27.

4.3.3. Expression screening

Figure 29 shows the result of expression of PCC 7420 peroxidase clones 14/1-5. The expected protein should have a molecular weight of 61928 Da according to the predictions in section 4.1.2. The chosen protein marker of Invitrogen (Mark 12) exhibit amongst others two proteins with a molecular weight of 55.4 kDa and 66.3 kDa and the expected protein should be exactly in the middle of these two bands (Cp Figure 29).

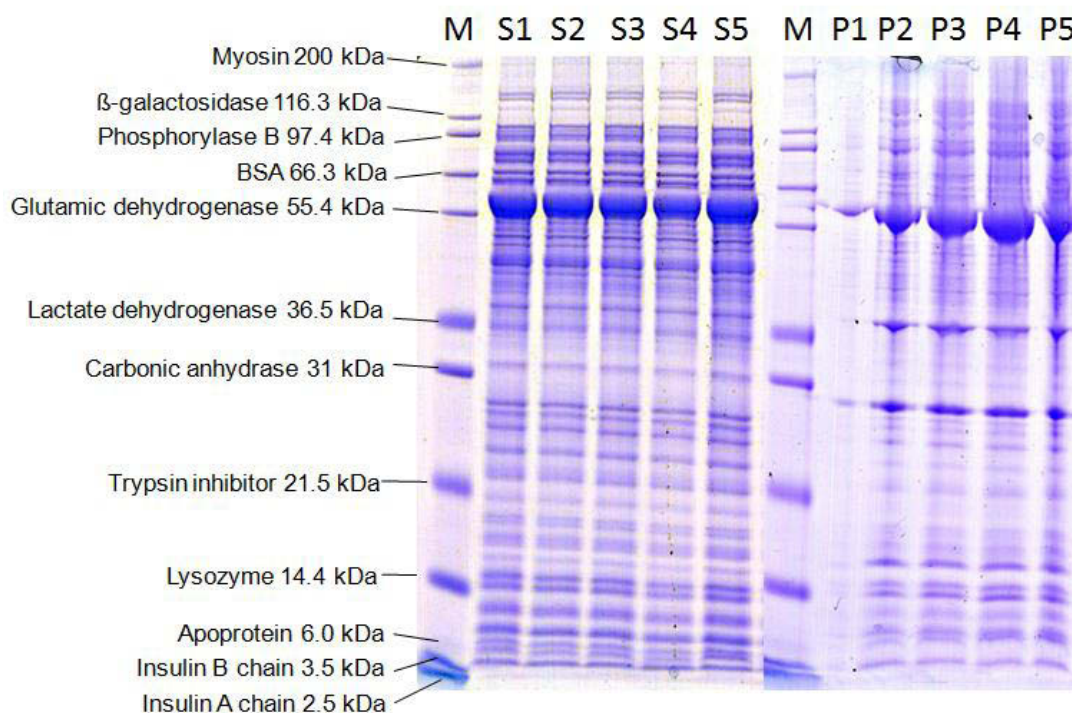


Figure 29. Precast system; NuPAGE® Novex 12% Bis-Tris Gel 1.0 mm, 15 well, from Invitrogen. M is Mark 12 protein marker from Invitrogen consisting of the proteins labeled on the left side. 5 μ L of the Mark 12 solution were used in both lanes. S1-5 were the investigation of the supernatant of PCC 7420 peroxidase clones 14/1-5 and P1-5 of the respective pellets. 10 μ L were loaded on the gel. The gel was stained with Coomassie blue R-250.

Actually, an intense clear discernible protein band appeared with a molecular weight of approximately 60 kDa at all of the investigated samples (Figure 29). During expression screening the cells were treated in almost the same manner like in the larger scaled enzyme purification performed later in this work. Only the supernatant was used for the purification by using the metal chelate affinity chromatography and that is why the results of lanes S1-5 were seen as positive result. The result of lanes P1-5 suggested that respectable amounts of protein were remaining within the cell debris but this fact was accepted and the cell pellet was discarded. Moreover the strongest protein band of the gel, P5 was finally chosen as clone for final protein expression.

4.3.4 DNA Sequencing

In accordance with the Barcode Sequencing Service the plasmid of *E. coli* clone 14/5 contained a complete and correct PCC 7420 peroxidase gene insert.

4.4.1 Enzyme purification

The UV-Vis spectra of the two cyanobacterial peroxidases were determined in 10 mM phosphate buffer pH 7.0 and 25°C. Both spectra are compared with those of bovine LPO and human MPO (Cp. Chart 5).

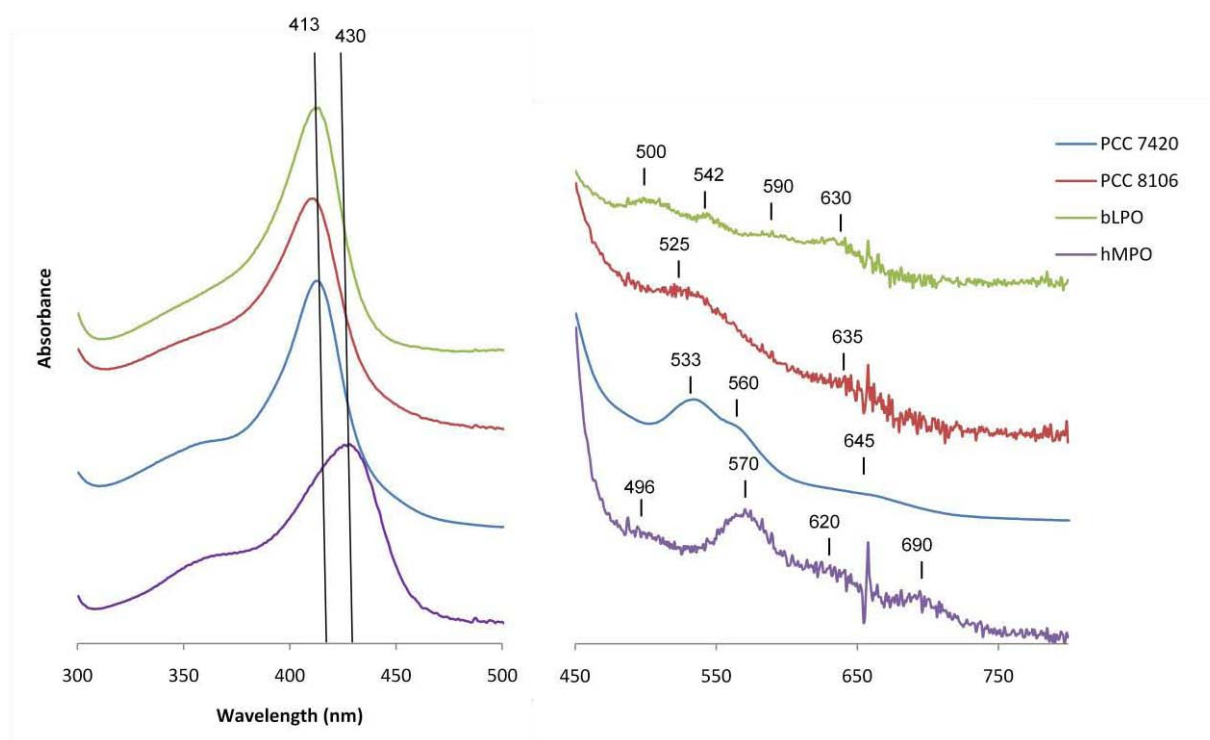


Chart 6. Spectral features of the peroxidases of PCC 7420 (blue) and PCC 8106 (red) compared with that of bovine LPO (green), human MPO (violet) at pH 7 (10 mM phosphate buffer) and a wavelength range from 300 nm to 800 nm. Each spectrum of the wavelength range from 450-800 nm was increased with a proper factor to make the characteristically peaks identifiable.

Both cyanobacterial enzymes showed a Soret peak at ~412 nm which was comparable to the Soret peak of bovine LPO (Chart 6). With regard to the sequence alignment this actuality made

sense, also the contrast to the red shifted Soret peak of MPO (430 nm) as a consequence of the third heme to protein link [12]. The bands in the range of 450-800 nm of the cyanobacterial peroxidases were comparable whereas both showed no similarities with the depicted (Chart 6) mammalian peroxidases.

Despite of the desalting process it could not be verified that the enzyme solution was fully free of other potential ligands than H₂O for the heme iron like imidazole which would lead to spectral changes. The bands between 530 and 560 nm of the PCC 7420 peroxidase indicated the presence of low-spin states due to binding of distal ligand.

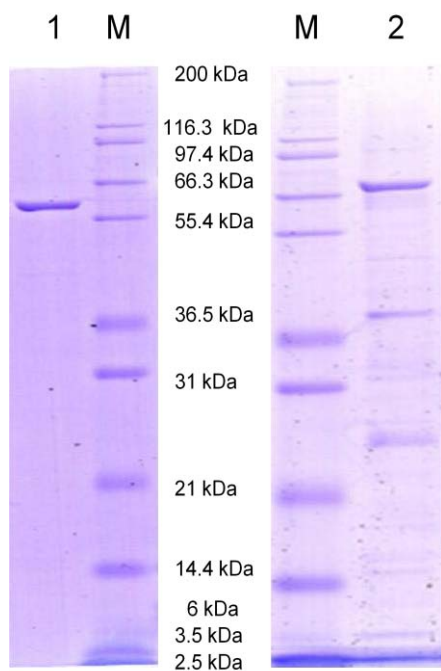


Figure 30 shows the electrophoretical investigation of the MCAC purified, concentrated and desalted PCC 7420 and PCC 8106 peroxidases. The purification of PCC 7420 peroxidase was successful, a clear protein band with expected size and marginal impurity was monitored. In contrast, PCC 8106 peroxidase was not pure. This could be a consequence of the purification with Ni²⁺ ions which exhibit a higher affinity to surface histidine, cysteine, and tryptophan residues than zinc ions. Hence more proteins bind to the column and were eluted afterwards with a higher concentration of imidazole.

Figure 30 Precast system; NuPAGE® Novex 12% Bis-Tris Gel 1.0 mm, 15 well, from Invitrogen. M is Mark 12 protein marker from Invitrogen. 1 is PCC 7420 peroxidase and 2 the PCC 8106 peroxidase, both after MCAC purification.

4.5. Spectroscopic analysis of cyanobacterial peroxidases.

4.5.1 UV-Vis spectroscopy

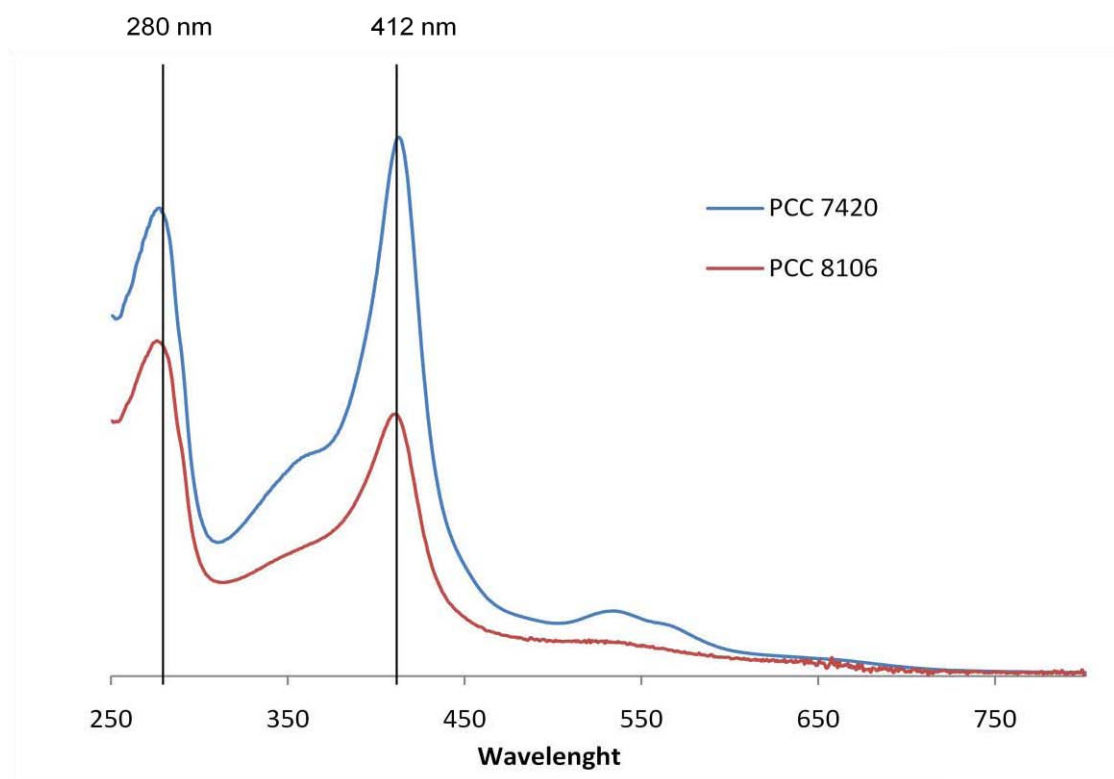


Chart 7 UV-Vis absorbance spectra (wavelength range 250-800 nm) of PCC 7420 (blue) and PCC 8106 (red) peroxidase solutions.

According to equations (1) and (2) (Section 3) based on the data of Chart 7 following values were calculated. The concentration of PCC 7420 peroxidase was $9.13 \mu\text{mol/L}$ and the RZ 1.17. The concentration of PCC 8106 peroxidase was $4.43 \mu\text{mol/L}$ and the RZ 0.80. The higher RZ of the *M. chthonoplastes* PCC 7420 containing solution was a confirmation of the data depicted in Figure 30.

4.5.2 CD spectroscopy

Chart 8 shows the far UV circular dichroism spectra from 190 to 260 nm. The range from 260-290 nm is removed from the Chart because the enzyme solutions in the 1 mm cuvette delivered a negligible small CD signal in this region. Table 27 shows the secondary structure content calculated from the far UV spectrum. For the calculation the actual protein concentration was

necessary, which was determined with the aid of the heme peak of each enzyme (not shown here).

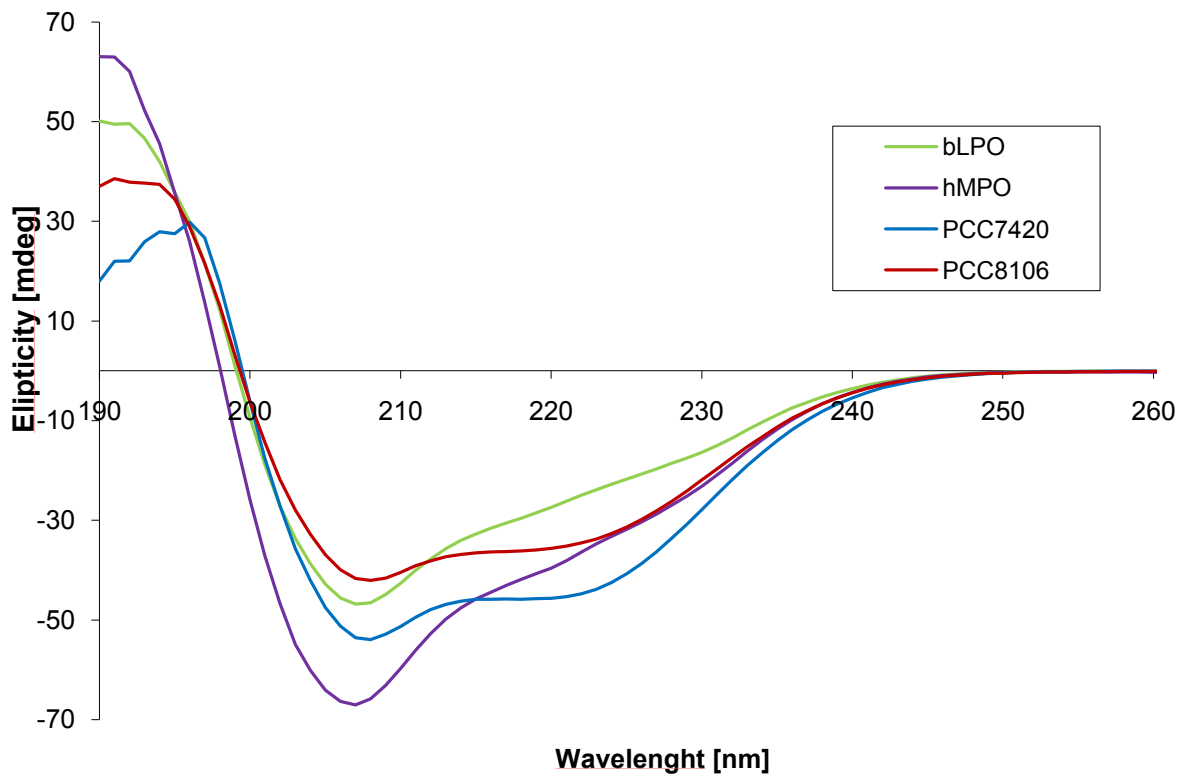


Chart 8 Far UV circular dichroism spectra (190-260 nm) of the cyanobacterial peroxidases of PCC 8106 (red) and PCC 7420 (blue) compared with that of human MPO (violet) and bovine LPO (green). The protein samples were measured in 10 mM phosphate buffer pH 7.0 and 25°C. The absorption of each enzyme solution at 280 nm was 0.6 related to a 10 mm cuvette. Pathlength of the measuring cuvette was 1 mm.

Tab. 27 Contents of secondary structure based on the result of the range of 195-260 nm computed with the aid of the Chirscan software and the diagnostic tools of Applied Photophysics Ltd.

	bLPO	hMPO	PCC7420	PCC8106
	195-260 nm	195-260 nm	195-260 nm	195-260 nm
Helix	25,00%	32,00%	49,02%	36,1%
Antiparallel	16,70%	12,70%	5,10%	9,20%
Parallel	10,40%	7,80%	4,80%	7,2%
Beta-Turn	18,90%	17,80%	14,70%	16,70%
Rndm. Coil	33,90%	25,10%	17,10%	25,50%
Total Sum	105,00%	95,40%	90,90%	94,70%

The far UV CD spectra of the two cyanobacterial peroxidases revealed that both proteins are assembled predominantly by α -helices and both have a lower content of β -sheets than the mammalian peroxidases. The total sum should be ideally 100%, which is not the case for all enzymes. However, the α -helix content of both enzymes matched well with the secondary structure prediction described in section 4.1.2.2. For *M. chthonoplastes* PCC 7420 peroxidase a α -helix content of 43.7% was predicted and the result of the CD measurement was 49.02%. In the same way for *Lyngbya sp.* PCC 8106 peroxidase the predicted α -helix content was 34.6% compared with the 36.1% due to the CD measurement.

Chart 9 pictures the near UV/Vis circular dichroism spectra from 250 to 500 nm. Because of the much smaller values for the ellipticity compared to the far UV region the 1 cm cuvette was used.

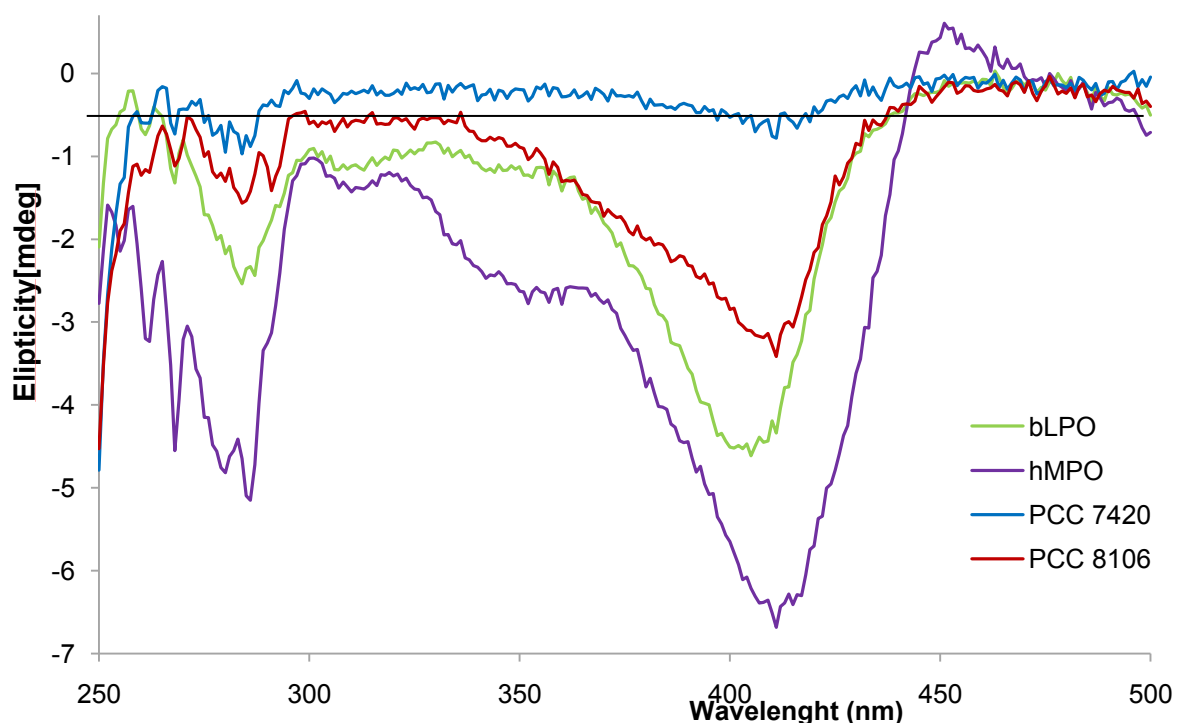


Chart 9 Near UV/Vis circular dichroism spectra (250-500 nm) of the cyanobacterial peroxidases of PCC 8106 (red) and PCC 7420 (blue) compared with that of human MPO (violet) and bovine LPO (green). The protein samples were measured in 10 mM phosphate buffer pH 7.0 and 25°C. The absorption of each enzyme solution at 280 nm was 0.6 related to a 10 mm cuvette. Pathlength of the measuring cuvette was 10 mm.

The so-called fingerprint region within the near UV range as described in 3.5.2.1 is often used to compare the native form of an enzyme with a recombinant produced wild type/variant form of enzyme. It indicates a correct folding of a recombinant protein. Due to the fact that no native peroxidase of both cyanobacterial organisms was available, the interpretation of this region was difficult. More important in this case was the heme spectrum around 412 nm that gives information about the correct integration of the prosthetic group. According to Chart 9 the native

enzymes of bovine LPO and human MPO showed the expected CD bands. Compared to that the peroxidase of *Lyngbya sp.* PCC 8106 also showed a clear CD band, whereas the interaction of the heme cavity with the heme group of the *M. chthonoplastes* PCC 7420 peroxidase seemed to be very weak.

4.6. Determination of peroxidase and halogenation activity

The peroxidase activities were detected in most cases spectrometrically. The slope of the respective time trace was recorded and determined by linear regression. Based on the value for the slope the specific activity [U⁵/mg] was calculated as described in detail below. Due to the huge amount of data only the specific activities are shown and compared in this section. The change of substrate concentration Δc [mol/L] per minute was calculated by using Lambert Beer's law and the measured slope ΔA (Change of Absorption per minute).

$$\Delta c = \frac{\Delta A}{\epsilon \cdot d} \quad (5)$$

ϵ Extinction coefficient of the respective substrate

d Diameter of the cuvette (1 cm)

Resulting Δc can be described as the amount of substrate that is oxidized by the used amount of peroxidase [U]. To convert the value into the specific activity [U/mg] it was necessary to fit the amount of enzyme to 1 mg.

The used amount of enzyme was determined as described below together with the used molecular weights of the peroxidases.

$$m \text{ [mg]} = n \text{ (mol of used enzyme)} \times M_w$$

Human MPO: 73000 Da ($\epsilon = 91000 \text{ M}^{-1}\text{cm}^{-1}$; $\lambda = 430 \text{ nm}$)

Bovine LPO: 78500 Da ($\epsilon = 112000 \text{ M}^{-1}\text{cm}^{-1}$; $\lambda = 413 \text{ nm}$)

Lyngbya sp. PCC 8106 peroxidase: 73198 Da ($\epsilon = 100000 \text{ M}^{-1}\text{cm}^{-1}$; $\lambda = 412 \text{ nm}$)

M. chthonoplastes PCC 7420 peroxidase: 61928 Da ($\epsilon = 100000 \text{ M}^{-1}\text{cm}^{-1}$; $\lambda = 412 \text{ nm}$)

⁵ One Unit U is defined as 1 μmol of substrate being converted per minute.

4.6.1. Iodination activity.

For rate calculation iodination the following pH-depended equilibrium must be considered.



However, the assay served as an confirmation of halogenation activity and gave a rough indication for the pH optimum. The calculated (analog 4.6) values for the specific activities are listed in Table 28 and pictured in Chart 10.

Tab. 28 Specific iodination activities (25°C) of the two cyanobacterial peroxidases, human MPO and bovine LPO, dependent on the pH. *The values for bovine LPO were set to 100%.

pH x	Specific iodination activity [U/mg]			
	PCC 8106 peroxidase	PCC 7420 peroxidase	bLPO	hMPO
pH 8.0	$6.20 \cdot 10^4$	$5.72 \cdot 10^3$		
pH 7.5	$3.99 \cdot 10^5$	$3.23 \cdot 10^4$		
pH 7.0	$5.13 \cdot 10^5$ 128.5%	$4.51 \cdot 10^4$ 11.2%	$3.99 \cdot 10^5$ 100%*	$6.76 \cdot 10^4$ 16.9%
pH 6.5	$4.67 \cdot 10^5$	$5.44 \cdot 10^4$		
pH 6.0	$3.32 \cdot 10^5$	$4.34 \cdot 10^4$		
pH 5.5	$1.99 \cdot 10^5$ 52.7%	$3.91 \cdot 10^4$ 10.3%	$3.78 \cdot 10^5$ 100%*	$2.13 \cdot 10^5$ 56.3%
pH 5.0	$1.61 \cdot 10^5$	$2.33 \cdot 10^4$		
pH 4.5	$8.46 \cdot 10^4$	$1.39 \cdot 10^4$		
pH 4.0	$5.31 \cdot 10^4$	$8.36 \cdot 10^3$		
pH 3.5	$3.15 \cdot 10^4$	$3.39 \cdot 10^3$		
pH 3.0	$1.98 \cdot 10^4$	$1.67 \cdot 10^3$		

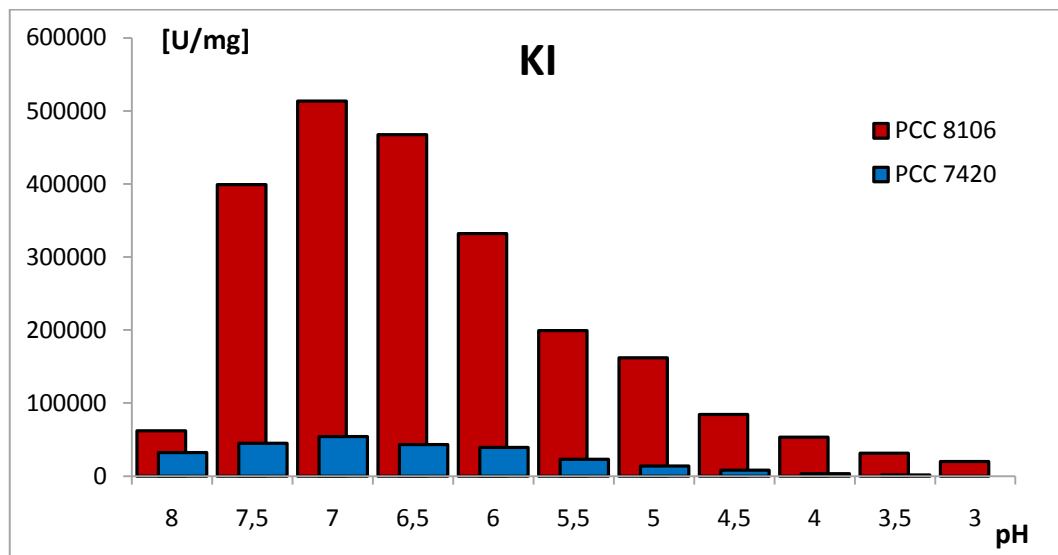


Chart 10 shows the specific iodination activities [U/mg] according to Table 22 of PCC 8106 peroxidase (red) compared to PCC 7420 peroxidase (blue).

The pH optimum for iodination was around pH 7 for both cyanobacterial peroxidases. For *Lyngbya sp.* (PCC 8106) peroxidase the specific activity was comparable to that of both MPO and LPO.

4.6.2 Bromination activity

The calculated (analog 4.6) values for the specific activities are listed in Table 29 and pictured in Chart 11.

Tab. 29 Specific bromination activities (25°C) of the two cyanobacterial peroxidases, human MPO, bovine LPO, and human EPO dependent on the pH. *The values for bovine LPO were set to 100%.

pH x	Specific bromination activity [U/mg]				
	PCC 8106 peroxidase	PCC 7420 peroxidase	bLPO	hMPO	hEPO
pH 7.0	71.16 147.4%	39.68 82.2%	48.29 100%*	22.28 46.2%	155.00 320.9%
pH 6.5	280.79	92.10			
pH 6.0	249.53	106.19			
pH 5.5	201.72	69.73			
pH 5.0	96.32 46.8%	28.57 13.5%	205.83 100%*	-	-
pH 4.5	57.19	8.94			
pH 4.0	40.56	3.60			
pH 3.5	23.31	1.69			
pH 3.0	13.30	0.00			

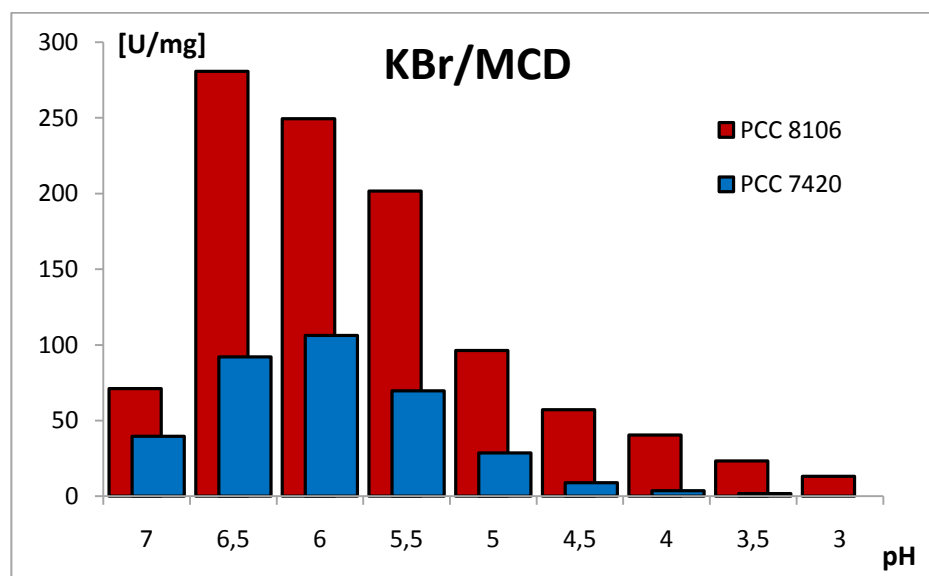


Chart 11 shows the specific bromination activities [U/mg] according to Table 22 of PCC 8106 peroxidase (red) compared to PCC 7420 peroxidase (blue).

Chart 11 demonstrates that PCC 7420 peroxidase had also a feasible bromination activity compared to PCC 8106 peroxidase. Both activities are in the range of the mammalian

peroxidases. The bromination pH optimum of the cyanobacterial peroxidases seemed to be between 6 and 6.5, whereas that for mammalian peroxidases is around 5-5.5 [12].

4.6.3 Chlorination activity

The calculated (analog 4.6) values for the specific activities are listed in Table 30 and pictured in Chart 12.

Tab. 30 Specific MCD chlorination activities of *Lyngbya sp.* PCC 8106 peroxidase compared to human MPO (25°C)

pH x	Specific iodination activity [U/mg]	
	PCC 8106 peroxidase	hMPO
pH 7.0	0	4.11
pH 6.5	0	
pH 6.0	0.12	8.56
pH 5.5	3.55	11.75
pH 5.0	13.67	7.77
pH 4.5	23.74	1.37
pH 4.0	17.45	
pH 3.5	8.28	
pH 3.0	1.50	

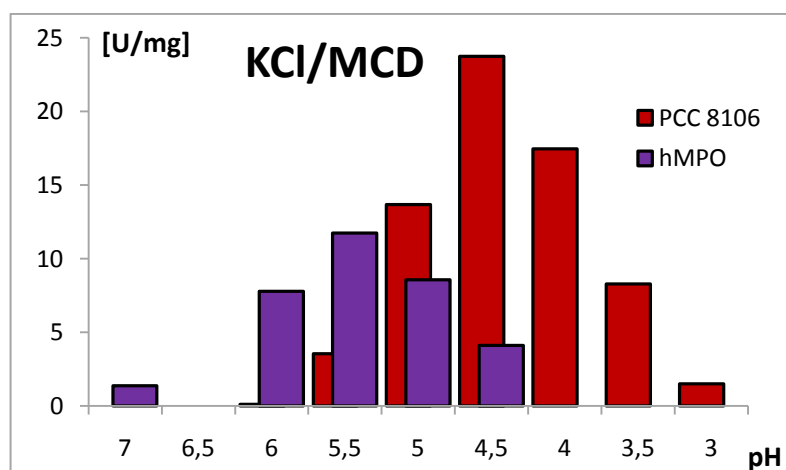


Chart 12 shows the specific chlorination activities [U/mg] according to Table 22 of PCC 8106 peroxidase (red) compared to human MPO (violet)

This result was remarkable. Although at pH values above 6.5 no activity with chloride and MCD was observed the cyanobacterial peroxidase at lower pH values showed values even higher than human MPO. For the interpretation of this result it should be considered that the concentration of the enzyme solutions were adjusted with the aid of the heme peak and the respective extinction coefficient. Thereby both extinction coefficients for the cyanobacterial Soret bands were set to $100000 \text{ M}^{-1}\text{cm}^{-1}$, which could differ from the real coefficient and consequently the used enzyme concentration of this assay also could differ. However this result should be elucidated, the next step could be a much more accurate stopped flow of the reaction. Stopped flow analysis with chloride as substrate were not performed in this work.

4.6.4 ABTS peroxidase activity

The calculated (analog 4.6) values for the specific ABTS activities are listed in Table 31 and pictured in Chart 13.

Tab. 31 Specific ABTS activities (25°C) of the two cyanobacterial peroxidases, human MPO, bovine LPO, dependent on the pH. *The values for bovine LPO were set to 100%.

pH x	Specific ABTS activity [U/mg]			
	PCC 8106 peroxidase	PCC 7420 peroxidase	bLPO	hMPO
pH 9.0	0.00	0.00		
pH 8.0	0.45	0.15		
pH 7.5	0.65	0.23		
pH 7.0	0.89	0.30	69.10	1.87
	1.3%	0.4%	100%	2.7%
pH 6.5	2.18	0.39		
pH 6.0	3.96	0.43		
pH 5.5	10.99	0.60		
pH 5.0	49.17	0.95	258.76	105.80
	19.0%	0.4%	100%	40.9%
pH 4.5	92.94	1.51	105.02	305.55
	88.5%	1.4%	100%	291.0%
pH 4.0	104.37	2.95	67.46	212,43
	154.7%	4.4%	100%	314.9%
pH 3.5	72.12	3.26		
pH 3.0	34.99	1.60	8,02	48,67
	436.1%	20.0%	100%	606.7%

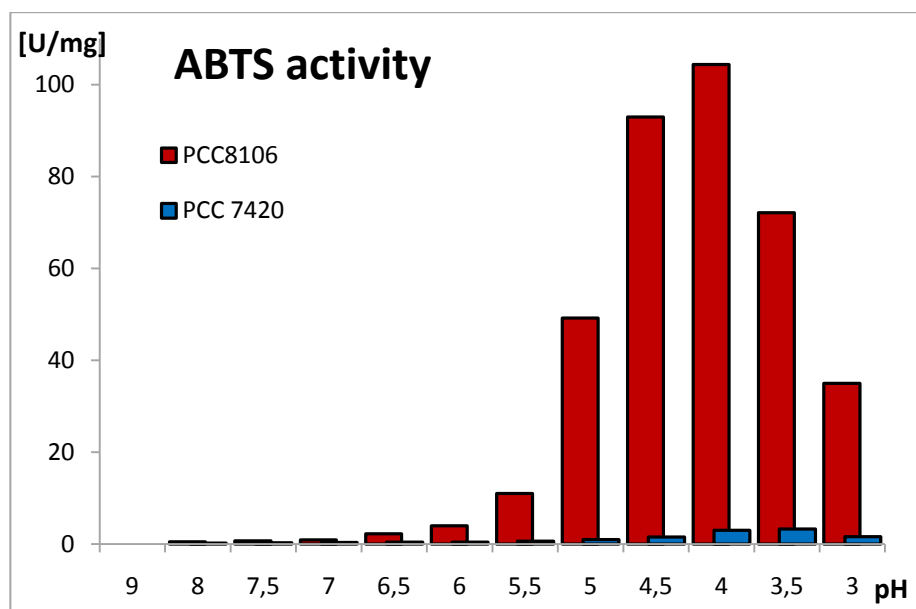


Chart 13 shows the specific ABTS activities [U/mg] according to Table 22 of PCC 8106 peroxidase (red) compared to PCC 7420 peroxidase (blue).

Although PCC 7420 peroxidase solution exhibited a very weak ABTS activity it was a clear evidence for a peroxidase activity in general, especially at lower pH values. The PCC 8106 peroxidase solution showed a pronounced ABTS activity, with absolute values [U/mg] comparable but significant lower than the mammalian peroxidases (Cp. Table 31). All measured peroxidases had a very weak peroxidase activity at pH 7 compared to bovine LPO and in almost the same manner the two cyanobacterial peroxidase and human MPO showed their highest activities at very low pH values (Cp. Table 28).

4.6.5 Guaiacol peroxidase activity

The calculated (analog 4.6) values for the specific ABTS activities are listed in Table 32 and pictured in Chart 14.

Tab. 32 Specific guaiacol activities of the two cyanobacterial peroxidases, human MPO, bovine LPO, at the pH values 7.0 and 5.5 and 25°C. *The values for bovine LPO were set to 100%.

pH x	Specific ABTS activity [U/mg]			
	PCC 8106 peroxidase	PCC 7420 peroxidase	bLPO	hMPO
pH 7.0	0.39	0.07	7.31	3.62
	5.3%	0.9%	100%	49.5%
pH 5.5	0.56	0.17	11.47	3.51
	4.9%	1,4%	100%	30.6%

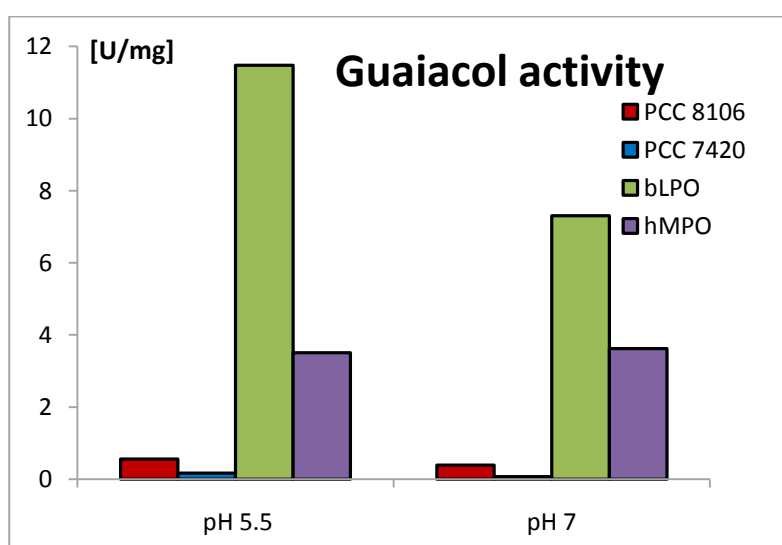


Chart 14 shows the specific Guaiacol activities [U/mg] according to Table 32 of PCC 8106 peroxidase (red) compared to PCC 7420 peroxidase (blue), bovine LPO (green), and human MPO (violet).

Guaiacol was not a convenient substrate for testing the peroxidase activity because the product formation was very low and it was hard to focus on the initial linear part of the product formation curve. The specific activities were range from 1-5% compared to the guaiacol activities of bovine LPO.

4.6.6. Tyrosine peroxidase activity

The results are denoted in fluorescence units (FU) which are determined according to Zederbauer et al. FU are obtained from the fluorometric monitoring of dityrosine formation and are defined as the slope of product formation per minute and mg enzyme [$\text{FUmin}^{-1}\text{mg}^{-1}$]. The results are listed in Table 33 and pictured in Chart 15.

Tab. 33 Specific tyrosine activities of the two cyanobacterial peroxidases, human MPO, bovine LPO, at the pH values 7.0 and 25°C. *The value for bovine LPO was set to 100%.

Tyrosine activity [$\text{FUmin}^{-1}\text{mg}^{-1}$]					
		PCC 8106 peroxidase	PCC 7420 peroxidase	bLPO	hMPO
pH 7.0		296734,975	7095,07816	319890,268	623188,146
		92.7%	2,2%	100%	194.8%

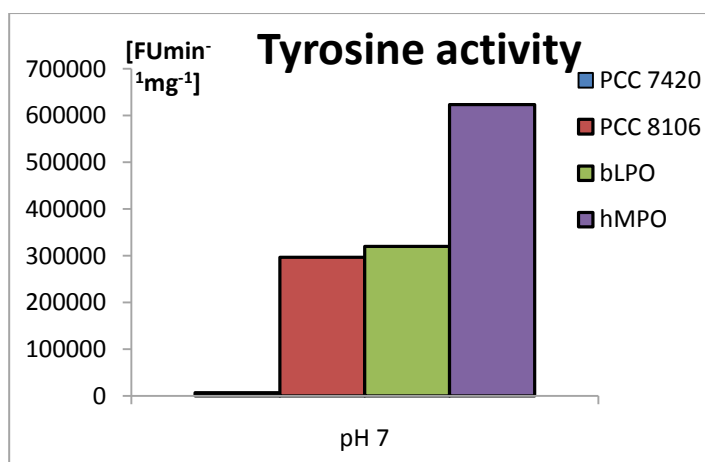


Chart 15 shows the specific tyrosine activities [U/mg] according to Table 33 of PCC 8106 peroxidase (red) compared to PCC 7420 peroxidase (blue), bovine LPO (green), and human MPO (violet).

The activity assay with tyrosine also showed like almost all previous activity assays that the PCC 7420 peroxidase exhibit a weak activity and the PCC 8106 peroxidase had an activity in the range of the mammalian peroxidases.

4.7. Cyanide binding

4.7.1. Spectrophotometrical cyanide titration

4.7.1.1 *Lyngbya sp.* PCC 8106 peroxidase

Chart 16 shows the spectral changes upon addition of cyanide to the ferric proteins. All in all 17 concentrations are depicted, the red graph showing the high-spin state, whereas the yellow one represents the low-spin cyanide complex.

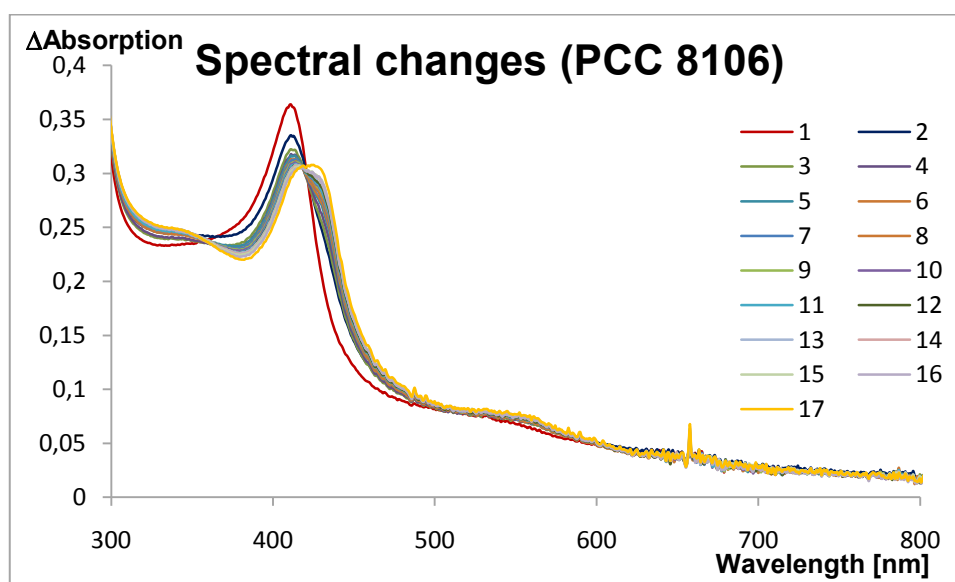


Chart 16 Shows the spectral changes from 300 to 800 nm of PCC 8106 peroxidase at pH 7 and 25°C with raising cyanide concentration. The red graph is the enzyme without CN^- and the yellow graph is the "endpoint" of shifting.

The spectral shift of PCC 8106 peroxidase appeared to be incomplete in contrast to the usual spectral changes of mammalian peroxidases, but no further shift of the Soret peak was achieved with further cyanide addition. Moreover, the spectral changes in the region of 500-600 nm could not be used for calculating due to negligible absorbance.

Chart 17 shows the difference spectra of the 17 graphs from Chart 16. The difference spectra were the basis for the choice of wavelength for further analysis.

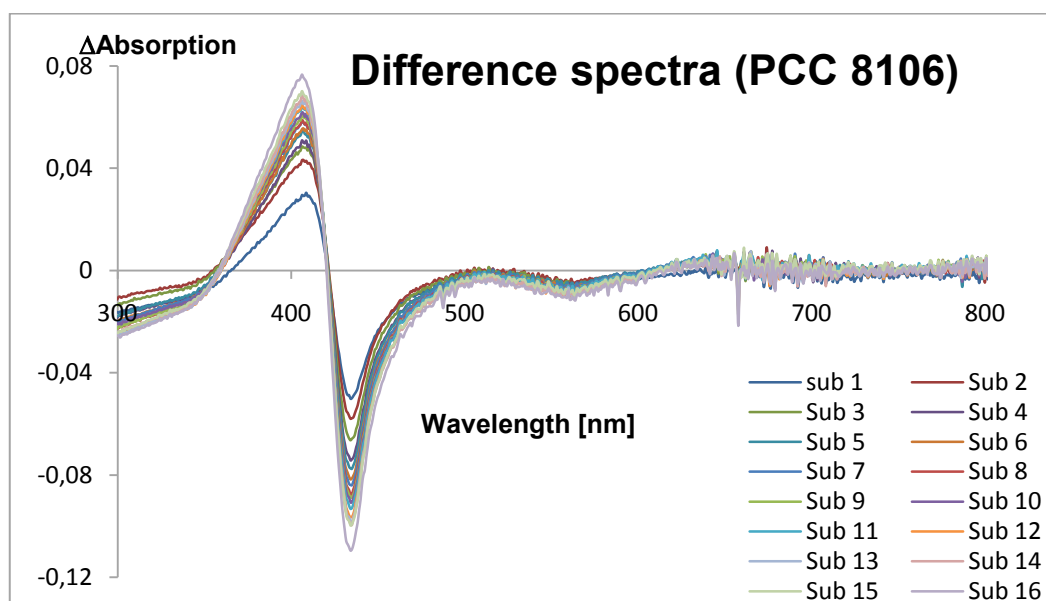


Chart 17 Difference spectra of PCC 8106 peroxidase.

The Δ Absorption values at 434 nm were consulted for following analysis and are listed in Table 34 for all measured cyanide concentrations.

Tab. 34 Absolute values for the Δ Absorption and the respective CN^- concentrations at 434 nm

Cyanide [mM]	Δ Absorption	Cyanide [mM]	Δ Absorption
0	0	0.8	0.0983
0.05	0.0501	0.9	0.0992
0.1	0.0580	1	0.0998
0.15	0.0664	1.25	0.1023
0.2	0.0743	1.75	0.1056
0.25	0.0775	2.25	0.1083
0.3	0.0816	2.75	0.1096
0.35	0.0839	3.75	0.1104
0.4	0.0877	4.75	0.1116
0.5	0.0907	7.5	0.1130
0.6	0.0933	10	0.1134
0.7	0.0965	15	0.1147

These values are plotted in Chart 18.

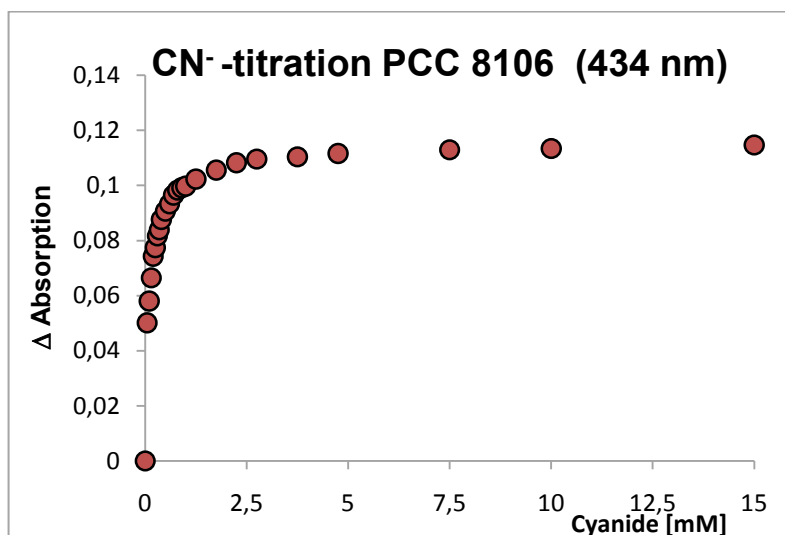


Chart 18 Plot of Δ Absorption against the cyanide concentration according to Table 34 resulting from spectral analysis

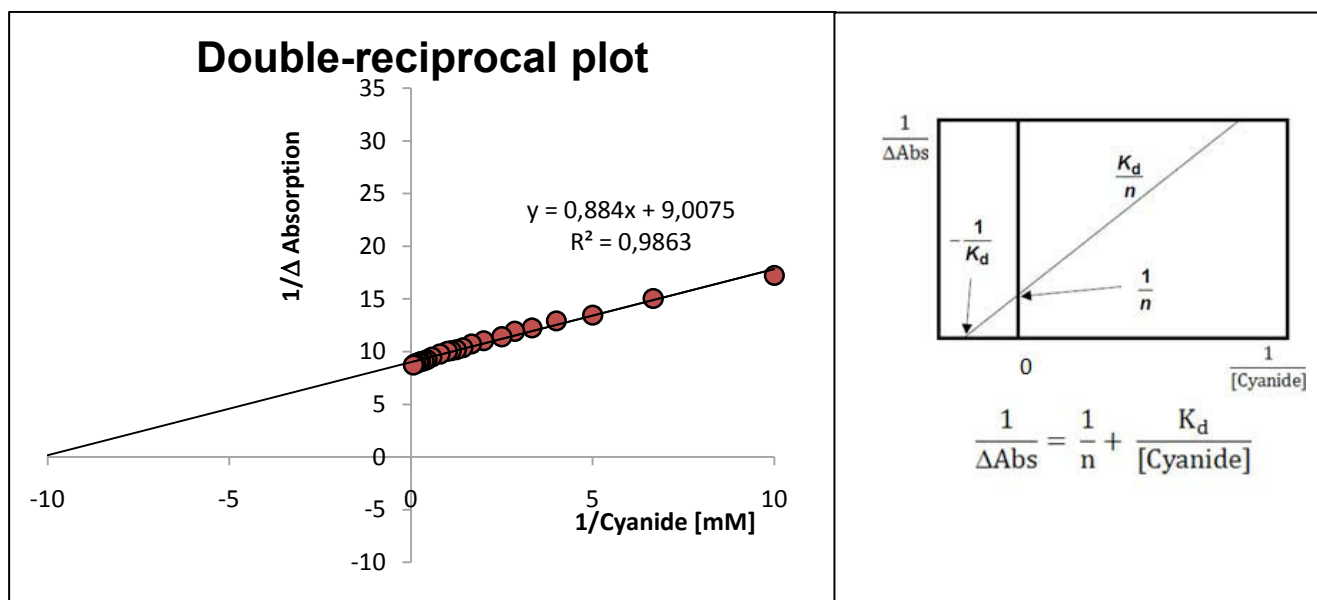


Chart 19 Double reciprocal plot of the values according to Table 34 and additionally the calculation method is shown.

In accordance to the double reciprocal plot the apparent K_d value of the PCC 8106 peroxidase with cyanide was 98.1 μ M.

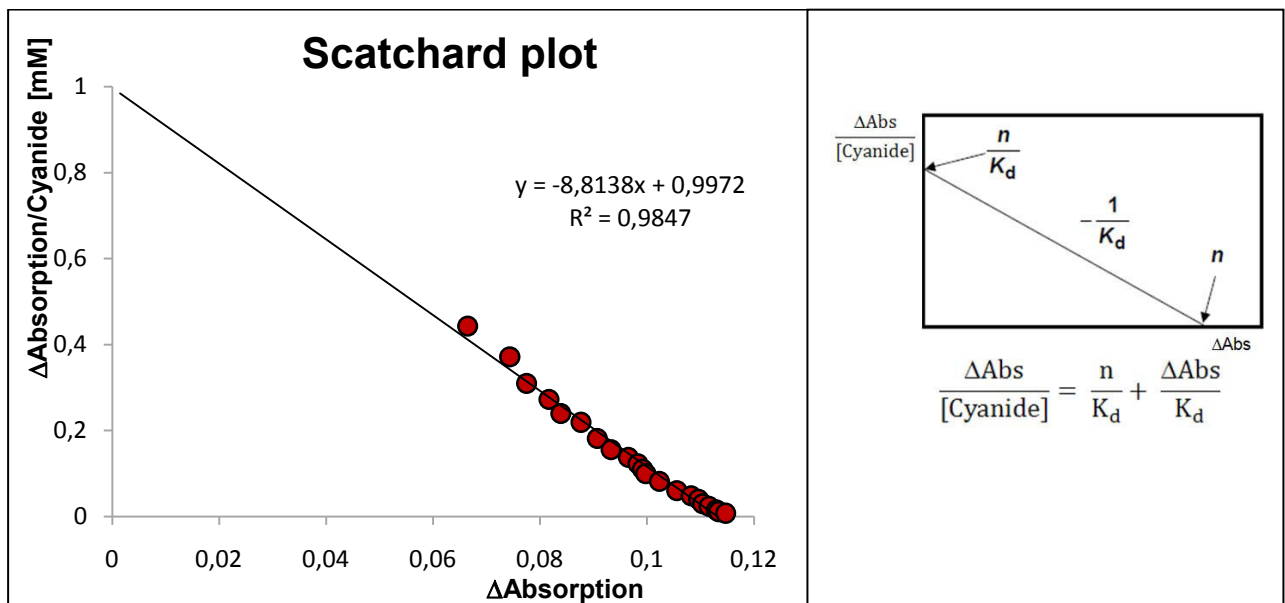


Chart 20 Scatchard Plot of the values according to Table 34 and additionally the calculation method is shown.

In accordance to the Scatchard plot the apparent K_d value of the PCC 8106 peroxidase with cyanide was 113.4 μM .

4.7.1.2 PCC 7420 peroxidase

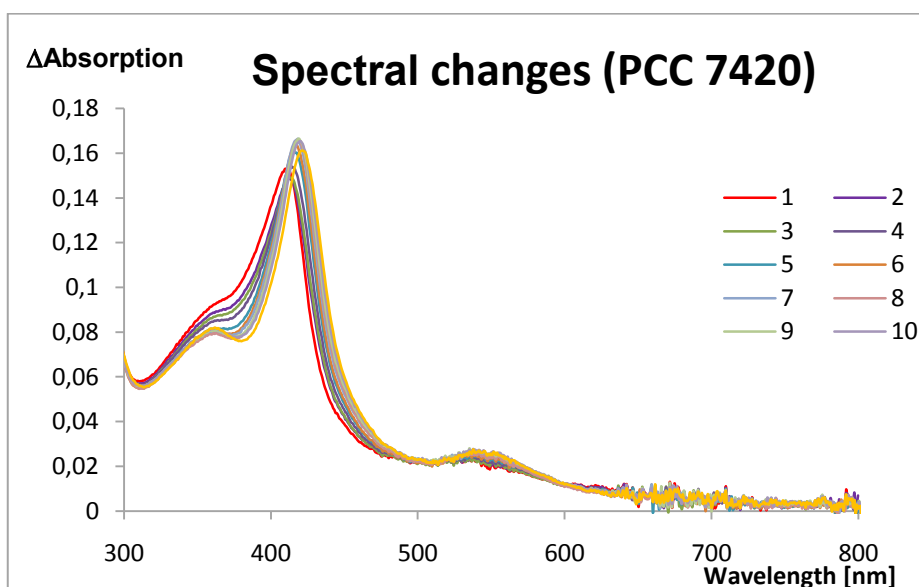


Chart 21 Shows the spectral changes from 300 to 800 nm of PCC 7420 peroxidase at pH 7 and 25°C with raising cyanide concentration. The red graph is the enzyme without CN^- and the yellow graph is the "endpoint" of shifting. In this case the lower absorption maximum of the yellow graph was due to dilution originating from CN^- stock solution.

The spectral shift of the PCC 7420 peroxidase also appeared to be incomplete in contrast to the usual spectral changes of mammalian peroxidases. But compared to the PCC 8106 peroxidase the Soret band red-shifted and increased in absorbivity. Moreover, the spectral changes in the region of 500-600 nm could not be used for calculating due to negligible absorbance.

Chart 17 shows the difference spectra of the 11 graphs from Chart 16. The difference spectra were the basis for the choice of wavelength for further analysis.

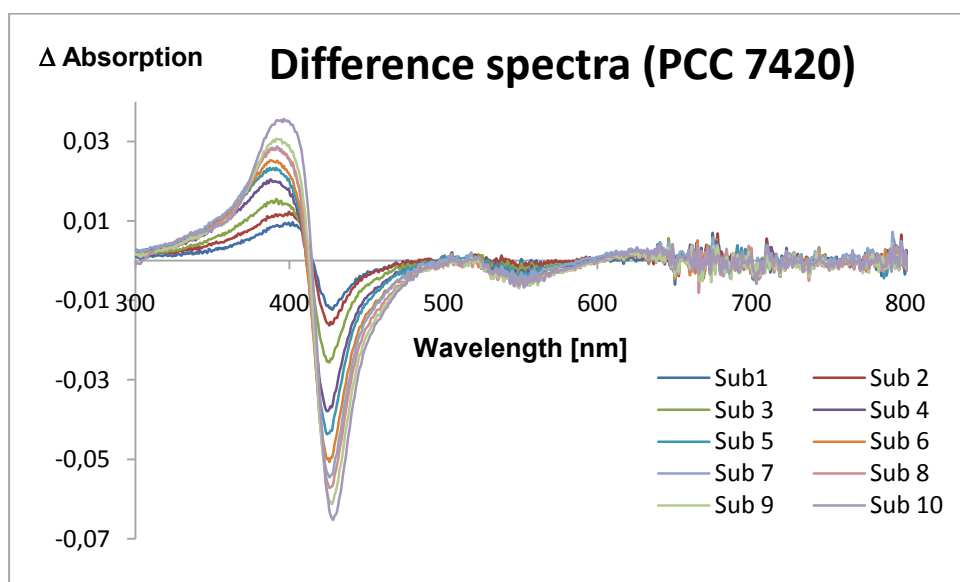


Chart 22 Difference spectra of PCC 7420 peroxidase.

The Δ Absorption values at 428 nm were consulted for following analysis and are listed in Table 35 for all measured cyanide concentrations.

Tab. 35 Absolute values for the Δ Absorption and the respective CN^- concentrations at 428 nm

Cyanide [mM]	Δ Absorption	Cyanide [mM]	Δ Absorption
0	0	4	0.0445
0.25	0.0121	5	0.0485
0.5	0.0157	6	0.0513
1	0.0241	7	0.0531
1.5	0.0300	8	0.0562
2	0.0354	10	0.0606
2.5	0.0383	15	0.0629
3	0.0408	25	0.0653

The values of Table 35 are plotted in Chart 23.

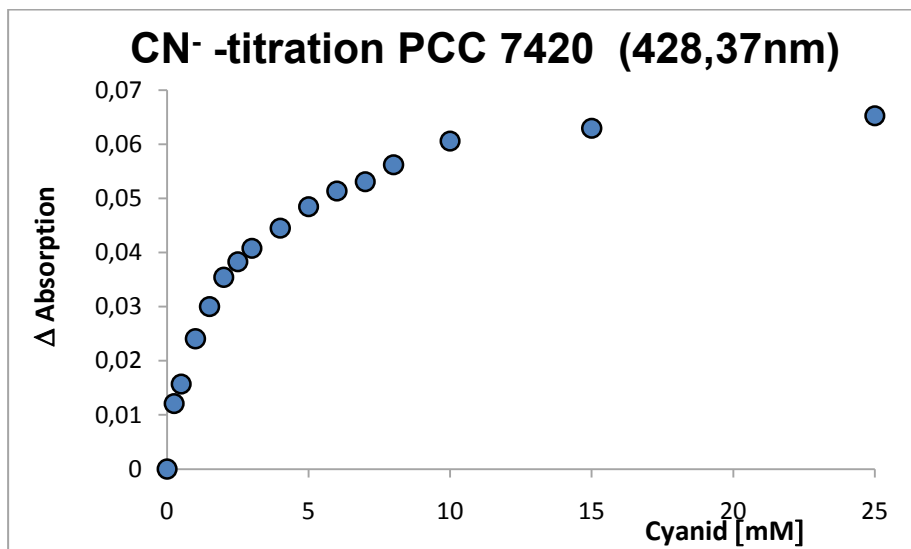


Chart 23 Plot of Δ Absorption against the cyanide concentration according to Table 35 resulting from spectral analysis

Chart 23 indicated that cyanide binding to the active site of PCC 7420 peroxidase occurred not as fast as to PCC 8106 peroxidase and in addition was not monophasic.

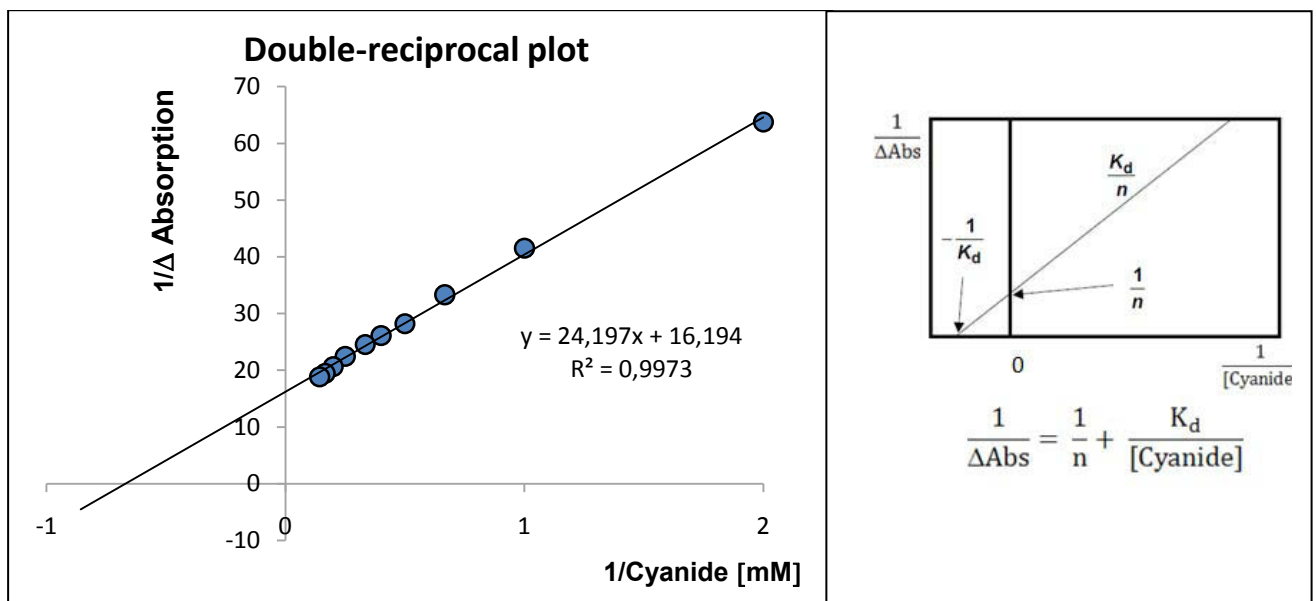


Chart 24 Double Reciprocal Plot of the values according to Table 35 and additionally the calculation method is shown. Data were taken from the first (high affinity) phase of the plot depicted in Chart 23.

In accordance to the double reciprocal plot the apparent K_d value of the PCC 7420 peroxidase with cyanide was 1.49 mM.

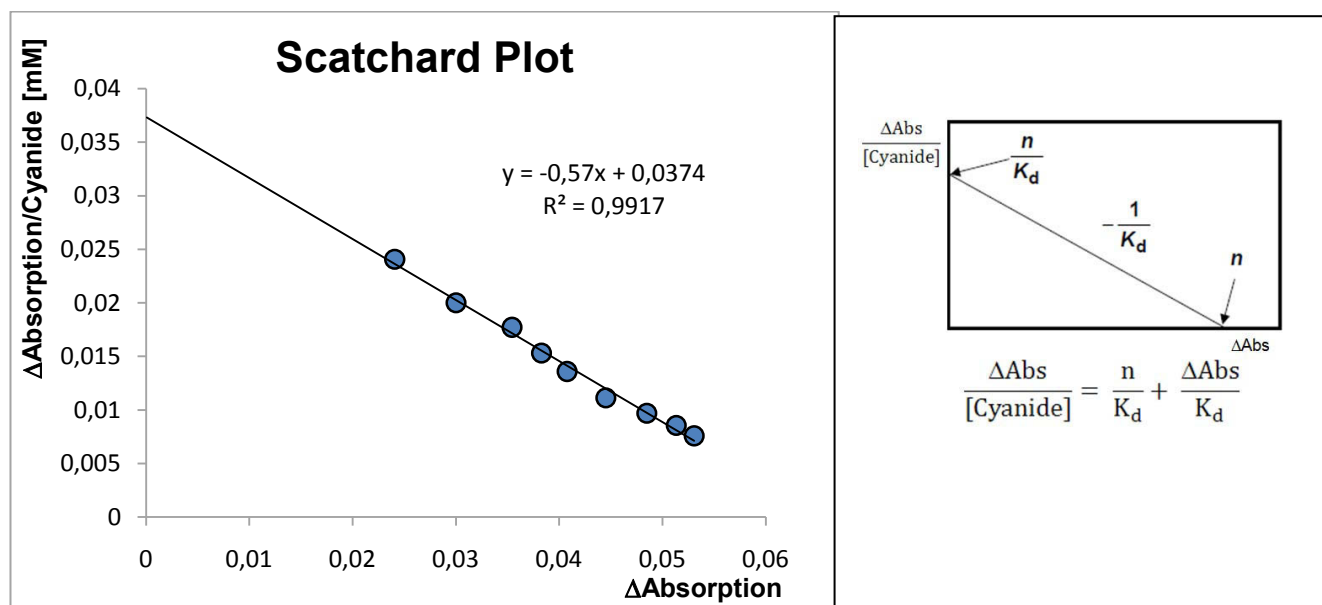


Chart 25. Scatchard Plot of the values according to Table 34 and additionally the calculation method is shown.

In accordance to the Scatchard plot the apparent K_d value of the PCC 7420 peroxidase with cyanide was 1.75 mM.

4.7.2 Kinetics of cyanide binding

4.7.2.1 Cyanide binding of PCC 8106 peroxidase

Figure 31 shows the results of the stopped-flow diode array measurement, analyzed by means of the Pro-K simulation program from Applied Photophysics.

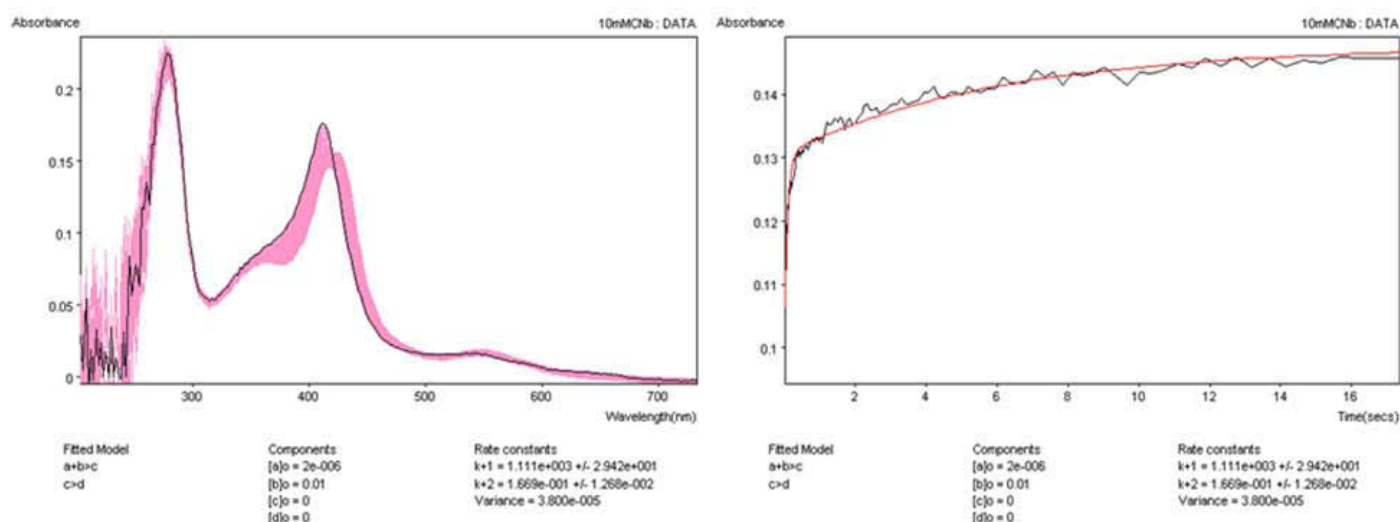


Figure 31 shows the stopped-flow diode array analysis of PCC 8106 peroxidase binding cyanide (25°C; 100 mM phosphate buffer pH 7; ~ 2 μ M enzyme). On the left side the spectral changes from 200 to 730 nm caused by addition of 10 mM cyanide (c_{end}) are shown. On the right side a 20 s time trace at 431.5 nm is pictured.

The spectral changes of PCC 8106 peroxidase were similar to that observed with cyanide titration. The time trace revealed that after the initial rapid phase there was a further much slower second phase which was not finished even after 20 seconds. The reason for this could be that the enzyme solution maybe contained some wrong folded protein with an blocked active site.

Chart 26 shows the pseudo-first-order rate constant (k_{obs}) plotted versus the cyanide concentration. The fit range for k_{obs} values was 0.73 seconds.

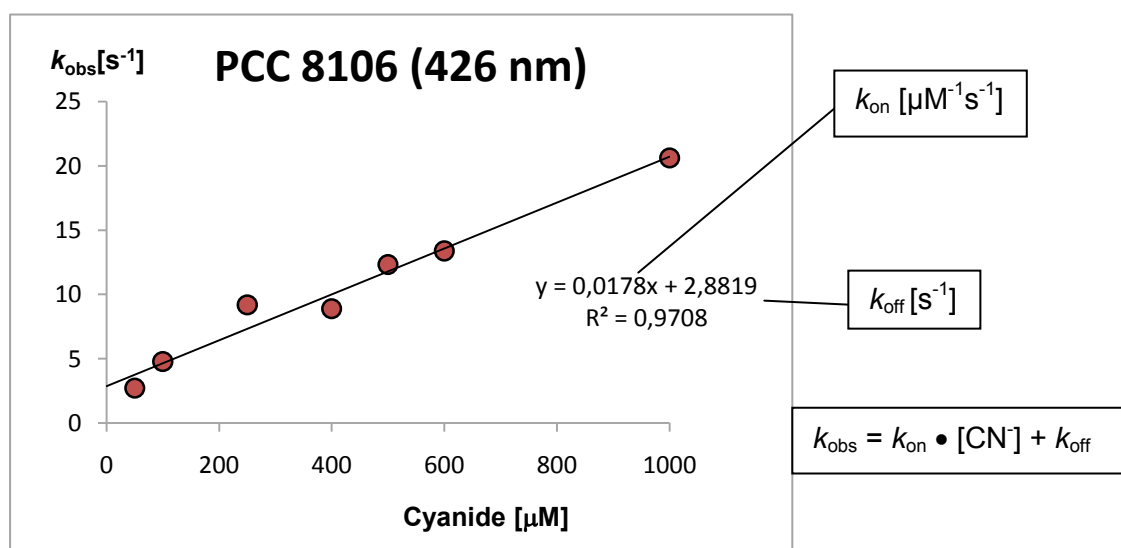


Chart 26 k_{obs} values plotted toward the used cyanide concentrations, measured with the stopped-flow single wavelength mode at 426 nm 22°C and 100 mM phosphate buffer pH 7.0 (~ 2 μ M enzyme).

The calculated apparent binding rate k_{on} was $1.78 \times 10^4 \text{ M}^{-1}\text{s}^{-1}$ and the dissociation rate k_{off} 2.88 s^{-1} . The K_d value is calculated according to equation (6).

$$K_d = \frac{k_{off}}{k_{on}} \quad (6)$$

The resultant K_d value $161.9 \mu\text{M}$ compares with $98.1 \mu\text{M}$ and $113.4 \mu\text{M}$ obtained from the equilibrium studies.

4.7.2.2 Cyanide binding of PCC 7420 peroxidase

Figure 32 shows the results of the stopped-flow diode array measurement, analyzed by means of the Pro-K simulation program from Applied Photophysics.

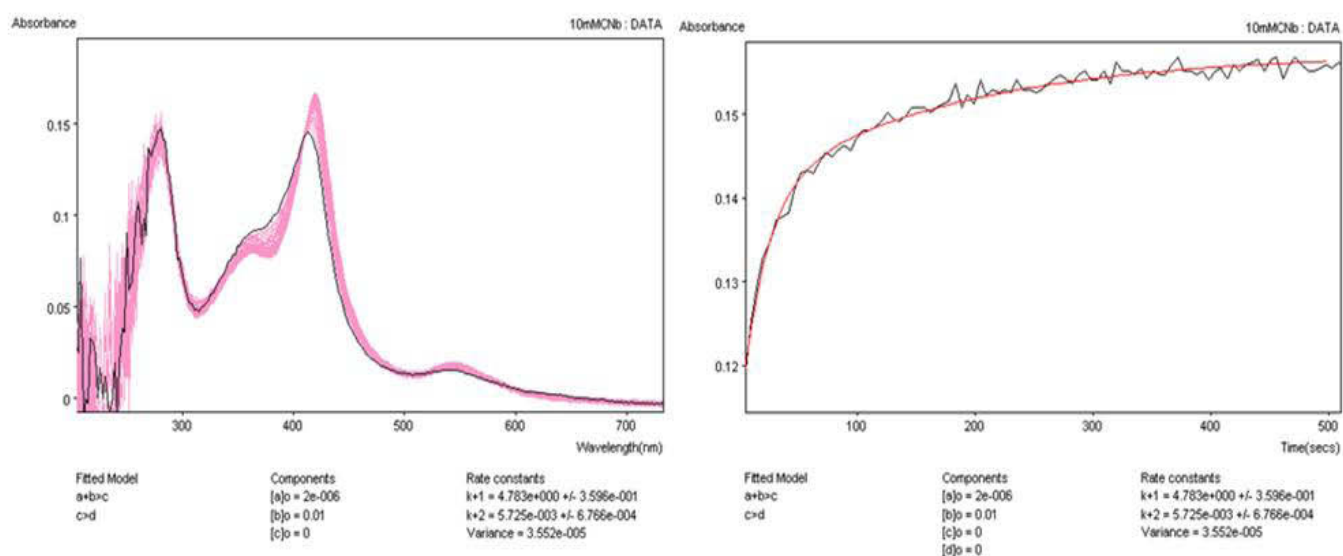


Figure 32 shows the stopped flow diode array analysis of PCC 7420 peroxidase with cyanide (25°C; 100 mM phosphate buffer pH 7.0; $\sim 2 \mu\text{M}$ enzyme). On the left side the spectral changes from 200 to 730 nm caused by addition of 10 mM cyanide (C_{end}) are shown. On the right side a 500 s time trace at 425.1 nm is pictured.

The spectral changes of PCC 7420 peroxidase were similar to that observed with cyanide titration. The time trace revealed that after the initial rapid phase there was a further much slower second phase which was not finished even after 500 seconds. The reason for this could be that the enzyme solution maybe contained some wrong folded protein with an blocked active site.

Chart 27 shows the pseudo-first-order rate constant (k_{obs}) plotted toward the cyanide concentration. The reaction curve was fitted with a triple exponential equation and consequently no fit range is denoted. For calculation of apparent k_{on} k_{obs} -values from the rapid (first) phase were taken.

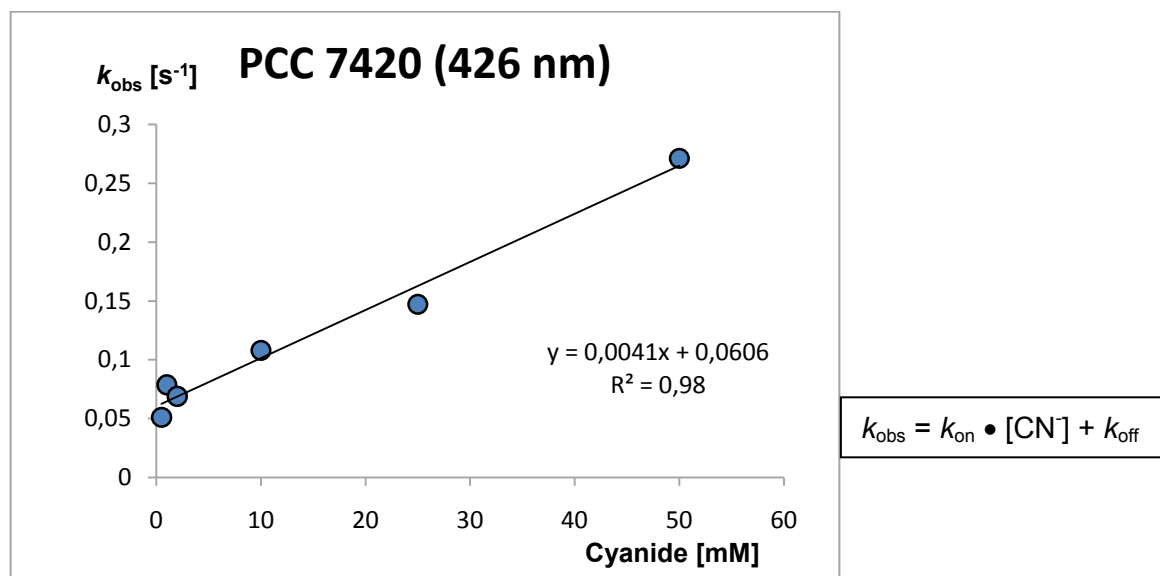


Chart 27 k_{obs} values plotted toward the used cyanide concentrations, measured with the stopped-flow single wavelength mode at 426 nm 22°C and 100 mM phosphate buffer pH 7.0 (~ 2 μM enzyme). k_{obs} value for 5 mM CN^- concentration was an outlier and consequently removed.

The calculated apparent binding rate k_{on} was $4.1 \text{ M}^{-1}\text{s}^{-1}$ and the dissociation rate k_{off} 0.06 s^{-1} . The K_{d} value is calculated according to equation (6).

The resultant K_{d} value 14.8 mM was about 10 times higher than the values obtained from the equilibrium studies (1.49 mM and 1.75 mM). The differences between the K_{d} values were due to the non-monophasic reaction.

4.8 Kinetics of hydrogen peroxide reduction

4.8.1 PCC 8106 peroxidase

Figure 33 shows the results of the stopped flow diode array measurement of PCC 8106 peroxidase with H_2O_2 , analyzed by means of the Pro-K simulation program from Applied Photophysics.

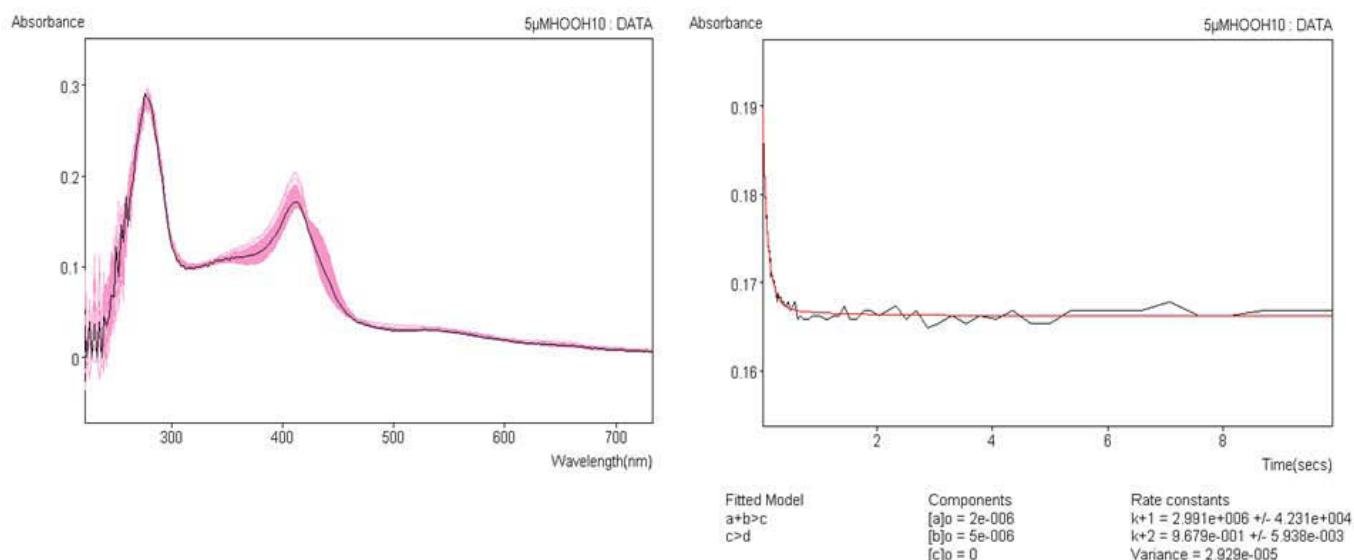


Figure 33 shows the stopped-flow diode array analysis of PCC 8106 peroxidase with H_2O_2 (23°C; 100 mM phosphate buffer pH 7.0; ~ 2 μM enzyme). On the left side the spectral changes from 200 to 730 nm caused by addition of 5 μM H_2O_2 (c_{end}) are shown. On the right side a 10 s time trace at 412.2 nm is pictured.

After the addition of 5 μM of H_2O_2 to the PCC 8106 peroxidase a decay and a red shift of the Soret peak was observed. The decay of the Soret was putatively the Compound I in conformity with the mammalian peroxidases and consequently the rate for Compound I formation was determined at the single wavelength mode at 406 nm. Additionally the red shift supposed to be the Compound II formation was followed at 428 nm. The resulting k_{obs} values at the respective concentrations are displayed in Chart 28. The used H_2O_2 concentrations were described in 3.7.2.

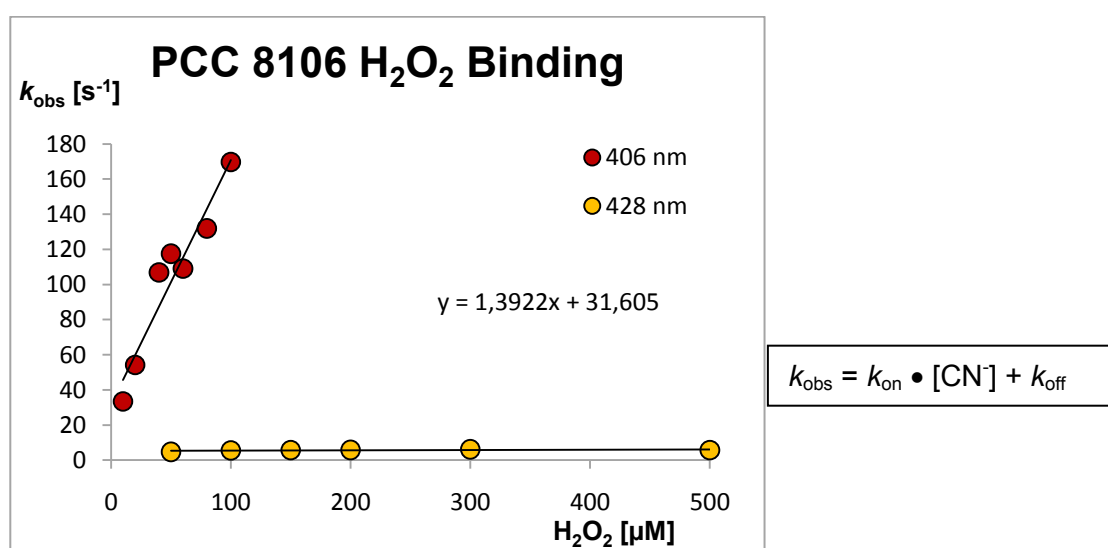


Chart 28 The velocity of the decrease of absorption at 406 nm with raising H_2O_2 concentrations are labeled red, and in the same way the values for increase of absorption at 428 nm are labeled yellow.

The calculated apparent second-order-rate constant for Compound I formation by hydrogen peroxide at pH 7 and 22°C was $2.2 \times 10^5 \text{ M}^{-1}\text{s}^{-1}$, which was significantly lower than that of LPO, MPO and EPO with H_2O_2 (1.7 and $4.3 \times 10^7 \text{ M}^{-1}\text{s}^{-1}$) [12, 16]. The observed spectral shift to 428 nm was not dependent on hydrogen peroxide concentration (Chart 28).

4.8.2 Results of the PCC 7420 peroxidase

Preliminary test showed the very high hydrogen peroxide concentrations were required thus the analysis were accompanied by absorption changes due to protein decomposition. Figure 34 shows the results of the stopped flow diode array measurement of PCC 7420 peroxidase with H_2O_2 , analyzed by means of the Pro-K simulation program from Applied Photophysics.

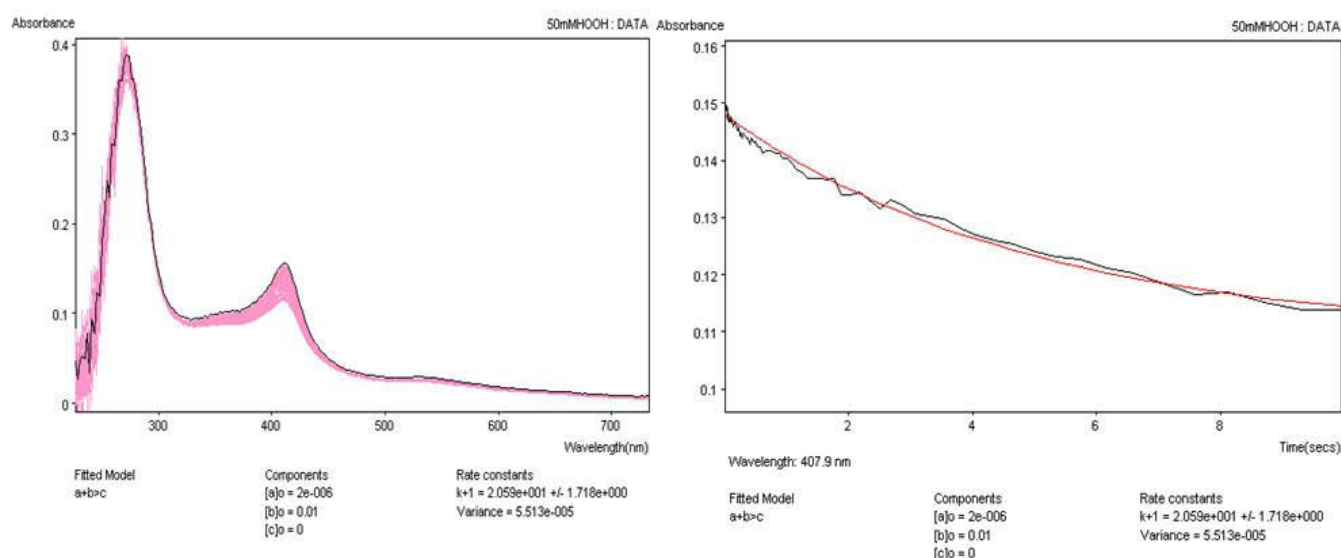


Figure 34 shows the stopped-flow diode array analysis of PCC 7420 peroxidase reaction with H_2O_2 (23°C; 100 mM phosphate buffer pH 7.0; $\sim 2 \mu\text{M}$ enzyme). On the left side the spectral changes from 200 to 730 nm caused by addition of 50 mM H_2O_2 (c_{end}) are shown. On the right side a 10 s time trace at 407.9 nm is pictured.

As easy noticeable in Figure 34 Compound I formation occurred very slowly despite high substrate concentrations. Nevertheless, a rate-constant for Compound I formation was determined as pictured in Chart 29.

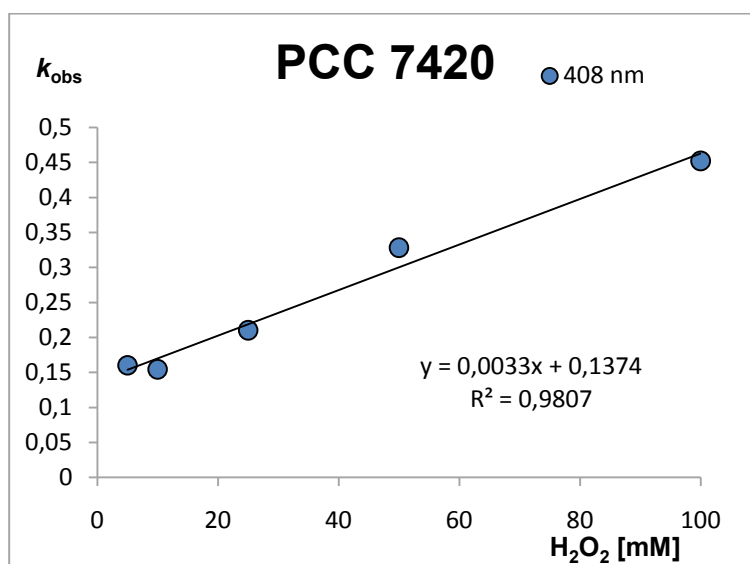


Chart 29 k_{obs} values of PCC 7420 peroxidase plotted toward the H_2O_2 concentration. The enzyme was measured at 23°C and pH 7.0 (100 mM phosphate buffer pH 7.0).

The calculated apparent second-order-rate constant for Compound I formation by hydrogen peroxide at pH 7 and 22°C was $4.2 \times 10^2 \text{ M}^{-1}\text{s}^{-1}$ which was much slower than the values of PCC 8106 peroxidase and the mammalian peroxidases.

5. Conclusions

Cloning

Cloning of the *Microcoleus chthonoplastes* (PCC 7420) peroxidase using the *E. coli* expression strain BL21 (DE) Star was successful. The expression screening showed that active enzyme occurred in both supernatant as well as in the cell pellet. For protein purification only peroxidase from the supernatant was used. Occurrence in cell debris could be caused by incomplete cleavage of the predicted leader peptide or trapping of the recombinant protein in the periplasmic space of the *E. coli* cells. This problem could be solved with an additional digestion solution during the cell lysis.

Overexpression and Purification

Although the complete structure of both cyanobacterial peroxidases is not clarified till yet, one could suppose that a big part of the PCC 7420 peroxidase was not folded correctly in contrast to the PCC 8106 peroxidase. The induction of expression with lactose instead of IPTG was a big improvement related to protein folding and activity. Preliminary tests with enzymes expressed by using IPTG are not shown in this work. However with regard to the protein expression and purification there is enough space for further developments. For example under modified buffer conditions a MCAC purification of the PCC 8106 peroxidase again with Zn^{2+} ions instead of Ni^{2+} ions is thinkable.

Under expression and purification conditions, like described in this work further treatment of PCC 7420 peroxidase could be performed. Provided that incorrect folded protein is less stable, additionally repeated centrifugation and freezing steps could potentially increase the part of correctly folded enzyme in obtained solution. However this would lead to much lower yields.

Sequence alignment and parameter prediction

The results of the sequence alignment (4.1.1) suggested that the recombinant production of both cyanobacterial enzymes should deliver a working peroxidase. Almost all well investigated amino acids in the active site of mammalian peroxidases were present in both cyanobacterial amino acid sequences. If they reside at the right place could only be confirmed by a crystal structure analysis.

Due to completeness the motif of the hydrogen bond chain to the surface of the MPO molecule [27] was also aligned and the cyanobacterial peroxidases showed surprising similarities. 4 of the 6 involved amino acids were identical. The only difference was the amino acid at the edge of the MPO molecule. Generally, for investigation if these amino acids are essential for the enzyme activity is more convenient by means of a bacterial expressed protein.

Further remarkably results of the prediction work were the high content of α -helices, the missing cysteins and the low p/s. The functionality of the mammalian peroxidases like binding to a membrane is strongly determined by their isoelectric properties. If the cyanobacterial peroxidases served the organisms as a defense or attack against foreign organisms there must have been an alternatively way of "targeting".

Both cyanobacterial peroxidases contained no cysteine which indicates maybe a low protein stability, but this section remains to be elucidated.

It should also be noticed that prediction of secondary structure starting from primary structure is still in its infancy (75% accuracy)

Spectroscopic conclusions

The UV-Vis spectra of the cyanobacterial heme peroxidases exhibited a Soret peak likewise to that of LPO and EPO. Additionally a shoulder at 370 nm was detected in particular in the PCC 7420 peroxidase spectra and less pronounced and LPO like in PCC 8106 peroxidase spectra, which might be caused by improperly incorporated heme. In the region from 490 to 700 nm no similarities to the mammalian peroxidases were found. The cyanide binding assay suggested the existence of a high spin and low spin state, despite their spectral changes appeared to be incomplete in contrast to the mammalian peroxidases. Moreover the slow spectral changes of the *Microcoleus chthonoplastes* PCC 7420 peroxidase in the substrate binding assays suggested an incorrect protein folding.

The predicted α -helix and β -sheet was compared with the results of far UV CD spectroscopy. Especially the predicted and the measured α -helix content of the PCC 8106 peroxidase matched well together. Moreover the near UV-Vis spectroscopy delivered a good estimation about the incorporation of the heme group. The Soret region of the PCC 7420 peroxidase showed a very weak signal whereas the CD band in this region of the PCC 8106 peroxidase was comparable to that of mammalian peroxidases MPO and LPO (4.5.2). The consequent supposition of a better folded protein was confirmed by a higher peroxidase and halogenation activity of the PCC 8106 peroxidase in contrast to the PCC 7420 peroxidase.

Peroxidase and halogenation activity

Both cyanobacterial peroxidases showed peroxidase and halogenation activity. The *Microcoleus chthonoplastes* PCC 7420 exhibited a weak activity whereas the *Lyngbya* sp. PCC 8106 peroxidase showed activities which were comparable to that of the mammalian peroxidases. Especially the MCD chlorinating activity of the PCC 8106 peroxidase at lower pH values was remarkably. Similar to that the EPO is known to exhibit weak chlorinating activity at pH 7 and significant higher activities at lower pH values due to raising reduction potential [41]. This property could be elucidated in detail because no chloride oxidation product was determined and the MCD assay was the first clear test for chlorinating activity.

In general both cyanobacterial peroxidases are halophil organisms and their most abundant substrate chloride is present in very high concentration. Due to osmotic pressure one can suppose that the salt concentrations inside the cells are also very high. Consequently a chlorination activity would not make sense because the high amount of produced antimicrobial agents would also kill themselves. But besides the fact that PCC 8106 peroxidase showed no chlorination activity at in the sea prevailing pH regions, natural expression levels of both cyanobacterial enzymes are not known. Furthermore it has not been clarified if special conditions or an inductor are necessary for enzyme expression.

References

- [1] Muller W.A., Leukocyte-Endothelial Cell Interactions in the Inflammatory Response., *Lab Invest* 2002, 82: 521–533
- [2] Riikka I., Vuokko L., Jorma T. Origin, structure, and biological activities of peroxidases in human saliva. *Arch Biochem Biophys.* 2006 Jan 15 ;445(2): 261-268.
- [3] Wang J., Slungaard A., Role of eosinophil peroxidase in host defense and disease pathology. *Arch. Biochem. Biophys.* 2006 Jan 15; 445(2):256-60.
- [4] Arlandson M., Decker T., Roongta V.A., Bonilla L., Mayo K.H., MacPherson J.C., Hazen S.L., Slungaard A. Eosinophil peroxidase oxidation of thiocyanate. *J. Biol Chem.* 2001 Jan 5;276(1):215-224.
- [5] Klebanoff S.J., Myeloperoxidase: friend and foe. *J Leukoc Biol.* 2005 May;77(5):598-625
- [6] Malle E., Furtmüller P.G., Sattler W., Obinger C., Myeloperoxidase: a target for new drug development? *Br. J. Pharmacol.* 2007 Nov;152(6):838-54. Review.
- [7] Zamocky M., Jakopitsch C., Furtmüller P.G., Dunand C., Obinger C., The peroxidase-cyclooxygenase superfamily: Reconstructed evolution of critical enzymes of the innate immune system. *Proteins.* 2008 Aug;72(2):589-605.
- [8] Obinger C. Heme peroxidase biochemistry-facts and perspectives. *Arch. Biochem. Biophys.* 2010 Aug 1;500(1):1-2.
- [9] Davies M.J., Hawkins C.L., Pattison D.I., Rees M.D., Mammalian heme peroxidases: from molecular mechanisms to health implications. *Antioxid Redox Signal.* 2008 Jul;10(7):1199-234.
- [10] Reynolds W.F., Rhees J., Maciejewski D., Paladino T., Sieburg H., Maki R.A., Masliah E., Myeloperoxidase polymorphism is associated with gender specific risk for Alzheimer's disease. *Exp. Neurol.* 1999 Jan;155(1):31-41.
- [11] Hansson M., Olsson I., Nauseef W.M., Biosynthesis, processing, and sorting of human myeloperoxidase. *Arch. Biochem. Biophys.* 2006 Jan 15;445(2):214-24.
- [12] Furtmüller P.G., Zederbauer M., Jantschko W., Helm J., Bogner M., Jakopitsch C., Obinger C., Active site structure and catalytic mechanisms of human peroxidases. *Arch. Biochem Biophys.* 2006 Jan 15;445(2):199-213.

- [13] Carpena X., Vidossich P., Schroettner K., Calisto B.M., Banerjee S., Stampler J., Soudi M., Furtmüller P.G., Rovira C., Fita I., Obinger C., Essential role of proximal histidine-asparagine interaction in mammalian peroxidases. *J. Biol Chem.* 2009 Sep 18;284(38):25929-37.
- [14] Iwamoto H., Kobayashi T., Hasegawa E., Morita Y. Reaction of human myeloperoxidase with hydrogen peroxide and its true catalase activity. *J Biochem.* 1987 Jun;101(6):1407-12.
- [15] Kettle A.J., Winterbourn C.C. A kinetic analysis of the catalase activity of myeloperoxidase. *Biochemistry.* 2001 Aug 28;40(34):10204-12.
- [16.] Furtmüller P.G., Burner U., Jantschko W., Regelsberger G., Obinger C., Two-electron reduction and one-electron oxidation of organic hydroperoxides by human myeloperoxidase. *FEBS Lett.* 2000 Nov 3;484(2):139-43.
- [17] Furtmüller P.G., Burner U., Jantschko W., Regelsberger G., Obinger C. The reactivity of myeloperoxidase Compound I formed with hypochlorous acid. *Redox Rep.* 2000;5(4):173-8.
- [18] Jantschko W., Furtmüller P.G., Zederbauer M., Jakopitsch C., Obinger C., Kinetics of oxygen binding to ferrous myeloperoxidase. *Arch Biochem Biophys.* 2004 Jun 1;426(1):91-7.
- [19] Jantschko W., Furtmüller P.G., Zederbauer M., Neugschwandtner K., Jakopitsch C., Obinger C., Reaction of ferrous lactoperoxidase with hydrogen peroxide and dioxygen: an anaerobic stopped-flow study. *Arch Biochem Biophys.* 2005 Feb 1;434(1):51-9.
- [20] Jantschko W., Furtmüller P.G., Zederbauer M., Lanz M., Jakopitsch C., Obinger C., Direct conversion of ferrous myeloperoxidase to Compound II by hydrogen peroxide: an anaerobic stopped-flow study. *Biochem Biophys Res Commun.* 2003 Dec 12;312(2):292-8.
- [21] Jakopitsch C., Regelsberger G., Furtmüller P.G., Rümer F., Peschek G.A., Obinger C., Catalase-peroxidase from *synechocystis* is capable of chlorination and bromination reactions. *Biochem Biophys Res Commun.* 2001 Sep 28;287(3):682-7.
- [22] Bolhuis H., Severin I., Confurius-Guns V., Wollenzien U.I., Stal L.J., Horizontal transfer of the nitrogen fixation gene cluster in the cyanobacterium *Microcoleus chthonoplastes*. *ISME J.* 2010 Jan;4(1):121-30.
- [23] Stal L.J, Grossberger S., Krumbein W.E., Nitrogen fixation associated with the cyanobacterial mat of a marine laminated microbial ecosystem Volume 82, Number 3, 217-224
- [24] Joergensen B.B., Cohen Y., Revsbech N.P. Transition from Anoxygenic to Oxygenic Photosynthesis in a *Microcoleus chthonoplastes* Cyanobacterial Mat *Applied and Environmental Microbiology*, Feb. 1986, p. 408-417 Vol. 51, No. 2

- [25] Abu-Soud H.M., Khassawneh M.Y., Sohn J.T., Murray P, Haxhiu M.A., Hazen S.L. Peroxidases inhibit nitric oxide (NO) dependent bronchodilation: development of a model describing NO-peroxidase interactions. *Biochemistry*. 2001 Oct 2;40(39):11866-75.
- [26] Furtmüller P.G., Jantschko W, Zederbauer M., Schwanninger M., Jakopitsch C, Herold S, Koppel W.H., Obinger C. Peroxynitrite efficiently mediates the interconversion of redox intermediates of myeloperoxidase. *Biochem Biophys Res Commun*. 2005 Nov 25;337(3):944-54.
- [27] Tristan J. Fiedler, Curt A. Davey, and Roger E. Fenna. X-ray Crystal Structure and Characterization of Halide-binding Sites of Human Myeloperoxidase at 1.8 Å Resolution *The Journal of biological chemistry* Vol. 275, No. 16, Issue of April 21, pp. 11964–11971, 2000
- [28] Zederbauer M., Furtmüller P.G., Brogioni S., Jakopitsch C., Smulevich G., Obinger C., Heme to protein linkages in mammalian peroxidases: impact on spectroscopic, redox and catalytic properties. *Nat Prod Rep*. 2007 Jun;24(3):571-84.
- [29.] Furtmüller P.G., Obinger.C. Practical course in Biochemistry 2. University of Natural Resources and life science. 2010
- [30] Jeanmougin F., Thompson J.D., Gouy M., Higgins M. Gibson T.J. Multiple sequence alignment with ClustalX. *Trends Biochem Sci* 1998; 23:403-405.
- [31] Nicholas K.B., Nicholas H.B., Genedoc a tool for editing and annotating multiple sequence alignments. Distributed by the author. 1997
- [32] Ueda T, Sakamaki K, Kuroki T, Yano I, Nagata S Molecular cloning and characterization of the chromosomal gene for human lactoperoxidase. *Eur J Biochem*. 1997 Jan 15;243(1-2):32-41.
- [33] Von Heijne G., Patterns of Amino Acids near Signal-Sequence Cleavage Sites *Eur. J. Blochem*. 133, 17-21 (1983)
- [34] Nielsen H., Krogh A. Prediction of signal peptides and signal anchors by a hidden Markov model. *Proc Int Conf Intell Syst Mol Biol*. 1998;6:122-30
- [35] Nielsen H., Engelbrecht J., Brunak S., von Heijne G., Identification of prokaryotic and eukaryotic signal peptides and prediction of their cleavage sites. *Protein Eng*. 1997 Jan;10(1):1-6.
- [36] Mubarakshina M.M., Ivanov B.N., Naydov I.A., Hillier W., Badger M.R., Krieger-Liszkay A. Production and diffusion of chloroplastic H₂O₂ and its implication to signalling. *J Exp Bot*. 2010 Aug;61(13):3577-87.

- [37] Doerge D.R, Divi R.L., Churchwell M.I., Identification of the colored guaiacol oxidation product produced by peroxidases, *Analytic Biochemistry* 1997 Feb. 250, 10-17
- [38] Hiner A.N., Rodríguez-López J.N., Arnao M.B., Lloyd Raven E., García-Cánovas F., Acosta M., Kinetic study of the inactivation of ascorbate peroxidase by hydrogen peroxide. *Biochem J.* 2000 Jun 1;348 Pt 2:321-8.
- [39] Jakopitsch C., Spalteholz H., Furtmüller P.G., Arnhold J., Obinger C., Mechanism of reaction of horseradish peroxidase with chlorite and chlorine dioxide. *J Inorg Biochem.* 2008 Feb;102(2):293-302.
- [40] Zederbauer M. Jantschko W., Neugschwandtner K., Jakopitsch Ch., Moguilevsky N., Obinger Ch., Furtmüller P.G., Role of the Covalent Glutamic Acid 242- Heme Linkage in the Formation and Reactivity of Redox Intermediates of human Myeloperoxidase. *American Chemical Society, Biochemistry* 2005, 44, 6482-6491.
- [41] Spalteholz H., Panasenko O.M., Arnhold J.; Formation of reactive halide species by myeloperoxidase and eosinophil peroxidase. *Arch Biochem Biophys.* 2006 Jan 15;445(2):225-34